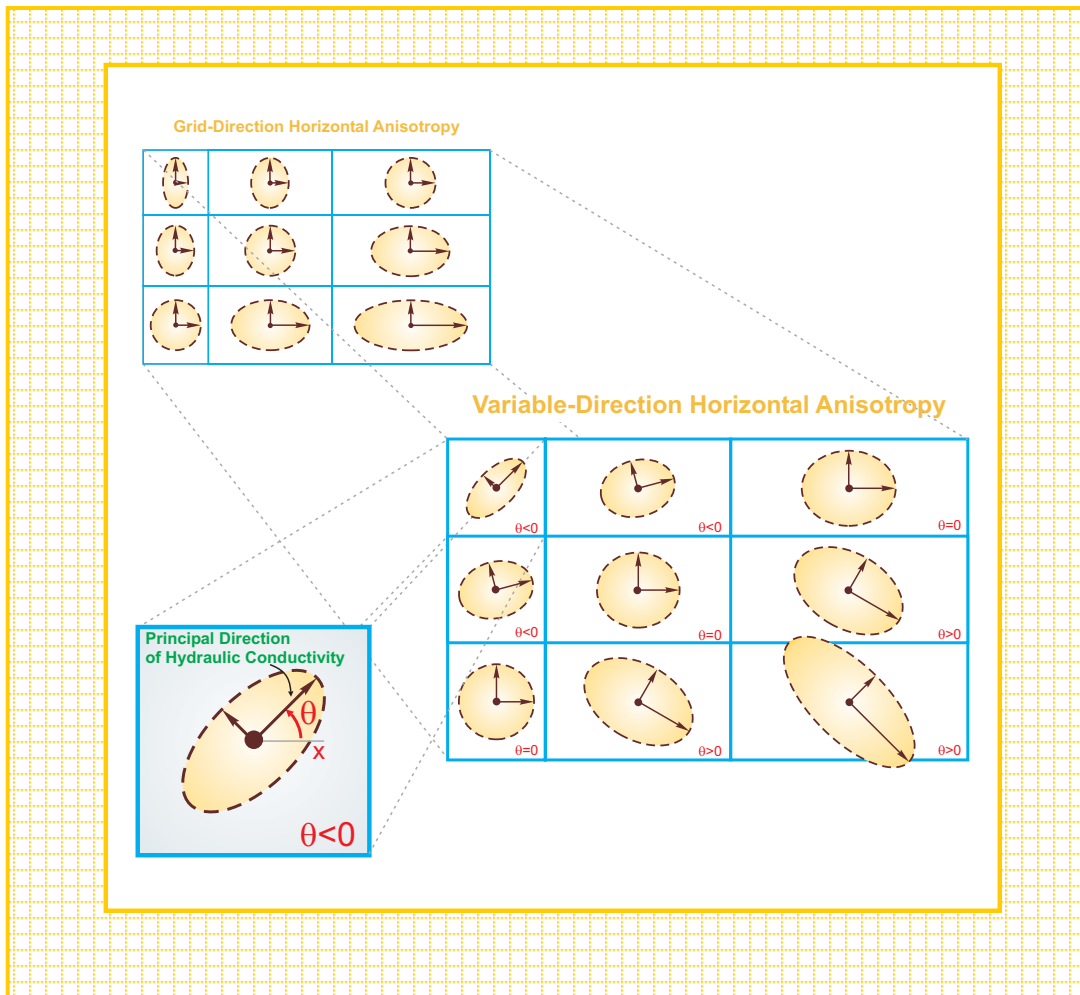




Prepared in cooperation with the
U.S. Department of Energy

MODFLOW-2000, THE U.S. GEOLOGICAL SURVEY MODULAR GROUND-WATER MODEL — DOCUMENTATION OF THE MODEL- LAYER VARIABLE-DIRECTION HORIZONTAL ANISOTROPY (LVDA) CAPABILITY OF THE HYDROGEOLOGIC-UNIT FLOW (HUF) PACKAGE

Open-File Report 02-409



U.S. Department of the Interior
U.S. Geological Survey

**MODFLOW-2000, THE U.S. GEOLOGICAL SURVEY
MODULAR GROUND-WATER MODEL —
DOCUMENTATION OF THE MODEL-LAYER VARIABLE-
DIRECTION HORIZONTAL ANISOTROPY (LVDA)
CAPABILITY OF THE HYDROGEOLOGIC-UNIT FLOW
(HUF) PACKAGE**

By Evan R. Anderman¹, Kenneth L. Kipp², Mary C. Hill³, Johan Valstar⁴, and Roseanna M. Neupauer⁵

**U.S. Geological Survey
Open-File Report 02-409**

**Prepared in cooperation with the
U.S. Department of Energy**

**DENVER, COLORADO
2002**

¹ Calibra Consulting LLC, Denver, CO, USA

² U.S. Geological Survey, Denver, CO, USA

³ U.S. Geological Survey, Boulder, CO, USA

⁴ Netherlands Institute of Applied Geophysics TNO – National Geological Survey, Utrecht, the Netherlands

⁵ University of Virginia, Charlottesville, VA, USA

U.S. DEPARTMENT OF THE INTERIOR
Gale A. Norton, *Secretary*
U.S. GEOLOGICAL SURVEY
Charles G. Groat, *Director*

The use of trade, product, industry, or firm names is for descriptive purposes only and does not imply endorsement by the U.S. Government.

For additional information write to:

Regional Research Hydrologist
U.S. Geological Survey
Box 25046, Mail Stop 413
Denver Federal Center
Denver, CO 80225-0046

Copies of this report can be
purchased from:

U.S. Geological Survey
Branch of Information Services
Box 25286
Denver, CO 80225-0425

PREFACE

The Model-Layer Variable-Direction Horizontal Anisotropy (LVDA) computer software described in this report is a new capability of the Hydrogeologic-Unit Flow (HUF) Package for MODFLOW-2000, the U.S. Geological Survey's three-dimensional ground-water flow parameter-estimation model. The software is designed to allow the primary axes of horizontal anisotropy to be oriented in directions other than along grid axes. The documentation presented here describes the methods used, the required new input file, the changes in how two parameter types in the HUF Package are used, and the output related to the new LDVA capability.

All code developed by the U.S. Geological Survey for MODFLOW-2000 is available for downloading over the Internet from a U.S. Geological Survey software repository. The repository is accessible on the World Wide Web from the U.S. Geological Survey Water Resources Information web page at URL

http://water.usgs.gov/software/ground_water.html

under the label 'MODFLOW-2000'.

The performance of the LVDA capability of the HUF Package has been tested in a variety of applications. Future applications, however, might reveal errors that were not detected in the test simulations. Users are requested to notify the U.S. Geological Survey of any errors found in this document or the computer program using the email address available on the website mentioned above. Updates might occasionally be made to both this document and to the LVDA capability of the HUF Package, and users are encouraged to check the website periodically.

CONTENTS

Preface	iii
Abstract	1
Introduction	2
Purpose and Scope.....	2
Methods	3
Issues for Users	4
Defining Variable-Direction Horizontal Anisotropy Using Model Layers.....	4
Defining Anisotropy Direction.....	4
Possible Solver Convergence Difficulties.....	4
Issue for Programmers: Coordinate system.....	4
Historical Perspective.....	5
Acknowledgments	5
Importance of Anisotropy Direction and Introduction of Some Basic Concepts.....	6
Conceptualization and Implementation of Model-Layer Variable-Direction Horizontal Anisotropy	10
Approach	10
Definition of Horizontal Anisotropy	12
Modifying the Equations for Traditional Solvers.....	12
Errors Caused by Model Layers that are Not Horizontal	13
Sensitivities.....	14
Simulation Examples.....	15
Tests of Hydraulic Heads and Cell-By-Cell Flows Simulated Using the LVDA Capability	15
Test of Hydraulic Head Using an Analytical Solution.....	15
Test of Hydraulic Heads Using a Numerical Solution	16
Test of Cell-By-Cell Flows Using an Analytical Solution.....	17
Illustration and Test of Sensitivities Calculated Using the LVDA Capability	18
References Cited.....	24
Appendix A: LVDA Input and Output.....	26
LVDA Input Instructions.....	26
Explanation of Variables Read by the LVDA Capability	26
Example LVDA Input File	27
LVDA Output.....	27
New Definition of Two Parameter Types of the HUF Package Input File.....	28
Execution Time Issues.....	28
Reference Cited	29
Appendix B: Mathematical Derivation for Simulating Variable-Direction Horizontal Anisotropy Using Block-Centered Finite Differences	30
Ground-Water Flow Equation	30
The Block-Centered Finite-Difference Grid and the Continuity Equation	31

Computational Coordinates	32
Finite-Difference Equations for Flow.....	34
Flow Equations in One Dimension	35
Flow Equations in Two Dimensions	36
Flow Continuity for the General Anisotropic Tensor.....	39
Flow Terms in the Finite-Difference Equation.....	43
Obtaining the Final Coefficients.....	49
Final Matrix Equation.....	50
Diagonal Dominance.....	51
Operator Splitting.....	51
Splitting at the Matrix Level	52
Splitting at the Flow Level	52
The Split Flow Components.....	52
Solving the Finite-Difference Equations	54
Semi-Implicit without Iteration	54
Semi-Implicit with Iteration	54
Stability	54
References Cited.....	55
Appendix C: Sensitivities.....	56
The f^9 Term.....	56
The f^5 Term.....	58
The Final Term.....	60
APPENDIX D: Calculation of Horizontal Cell-Face Velocities and Sensitivities.....	61
Horizontal Cell-Face Velocities	61
Horizontal Cell-Face Velocity Sensitivity.....	61

FIGURES

Figure 1. Nine cells from a MODFLOW model layer showing (A) grid-direction horizontal anisotropy defined for each grid cell, (B) variable-direction horizontal anisotropy defined for each grid cell, and (C) definition of the angle, θ , required to define variable-direction horizontal anisotropy. The angle is defined clockwise from the positive x direction, and can be assigned values between -90 and 90 degrees, inclusive, in the LVDA capability.	3
Figure 2: Typical actual and approximate representations of horizontal anisotropy for which (A) errors in flow directions and magnitudes are considered and (B) the analysis of errors would be equivalent if θ were measured from the y-axis instead of the x-axis. The angle θ is measured from the positive x-axis direction and clockwise angles are positive.	7
Figure 3. Error in flow magnitude as a function of horizontal anisotropy ratio (HANI) and angle relative to the hydraulic gradient direction.	9
Figure 4. Error in flow direction as a function of horizontal anisotropy ratio (HANI) and angle relative to the hydraulic gradient direction.	9

Figure 5: The flows calculated through the boundaries of each cell using the formulation presented in this report, shown for cell 1. Two flows are calculated for each grid-cell boundary instead of the single value described by McDonald and Harbaugh (1988, p. 5-3) 11

Figure 6. (A) Representation of the hydraulic-conductivity ellipse for the steady-state analytical solution. HANI is the horizontal anisotropy ratio. (B) Hydraulic-head solution using the LVDA capability in MODFLOW-2000. The LVDA capability nearly reproduces the analytical hydraulic-head distribution, for which the contours should be parallel and vertical. The slight angle of the head contours is caused by the approximate way that the LVDA capability accounts for specified-flow boundaries. (C) Hydraulic-head solution without the LVDA capability with the same boundary conditions as in (B) and isotropic hydraulic conductivity. This is the solution that is produced using previously existing capabilities of MODFLOW. 16

Figure 7. Hydraulic heads simulated in two ways that theoretically produce identical results rotated by 45 degrees. In both situations, the hydraulic head at the circular boundary 1000 m from the pumping well is 10 m. (A) Horizontal anisotropy is parallel to the grid directions simulated using MODFLOW without the LVDA capability. (B) Horizontal anisotropy at a 45 degree angle to the grid simulated using MODFLOW with the LVDA capability..... 17

Figure 8. Advective-transport paths simulated using the LDVA capability for the problem presented in figure 6. The paths are superimposed on the hydraulic-head solution from figure 6B. 18

Figure 9. Model grid, boundary conditions, observation locations, and hydraulic-conductivity zones for complex example used to test the calculation of sensitivities. (Modified from Hill and others, 2000.)..... 19

Figure 10. (A) Representation of the hydraulic-conductivity ellipse for zone 4; ANIV is the horizontal anisotropy ratio. (B) Hydraulic-head distribution with anisotropy in zone 4 defined parallel to the grid directions (black lines) and with anisotropy in zone 4 defined 45 degrees from the grid directions (red lines). (C) Change in hydraulic head produced by rotating the direction of horizontal anisotropy in zone 4 (outlined by thick black line) from 0 to 45 degrees..... 22

Figure 11. Composite scaled sensitivities at the true values for parameters listed in table 1. Sensitivities for the LVDA parameters shown with cross hatching. The composite scaled sensitivity for LVDA123 is zero because the related horizontal anisotropy ratio equals 1.0. . 23

Figure A- 1. Execution times for MODFLOW-2000 models run using the HUF Package without the LDVA capability and with the LVDA capability using angles of horizontal anisotropy of 0 and 45 degrees. The solutions without LDVA and with LDVA using an angle of 0 degrees are identical and execution times differ because of the extra effort required by the LDVA capability. Execution times are reported in seconds and relative to the execution time without the LDVA capability. The three-dimensional example is thought to be more representative of typical applications..... 29

Figure B-1. Two-dimensional cell-centered grid in x-y plane. The row indexing convention is the same as that used in MODFLOW, when observed from below, with j used to index the x axis and i used to index the y axis. 31

Figure B-2. A two-dimensional cell in the x-y plane mapped into a unit square cell in the ξ - η plane. For convenient referencing in the text, the four sides of the unit square are labeled N (north), S (south), E (east), and W (west). Δc_i is the cell dimension along the y axis, which is parallel to the columns of the grid; Δr_j is the cell dimension along the x axis, which is parallel to the rows of the grid. 33

Figure B-3. One-dimensional cells with piecewise linear hydraulic-head variation. 35

Figure B-4. Piecewise-linear basis functions. Global finite-difference nodes j and $j+1$ are shown with f , the location of the finite-difference cell boundary. Local coordinates which range from 0 to 1 for each cell also are shown 36

Figure B-5. Unit-square grid with areas covered by piecewise linear triangular basis functions shaded gray..... 38

Figure B-6. Areas covered by the triangular basis functions associated with the $j+\frac{1}{2}$ and $i+\frac{1}{2}$ faces of cell 1. For convenient referencing in the text, the four added nodes on the sides of the finite-difference cells are labeled N (north), S (south), E (east), and W (west). The I at the top of the figure identifies this set of four cells as cell 1 of figure B-5 plus bordering cells 2, 3, and 4..... 38

Figure B-7. Control volume quadrant flows..... 39

Figure B-8. Four subsets of the nine-cell grid associated with cell 1. Locations of additional hydraulic heads are marked by \times 's. Subset I was also shown in figure B-6 40

Figure B-9. Finite-difference grid showing local numbering and global indices used for the derivation of variable-direction horizontal anisotropy..... 50

TABLES

Table 1. Labels, descriptions and true and starting values for the parameters for the complex example 20

Table 2. Coordinate system notation used in this report 39

CONVERSION FACTORS AND ABBREVIATIONS

Divide	By	To Obtain
millimeters (mm)	0.03937	inch
meter (m)	3.28	foot
meter per day (m/d)	3.28	foot per day
square meter per day (m ² /d)	10.78	square foot per day
cubic meter per day (m ³ /d)	35.314	gallons per day
kilometer (km)	0.62	mile

Other abbreviations used in this report:

Length (L)

Time(T)

**MODFLOW-2000,
THE U.S. GEOLOGICAL SURVEY MODULAR GROUND-
WATER MODEL —

DOCUMENTATION OF THE MODEL-LAYER VARIABLE-
DIRECTION HORIZONTAL ANISOTROPY (LVDA)
CAPABILITY OF THE HYDROGEOLOGIC-UNIT FLOW
(HUF) PACKAGE**

By Evan R. Anderman, Kenneth L. Kipp, Mary C. Hill, Johan Valstar, and
Roseanna M. Neupauer

ABSTRACT

This report documents the model-layer variable-direction horizontal anisotropy (LVDA) capability of the Hydrogeologic-Unit Flow (HUF) Package of MODFLOW-2000. The LVDA capability allows the principal directions of horizontal anisotropy to be different than the model-grid row and column directions, and for the directions to vary on a cell-by-cell basis within model layers. The HUF Package calculates effective hydraulic properties for model grid cells based on hydraulic properties of hydrogeologic units with thicknesses defined independently of the model layers. These hydraulic properties include, among other characteristics, hydraulic conductivity and a horizontal anisotropy ratio. Using the LVDA capability, horizontal anisotropy direction is defined for model grid cells within which one or more hydrogeologic units may occur. For each grid cell, the HUF Package calculates the effective horizontal hydraulic conductivity along the primary direction of anisotropy using the hydrogeologic-unit hydraulic conductivities, and calculates the effective horizontal hydraulic conductivity along the orthogonal anisotropy direction using the effective primary direction hydraulic conductivities and horizontal anisotropy ratios. The direction assigned to the model layer effective primary hydraulic conductivity is specified using a new data set defined by the LVDA capability, when active, to calculate coefficients needed to solve the ground-water flow equation. Use of the LVDA capability is illustrated in four simulation examples, which also serve to verify hydraulic heads, advective-travel paths, and sensitivities calculated using the LVDA capability.

This version of the LVDA capability defines variable-direction horizontal anisotropy using model layers, not the hydrogeologic units defined by the HUF Package. This difference needs to be taken into account when designing model layers and hydrogeologic units to produce simulations that accurately represent a given field problem. This might be a reason, for example, to make model layer boundaries coincide with hydrogeologic-unit boundaries in all or part of a model grid.

INTRODUCTION

In models of ground-water systems, depositional, structural, and other conditions can result in hydraulic conductivity being different depending on the direction considered. This is called hydraulic-conductivity anisotropy. Correct representation of hydraulic-conductivity anisotropy is important for the accurate solution of hydraulic heads, flows, and transport, as demonstrated by Henry and others (1998). MODFLOW-2000 (Harbaugh and others, 2000) with either the Layer-Property Flow (LPF) Package (Harbaugh and others, 2000, p. 22) or the Hydrogeologic-Unit Flow (HUF) Package (Anderman and Hill, 2000) have been limited to grid-direction anisotropy (fig. 1A). That is, the simulated directions of anisotropy have been limited to being oriented along the grid axes. MODFLOW-2000 is more flexible than previous USGS-produced versions of MODFLOW in that it allows grid-direction horizontal anisotropy to vary within a layer by specifying different values of the horizontal grid-direction anisotropy ratio for each model grid cell (fig. 1A), but the limitation to grid directions remained. To address this limitation, the U.S. Geological Survey, in cooperation with the U.S. Department of Energy, developed the model layer variable direction horizontal anisotropy (LVDA) capability to make fully variable-direction horizontal anisotropy within model layers available in MODFLOW-2000's HUF Package.

Flexibility in the definition of horizontal anisotropy, such as that shown in figure 1B, is necessary because of the following. (1) In modeling natural systems, grid axes can not always be oriented parallel to major anisotropy directions. For example, major fracture groups in different parts of a single flow system may be oriented at angles other than 90 degrees. (2) Considerations other than horizontal anisotropy, for example, boundary shape, often are important in grid orientation, and flexibility for defining horizontal-anisotropy direction allows those other considerations to be better addressed. (3) Significant errors in the magnitude and direction of flow can result from inaccurately defined anisotropy direction, and this error can be quantified using the Ground-Water Flow and Sensitivity Processes of the new LVDA capability. As shown in this work, using the LDVA capability to simulate horizontal anisotropy that is not parallel to grid directions results in increased execution times, and this will need to be considered when designing a model grid.

Purpose and Scope

The purpose of this report is to document the conceptualization and implementation of the LVDA capability of the HUF Package. After reviewing selected aspects of the methodology that are important to users and programmers, some basic concepts are presented and errors that can be produced by incorrectly specifying the direction of anisotropy are investigated with an analytical solution. Next, the equations used to calculate heads and sensitivities in the new capability are derived; main points are presented in the text and details are presented in Appendices B and C. Then, the hydraulic heads simulated with the new capability are tested using an analytical solution and a numerical solution, and calculated sensitivities are tested using a heterogeneous three-dimensional test case. Appendix A describes the new input file required to use variable-direction horizontal anisotropy.

Methods

This section briefly discusses several aspects of the methods used in this work that are important to users and programmers using the LVDA capability. The issues important to users include: (1) variable-direction horizontal anisotropy is defined by model layer rather than hydrogeologic unit, (2) definition of the anisotropy direction, and (3) possible solver convergence difficulties. An issue important to programmers is the perspective of the MODFLOW coordinate system used in this work to develop the relevant equations and its relation to the model grid. Finally, the present work is put into perspective relative to selected existing models capable of representing variable-direction horizontal anisotropy.

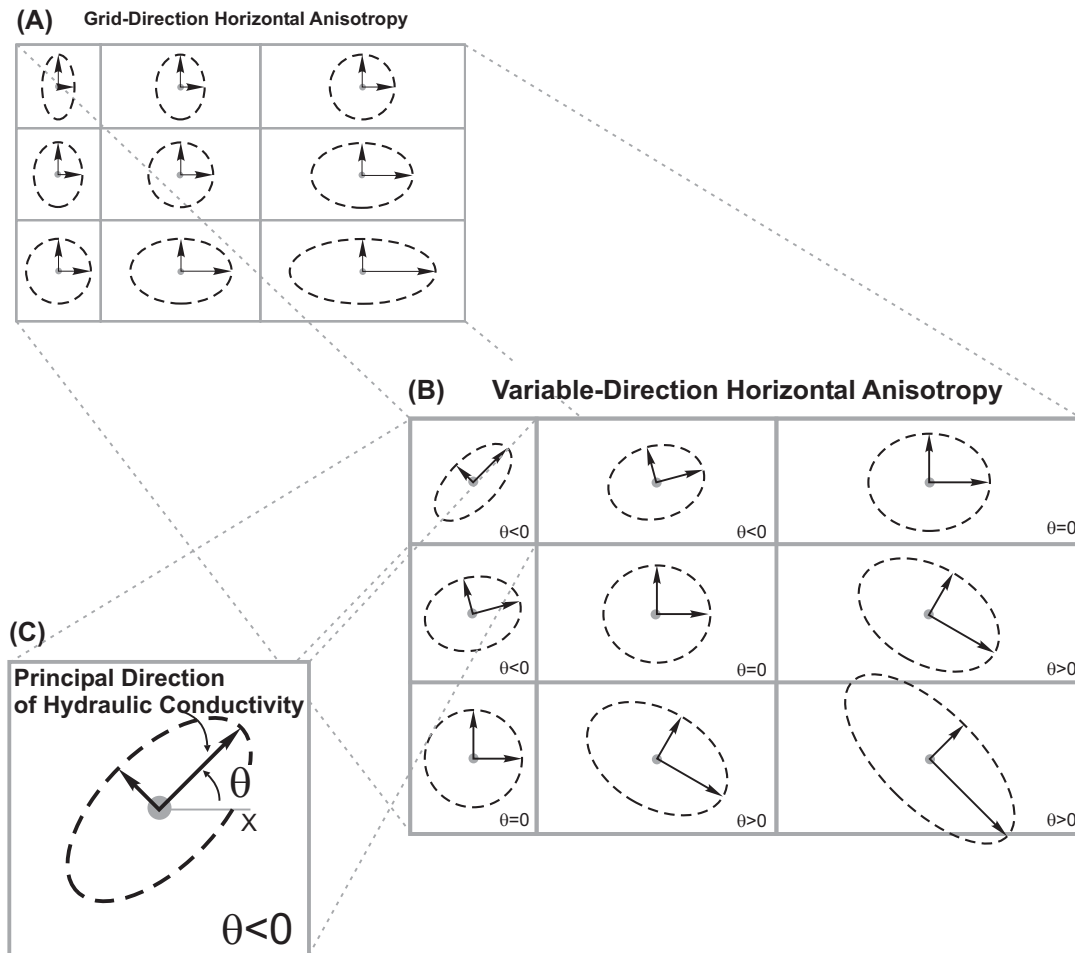


Figure 1. Nine cells from a MODFLOW model layer showing (A) grid-direction horizontal anisotropy defined for each grid cell, (B) variable-direction horizontal anisotropy defined for each grid cell, and (C) definition of the angle, θ , required to define variable-direction horizontal anisotropy. The angle is defined clockwise from the positive x direction, and can be assigned values between -90 and 90 degrees, inclusive, in the LVDA capability.

Issues for Users

Three issues that are likely to be of concern to users include defining variable direction horizontal anisotropy using model layers, defining the anisotropy direction, and possible solver difficulties.

Defining Variable-Direction Horizontal Anisotropy Using Model Layers

This version of the LVDA capability defines variable-direction horizontal anisotropy using model layers, not the hydrogeologic units defined by the HUF Package. This can affect how model layers and hydrogeologic units are best designed for given applications. For example, in areas where fracturing is thought to produce horizontal anisotropy principally in one hydrogeologic unit, more accurate simulations may be attained by making model layer boundaries coincide with the top and bottom of that hydrogeologic unit.

Defining Anisotropy Direction

For each model grid cell, the direction of horizontal anisotropy is defined using an angle from the direction of model rows. Angle values can range from +90 to -90 degrees. The angle is measured clockwise from the model-row direction, as shown in figures 1B and 1C. Parameter estimation may result in angles that are outside this range; if so, the value is converted to a number within this range. For parameters used to define the anisotropy angle, the scaling for dimensionless scaled sensitivities does not include multiplication by the parameter value.

Possible Solver Convergence Difficulties

Allowing the primary axes of horizontal hydraulic conductivity to vary within a model requires additional terms to be represented in the hydraulic-conductivity tensor (see equation B-2a and 2b in Appendix B). When horizontal anisotropy is aligned with the grid direction, only diagonal terms occur in the hydraulic-conductivity tensor; when the direction of horizontal anisotropy is not aligned with the grid, off-diagonal terms are required. This change results in more off-diagonal elements being added to the matrix difference equation for ground-water flow, which then no longer matches the difference stencil of solvers available in MODFLOW. A matrix with the standard stencil is shown in McDonald and Harbaugh (1988, p. 12-3). In this work, matrix splitting was employed to maintain the utility of popular solvers for MODFLOW. While all tests conducted thus far indicate the matrix splitting works well, good solver performance can not be guaranteed through mathematical proof, as discussed in Appendix B. Users therefore need to check for signs of solver failure. Solver failure generally is accompanied by lack of solver convergence or large global budget errors.

Issue for Programmers: Coordinate system

McDonald and Harbaugh (1988, p. 2-4) define a right-hand coordinate system for MODFLOW that has the advantage of being coordinated with a grid numbering system that is easy for users to understand. Grid row numbers increase from back to front and are indexed by i , column numbers increase from left to right and are indexed by j , and layer numbers increase from top to bottom and are indexed by k . The y axis points along columns toward increasing row numbers, the x axis points along rows toward increasing column numbers, and the z axis points downward.

The difficulty with this user-oriented MODFLOW coordinate system is that j indexes the x axis instead of the more common i ; i indexes the y axis instead of the more common j , and the z

axis points down instead of up. In this report, the MODFLOW convention of j denoting cell indexing along the x axis and i denoting cell indexing along the y axis is followed. However, for the two-dimensional (x - y) coordinate grid system needed for this work, graphs with the normal orientation of the x -axis pointing to the right and the y axis pointing up are shown. This corresponds to looking at a MODFLOW x - y nodal plane from a higher value along the z axis than the location of the plane. In the MODFLOW coordinate system, this means looking up at an x - y plane from below in the three-dimensional grid.

Historical Perspective

Historically, variable-direction anisotropy has been available only in finite-element models. For example, considering only three-dimensional finite-element models, FEMWATER (Lin and others, 2001), the newest version of SUTRA (Voss and Provost, 2002), and FEHM (Dash and others, 2002) allow mutually orthogonal anisotropy directions to be in any orientation, WATFLOW/WTC (Molson and Frind, 2002a) and FLOWNET/TRANS (Molson and Frind, 2002b) allow mutually orthogonal anisotropy directions, but one direction is required to be vertical, and PTC (Pinder, 2002) specifies the allowable coordinate directions for anisotropy. The capabilities of FEMWATER, SUTRA, and FEHM exceed those of MODFLOW-2000 with HUF and its LVDA capability because LVDA is limited to variable direction anisotropy only within model layers.

A method for developing equations for flow under general anisotropy in two dimensions has been presented by Edwards and Rogers (1998) for a block-centered finite-difference grid as used in MODFLOW. The Edwards and Rogers (1998) method was implemented for work discussed in this report, but only for orthogonal horizontal coordinates of a three-dimensional region. Thus, applicability is restricted to variable direction horizontal, orthogonal anisotropy for the hydraulic-conductivity tensor.

Acknowledgments

The authors acknowledge Frank D'Agnesse of the U.S. Geological Survey for his vision, encouragement, and support of this capability. Additionally, the authors acknowledge Ned Banta and Alden Provost for their critically thorough reviews that greatly improved the document.

IMPORTANCE OF ANISOTROPY DIRECTION AND INTRODUCTION OF SOME BASIC CONCEPTS

A simple analytical example developed by John L. Wilson (New Mexico Institute for Mining and Technology, written commun., 1999) is used to introduce some basic concepts such as the relation between the primary axes of horizontal anisotropy and the grid coordinate axes, and to illustrate the error in the magnitude and direction of the specific discharge vector when the primary axes of horizontal anisotropy are not aligned with the grid coordinate axes.

To relate the errors illustrated by the simple analytical example to MODFLOW, consider that previous MODFLOW capabilities allowed primary axes of horizontal anisotropy to be defined parallel to the grid directions only – that is, parallel to the x and y grid directions. Hydraulic-conductivity values were specified along rows (in the x direction) and multiplied by horizontal anisotropy to obtain hydraulic conductivity along columns (in the y direction).

To evaluate the error in the magnitude and direction of the simulated flow that occurs when the actual primary directions of horizontal anisotropy are not the grid directions, consider the problem shown in figure 2. K_{\max} and K_{\min} define the principal directions and magnitudes of the hydraulic conductivity field. The direction of K_{\max} is defined by θ , the angle between the x-coordinate direction and the K_{\max} direction, measured clockwise from the x axis. In this work, the direction of K_{\min} is always perpendicular to K_{\max} in the horizontal plane. The magnitude of K_{\max} is larger than or equal to that of K_{\min} ; the ratio of the magnitudes, K_{\min}/K_{\max} , is termed HANI in this report because that is the variable name used in MODFLOW-2000.

The relations between K_{xx} and K_{yy} , and K_{\max} , K_{\min} and θ , are as follows:

$$K_{xx} = \frac{K_{\max} + K_{\min}}{2} + \frac{K_{\max} - K_{\min}}{2} \cos(2\theta) \quad (1a)$$

$$K_{yy} = \frac{K_{\max} + K_{\min}}{2} - \frac{K_{\max} - K_{\min}}{2} \cos(2\theta) \quad (1b)$$

Previous versions of MODFLOW have not included the additional term, K_{xy} , calculated as:

$$K_{xy} = K_{yx} = \frac{K_{\max} - K_{\min}}{2} \sin(2\theta) \quad (1c)$$

In this evaluation, only errors in anisotropy direction that are less than or equal to 45 degrees need to be considered so that $K_{xx} \geq K_{yy}$. If the direction error exceeds 45 degrees, previous capabilities of MODFLOW would have allowed the anisotropy factor to be greater than 1.0, so that the higher hydraulic conductivity value could have been assigned to the y axis instead of the x axis. This relationship is shown in figure 2.

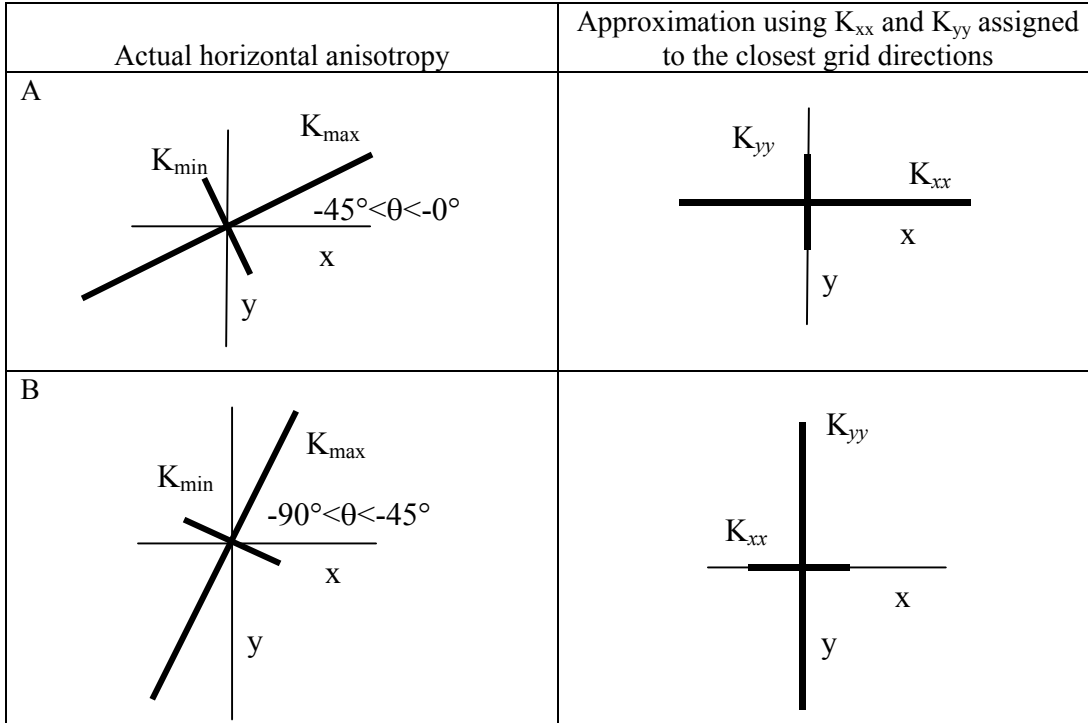


Figure 2: Typical actual and approximate representations of horizontal anisotropy for which (A) errors in flow directions and magnitudes are considered and (B) the analysis of errors would be equivalent if θ were measured from the y-axis instead of the x-axis. The angle θ is measured from the positive x-axis direction and clockwise angles are positive.

To evaluate the error in the magnitude and direction of the simulated flow that occurs when the actual primary directions of horizontal anisotropy are not the grid directions, consider the analytical equivalent of a MODFLOW simulation of a homogeneous ground-water system with a hydraulic gradient imposed parallel to the rows of the finite-difference grid. The direction of the hydraulic gradient is thus x direction, and the perpendicular horizontal direction along columns is the y direction. In this homogeneous problem, the same hydraulic-conductivity value, K_{xx} , is specified everywhere in the system in the x direction, and a different value, K_{yy} , is specified everywhere in the system in the y direction.

For a two-dimensional domain with the hydraulic gradient in the x direction only, the Darcy velocity vector, q (L/T), is

$$q = -K_{xx} \frac{\partial h}{\partial x} n_x - K_{xy} \frac{\partial h}{\partial x} n_y, \quad (2)$$

where,

K_{xx} and K_{xy} are components of the porous-medium hydraulic conductivity tensor [L/T];

h is the fluid hydraulic head [L]; and

n_x and n_y are unit vectors in the x - and y -directions, respectively, where n_x points in the x direction along rows, and n_y points in the y direction along columns.

The first term on the right-hand side of equation 2 is the flow parallel to the gradient direction and normal to the finite-difference cell faces crossed in this direction; it is often called

the normal flow. The second term is the flow perpendicular to the gradient direction and is often called the flow tangential to the face. The magnitude of the Darcy velocity, therefore, can depend significantly on K_{xy} , as can its direction.

If the primary axes of horizontal anisotropy are incorrectly assumed to be aligned with the coordinate axes, then K_{xy} is assumed to equal 0, and the approximation, \hat{q} , to the Darcy velocity vector is

$$\hat{q} = -K_{xx} \frac{\partial h}{\partial x} n_x \quad (3)$$

The importance of correctly accounting for anisotropy can be illustrated by evaluating the error in the magnitude and direction of the approximation \hat{q} relative to true specific discharge q .

The error in magnitude, ε_m , is defined as:

$$\varepsilon_m = \frac{|\hat{q}| - |q|}{|q|} = \frac{\sqrt{\left(-K_{xx} \frac{\partial h}{\partial x}\right)^2} - \sqrt{\left(-K_{xx} \frac{\partial h}{\partial x}\right)^2 + \left(-K_{xy} \frac{\partial h}{\partial x}\right)^2}}{\sqrt{\left(-K_{xx} \frac{\partial h}{\partial x}\right)^2 + \left(-K_{xy} \frac{\partial h}{\partial x}\right)^2}} = \frac{1 - \sqrt{1 + \left(\frac{K_{xy}}{K_{xx}}\right)^2}}{\sqrt{1 + \left(\frac{K_{xy}}{K_{xx}}\right)^2}}, \quad (4)$$

and represents the fractional error in the approximated \hat{q} . The percent error is obtained by multiplying by 100.

The error in direction, ε_d , is defined as the difference in angle between the true specific discharge and the approximation. The angle of the true specific discharge would be between the angle of the hydraulic gradient and the angle of the horizontal anisotropy (θ), and can be calculated as

$$\tan^{-1} \left(\frac{-K_{xy} \frac{\partial h}{\partial x}}{-K_{xx} \frac{\partial h}{\partial x}} \right) = \tan^{-1} \left(\frac{K_{xy}}{K_{xx}} \right). \quad (5a)$$

In the approximation, flow is along the x-axis so the angle of the approximation equals zero. Thus the error in direction, ε_d , equals:

$$\varepsilon_d = \tan^{-1} \left(\frac{K_{xy}}{K_{xx}} \right). \quad (5b)$$

These error measures, ε_m and ε_d , are plotted in figures 3 and 4, respectively, for several different anisotropy ratios and different directions (as represented by the angle θ) of horizontal anisotropy. The anisotropy ratio is defined as HANI = K_{\min}/K_{\max} . Values as small as 0.01 are considered; errors for smaller values were very similar to those for 0.01. As discussed previously, the maximum angle of deviation between the coordinate axes and principal directions of horizontal anisotropy that needs to be considered is 45 degrees, so the results in figures 3 and 4 are shown for $-45 \leq \theta \leq 45$ degrees.

For HANI=1 (isotropic) or $\theta = 0$, there are no errors in either the flow magnitude or the flow direction (figs. 3 and 4). As HANI decreases toward zero and the absolute value of θ

increases, the approximate flow magnitude becomes progressively smaller than the true flow magnitude (fig. 3), as simulated values differ from true values by as much as about 29 percent. In conjunction, the approximate flow direction, which is always parallel to the x direction, deviates from the true flow direction, which always tends towards the K_{\max} direction and is nearly parallel to the K_{\max} direction when $HANI=0.01$ (fig. 4). The errors are most severe for small HANI and for θ substantially different from zero.

This analysis does not consider the substantial error that can occur because anisotropy direction can be difficult to determine from field data. That error is not, of course, caused by limitations of any numerical solution, which is the subject of the present analysis. The LVDA capability does, however, provide the ability to quantify the effects of uncertainty in the horizontal anisotropy direction and ratio.

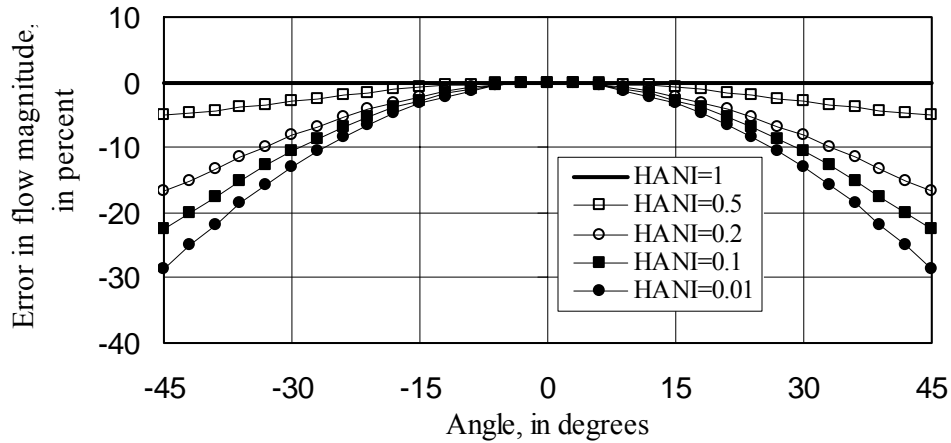


Figure 3. Error in flow magnitude as a function of horizontal anisotropy ratio (HANI) and angle relative to the hydraulic gradient direction.

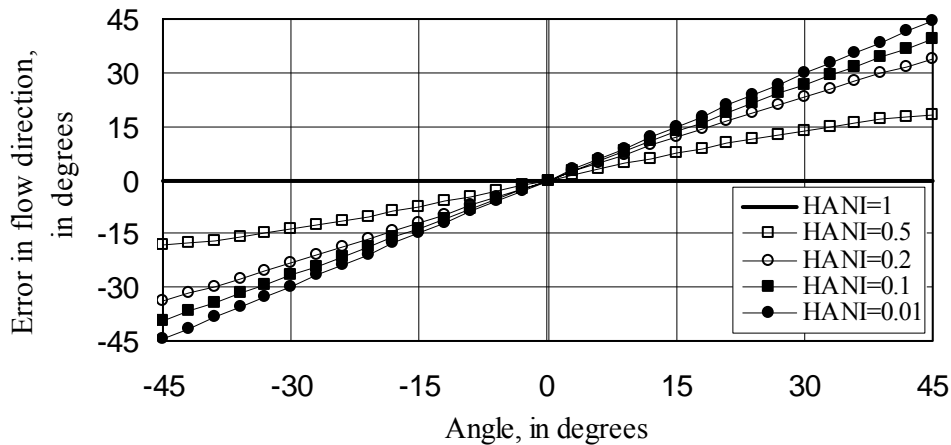


Figure 4. Error in flow direction as a function of horizontal anisotropy ratio (HANI) and angle relative to the hydraulic gradient direction.

CONCEPTUALIZATION AND IMPLEMENTATION OF MODEL-LAYER VARIABLE-DIRECTION HORIZONTAL ANISOTROPY

This section of the report briefly describes the LVDA capability and highlights aspects important to most users; a full derivation of the equations is presented in Appendix B. The development presented here is strongly based on the work of Edwards and Rogers (1998).

Approach

To develop a block-centered finite-difference approximation to the ground-water flow equation for the case of flow in a horizontally anisotropic, heterogeneous porous medium, the directions of the principal axes of hydraulic conductivity for each grid cell need to be defined. For variable-direction horizontal anisotropy, one of the principal axes of the hydraulic-conductivity tensor is aligned with the vertical z -coordinate axis, while the other two axes are free to point in any mutually orthogonal directions in the horizontal plane. The equations are developed using the two-dimensional form of the flow equation in the x - y plane, but the terms derived apply unchanged to a three-dimensional equation in which the z axis is perpendicular to the x - y plane.

The derivation of the equations begins by imposing the following assumptions and requirements.

- (1) Hydraulic conductivity is constant within each finite-difference cell but may differ from cell to cell. Thus, like the Hydrogeologic-Unit Flow (HUF) Package, the LVDA derivation is limited to harmonic averaging to obtain the conductance terms used to link cells within model layers. Other averaging options are available in the Layer Property Flow (LPF) Package documented by Harbaugh and others (2000, p. 22), but the LPF Package does not currently support the LVDA capability.
- (2) Mass needs to be conserved even when the media are highly heterogeneous. Conservation of mass is accomplished by imposing the same requirements that MODFLOW with harmonic averaging has always satisfied: that normal flow and the hydraulic head be continuous across cell boundaries, although the head gradient generally is discontinuous at cell boundaries.

As discussed in the previous section and shown in equation 2, the K_{xy} terms needed to account for variable-direction horizontal anisotropy produce tangential Darcy velocity terms that can be substantial. When the hydraulic gradient has $\frac{\partial h}{\partial x}$ and $\frac{\partial h}{\partial y}$ terms, the situation is more complicated and the generalization of equation 2 is

$$q = -K_{xx} \frac{\partial h}{\partial x} n_x - K_{xy} \frac{\partial h}{\partial y} n_x - K_{yx} \frac{\partial h}{\partial x} n_y - K_{yy} \frac{\partial h}{\partial y} n_y \quad (6)$$

The total Darcy velocity, q , can be divided into the Darcy velocity in the x and y directions as:

$$q_x = -K_{xx} \frac{\partial h}{\partial x} n_x - K_{xy} \frac{\partial h}{\partial y} n_x \quad (7a)$$

$$q_y = -K_{yy} \frac{\partial h}{\partial y} n_y - K_{xy} \frac{\partial h}{\partial x} n_y \quad (7b)$$

Equations 7a and 7b apply at a point on a cell face. Considering a cell face perpendicular to the x direction, q_x defines a normal Darcy velocity through the cell face and q_y defines a tangential Darcy velocity parallel to the cell face. Within the normal Darcy velocity, q_x , the first term on the right-hand side of equation 7a is the normal gradient component, and the second term is the tangential gradient component of this normal Darcy velocity. For a cell face perpendicular to the y direction, q_y defines a normal Darcy velocity through the cell face and q_x defines a tangential Darcy velocity parallel to the cell face. Within the normal Darcy velocity, q_y , the first term on the right-hand side of equation 7b is the normal gradient component, and the second term is the tangential gradient component of this normal Darcy velocity.

Across a cell face, the normal Darcy velocity is continuous, but the tangential Darcy velocity may be discontinuous because neighboring cells may have different hydraulic properties, including anisotropy direction. To approximate the effects of tangential Darcy velocities while conserving mass, the normal Darcy velocity is allowed to change in a piecewise fashion along each of the four cell boundaries, as illustrated in figure 5. This is accomplished by introducing one additional unknown hydraulic head at the center of each of the four cell faces. The eight flows for each cell, shown by the arrows in figure 5, are expressed in terms of only the node hydraulic heads by eliminating the hydraulic heads at the cell faces. The equation for any given flow takes the form of the sum of the products of a coefficient times one of the four nearby heads, where the coefficients are a function of the transmissivities of the four nearby cells.

The LVDA capability needs to produce cell-by-cell flow terms for calculating advective-transport paths and other types of transport and for other programs such as ZONEBUDGET (Harbaugh, 1990). This is accomplished by summing the two velocities through each cell side.

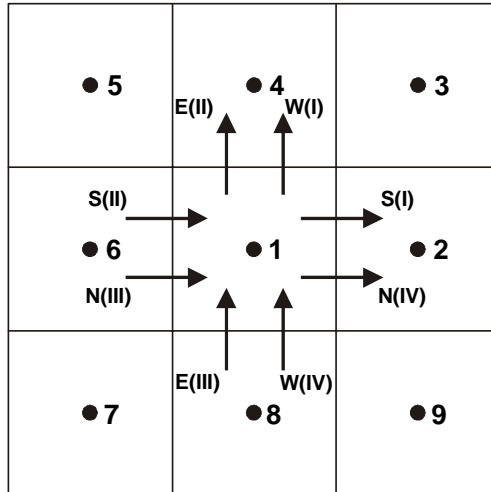


Figure 5: The flows calculated through the boundaries of each cell using the formulation presented in this report, shown for cell 1. Two flows are calculated for each grid-cell boundary instead of the single value described by McDonald and Harbaugh (1988, p. 5-3)

Definition of Horizontal Anisotropy

In the LDVA Capability, the horizontal anisotropy direction is defined as the angle from a line in the positive x direction (along a row of the finite difference grid) to the major axis of the anisotropy ellipse (fig. 1). The angle is taken as positive in the clockwise direction and can vary between -90 and 90 degrees. The horizontal hydraulic conductivity along the major axis of anisotropy, K_{max} , and the horizontal anisotropy ratio, HANI, are defined by the user; HANI values need to range from 0.0 and 1.0. The horizontal hydraulic conductivity along the minor axis of anisotropy is calculated by the program as $K_{min}=HANI \times K_{max}$.

Modifying the Equations for Traditional Solvers

The eight flow equations for each cell are assembled using a conservation-of-mass approach into a system of equations to solve the ground-water flow equation for the entire finite-difference grid. The resulting system of equations forms a matrix with a 9-point stencil for a two-dimensional problem or an 11-point stencil for a three-dimensional problem. These equations can not be solved using the solvers presently available for MODFLOW, which require a 5-point stencil for a two-dimensional problem and a 7-point stencil for a three-dimensional problem. Additionally, as a rule, the coefficient matrix is not diagonally dominant, and can be difficult for iterative solvers. For example, preconditioned conjugate gradient solvers such as PCG2 (Hill, 1990) and multi-grid solvers such as LMG (Mehl and Hill, 2001) require diagonally dominant matrices.

In addition, the matrix of difference equations no longer satisfies the maximum principle that applies when the principal axes of anisotropy are aligned with the coordinate axes. This noncompliance means that the solution for hydraulic head can have interior values that are greater or less than any boundary values (for example, local maxima or minima that exceed boundary values in magnitude can appear in the interior of the grid). This type of solution does not conform with the original partial-differential equation of flow and implies a deficient finite-difference approximation.

In this report these problems are addressed by splitting the equations into an explicit part that is multiplied by heads from the previous solver iteration and an implicit part that produces a diagonally dominant matrix with a traditional 5-point difference stencil (seven point in three dimensions) as in classical MODFLOW difference equations, as suggested by Edwards (1998; 2000). Splitting at the inter-cell flow level rather than at the matrix-coefficient level was done for consistency. Each flow equation was split into its normal-gradient component and tangential-gradient component (eq. 7a and 7b), as discussed in appendix B.

The matrix equation for a one-layer problem can be used to describe the matrix splitting, and can be expressed as:

$$\mathbf{A}^{(9)}h = f \quad (8)$$

where

- $\mathbf{A}^{(9)}$ is the matrix of finite-difference coefficients, where the superscript (9) indicates the number of diagonals in the matrix and would be (5) in the absence of variable-direction horizontal anisotropy [L^2/T];
- h is the vector of hydraulic heads at the node points [L]; and
- f is the vector of volumetric flow rates at each cell [L^3/T] (positive is into the cell).

Splitting the matrix guarantees a stable solution only under rather restrictive conditions, as discussed in Appendix B. The tests considered in this work violated the restrictive conditions as might be expected in practice, yet the solvers available in MODFLOW-2000 have performed well. There is, however, a possibility that the solvers will not perform well in some circumstances. In these circumstances, the solver may fail to converge or global budget errors are likely to be large.

Errors Caused by Model Layers that are Not Horizontal

The derivation for variable-direction horizontal anisotropy, like the derivation of the original discretized equations for MODFLOW, was developed in the context of model layers that are horizontal and model layers that are stacked vertically. Often, however, model layers are not horizontal for a number of reasons. For example, consider the following situations:

1. MODFLOW model layer thickness can vary on a cell-by-cell basis which can cause cell centers to deviate from being located on a horizontal plane.
2. A useful way of managing the nonlinearity and resulting solver-convergence problems caused by free-surface water-table conditions is to define model grids for which the top is located at the level of the approximate water table. Using such a grid, many simulations, and particularly many calibrated simulations, can produce reasonably accurate results with the top layer specified as confined. Only when large parts of the system experience large amounts of dewatering over a time period of interest for the purpose of calibration or prediction are the results produced by such a simulation likely to be significantly in error. The resulting grid often has the property that the model layers are not horizontal in some parts of the grid, while the model layers are still stacked vertically. Thus, the grid locally does not possess three mutually orthogonal grid axes.
3. Tilted hydrogeologic layers may be best represented by a model grid with three mutually orthogonal model-grid directions, but the model-grid directions may be tilted so that the two model-layer axes fall within the plane of the hydrogeologic layers, while the third axis is perpendicular so that it crosses the hydrogeologic layers. In this circumstance, the axes are no longer horizontal and vertical but are mutually orthogonal.

Situations 1 and 2 result in numerical errors that increase as the amount by which the directions are not orthogonal increases. The consequences of such errors on simulated heads and flows were studied by Henry and others (1998). In their example, a cross-sectional model had a no-flow bottom boundary that oscillated such that the system thickness changed by a factor of

two with slopes that were often at a 45 degree angle. The simulated hydraulic heads and flows were significantly in error. The extremity of this example, however, indicates that the magnitude of the errors displayed are rarely encountered in practice. In most practical circumstances, the error would be much smaller than in their example, and it is likely that some distortion is acceptable. Careful study of the errors caused by such grid distortions have not, however, been conducted for this report.

Situation 3 would not result in any numerical error, because the grid directions remain mutually orthogonal. Care would need to be taken when using such a grid, however, because vertical features such as wells could easily be represented inaccurately.

The experiences supporting much of the above discussion are with isotropic problems. Errors for anisotropic problems are expected to be similar, but analysis of anisotropic problems for these situations is beyond the scope of this report.

Sensitivities

The sensitivities of simulated results to the hydraulic-property parameters are obtained using the sensitivity-equation method described by Hill and others (2000) for steady-state situations in which no layers are convertible. The sensitivity equation is derived by taking the partial derivative of the flow equation with respect to any given parameter. It is not practical to derive the sensitivity-equation sensitivities of the transmissivity coefficients for the anisotropic case, and perturbation sensitivities are used instead. The method used is described in Appendix C. For problems in which the solver performs well so that the heads are calculated correctly, no special difficulties are expected when calculating sensitivities when the LVDA capability is used to represent variable-direction horizontal anisotropy.

SIMULATION EXAMPLES

To test the hydraulic heads simulated using the LVDA capability, two simulation examples were used – one analytical and one numerical. An additional example, modified from test case 2 of Harbaugh and others (2000) and Hill and others (2000), is presented to illustrate how the LVDA capability might be applied to a model with features common to a complex three-dimensional ground-water flow model and to test the calculation of sensitivities.

Tests of Hydraulic Heads and Cell-By-Cell Flows Simulated Using the LVDA Capability

Test of Hydraulic Head Using an Analytical Solution

The analytical solution example was suggested by Richard L. Naff (U.S Geological Survey, written commun., 2002) and tests the variable-direction horizontal anisotropy derivation and implementation. The hydraulic-conductivity tensor is defined using a primary-direction hydraulic conductivity of 1.5 m/d, a horizontal-anisotropy ratio of 1/3, and an angle of 45 degrees. The resulting model hydraulic-conductivity tensor is:

$$\mathbf{K} = \begin{bmatrix} 1 & \frac{1}{2} & 0 \\ \frac{1}{2} & 1 & 0 \\ 0 & 0 & 1 \end{bmatrix} \quad (9)$$

The model area is shown in figure 6. A single-layer model with a constant 50-m thickness is represented with a finite-difference grid of 51 rows and 51 columns covering an area 5,100 m long in the x direction and 5,100 m long in the y direction. The boundary conditions imposed are constant flow of 1.0 m³/d into the model across the left boundary and out of the model across the right boundary, and constant flow of 0.5 m³/d into the model at the top and exiting the model at the bottom. A system with only defined flow boundaries has no unique head solution, so an arbitrary head was specified at one cell at the center of the model grid.

The analytical solution to this problem is a planar head distribution with a non-zero gradient in the x direction and a zero gradient in the y direction, regardless of the size of the simulated area. The head distribution calculated using the LVDA capability in MODFLOW-2000 shown in figure 6B nearly matches the analytical solution, but it is not completely linear and is rotated slightly in the counterclockwise direction. The bias is introduced because the LVDA capability needs to be modified to make the nine-point stencil properly handle the absence of neighboring cells at no-flow boundaries.

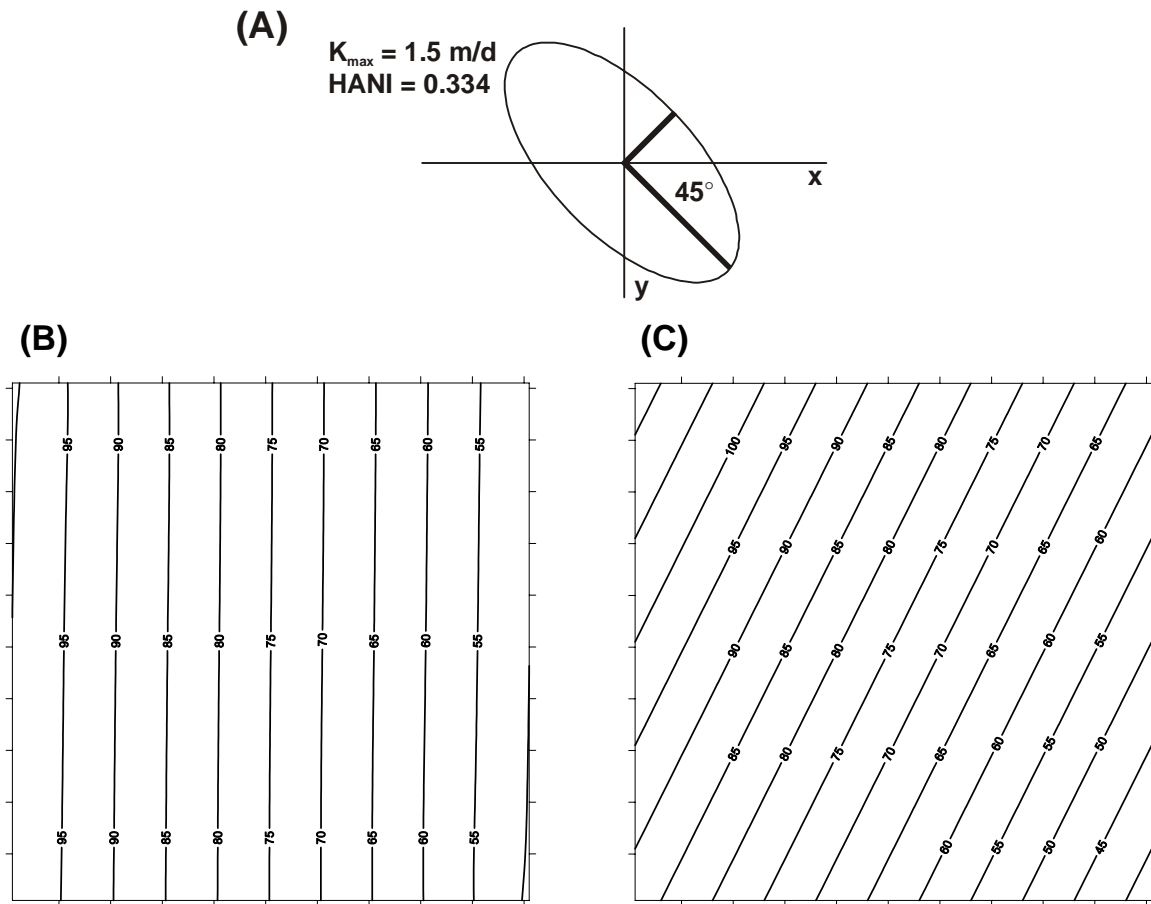


Figure 6. (A) Representation of the hydraulic-conductivity ellipse for the steady-state analytical solution. HANI is the horizontal anisotropy ratio. (B) Hydraulic-head solution using the LVDA capability in MODFLOW-2000. The LVDA capability nearly reproduces the analytical hydraulic-head distribution, for which the contours should be parallel and vertical. The slight angle of the head contours is caused by the approximate way that the LVDA capability accounts for specified-flow boundaries. (C) Hydraulic-head solution without the LVDA capability with the same boundary conditions as in (B) and isotropic hydraulic conductivity. This is the solution that is produced using previously existing capabilities of MODFLOW.

Test of Hydraulic Heads Using a Numerical Solution

The anisotropy capability was tested on a two-dimensional numerical example of a circular island with a confined aquifer and a pumping well in the center. The maximum hydraulic conductivity is 10 m/day; the horizontal anisotropy ratio of the hydraulic conductivity is 0.1. The aquifer thickness is 1 m. The pumping rate is 500 m³/day. The diameter of the island is 2000 m and the boundary condition at the edge of the island is a prescribed head of +10 m. The cell sizes used are 10 m in the x and y directions and the grid has 200 rows and 200 columns.

This example is simulated in two ways. First, the direction of maximum hydraulic conductivity was assumed to be parallel to grid columns and the problem was simulated using MODFLOW without the LVDA capability. In this simulation, the Block-Centered Flow (BCF) Package of MODFLOW-2000 was used. Second, the direction of maximum conductivity was

defined as 45 degrees and the problem was simulated using the LVDA capability of the Hydrogeologic-Unit Flow (HUF) package.

The resulting heads of both simulations are shown in figure 7. The two hydraulic-head distributions are almost identical except for a 45-degree rotation. The drawdown in the center of the grid differs only by 4 mm out of a total drawdown of over 14 m. When the LPF or HUF packages are used instead of the BCF package in the first simulation, the drawdown is identical.

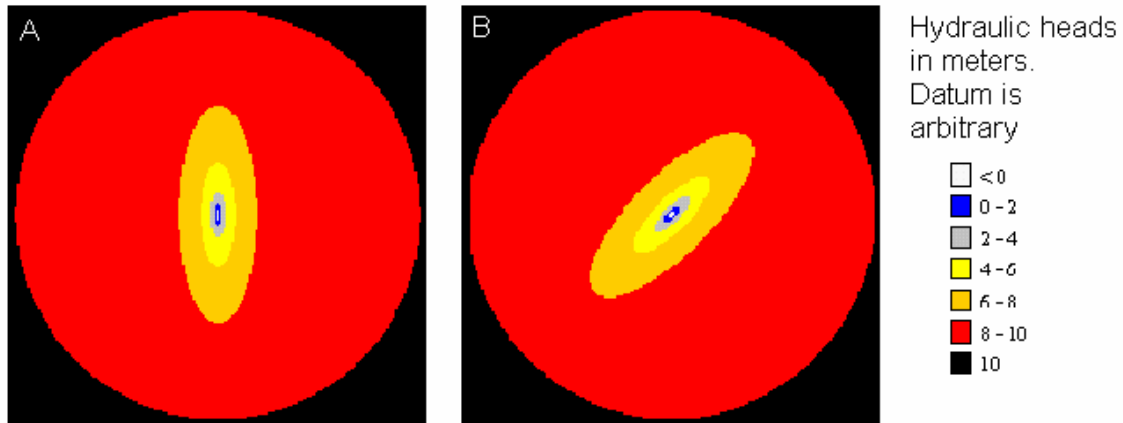


Figure 7. Hydraulic heads simulated in two ways that theoretically produce identical results rotated by 45 degrees. In both situations, the hydraulic head at the circular boundary 1000 m from the pumping well is 10 m. (A) Horizontal anisotropy is parallel to the grid directions simulated using MODFLOW without the LVDA capability. (B) Horizontal anisotropy at a 45 degree angle to the grid simulated using MODFLOW with the LVDA capability.

Test of Cell-By-Cell Flows Using an Analytical Solution

The analytical solution used to test hydraulic heads (fig. 6) is used here to test the calculation of cell-by-cell flows. This is accomplished by using the flows to calculate four advective-travel paths using the ADV2 Package of MODFLOW-2000 (Anderman and Hill, 2001). Theoretically the angle of transport should be 26.565 degrees; the simulated angle of the paths shown in figure 8 is 26.96 degrees, which is a 1.5% discrepancy. The small discrepancy is caused by the same boundary representation problem that affected the hydraulic-head solution, as discussed above.

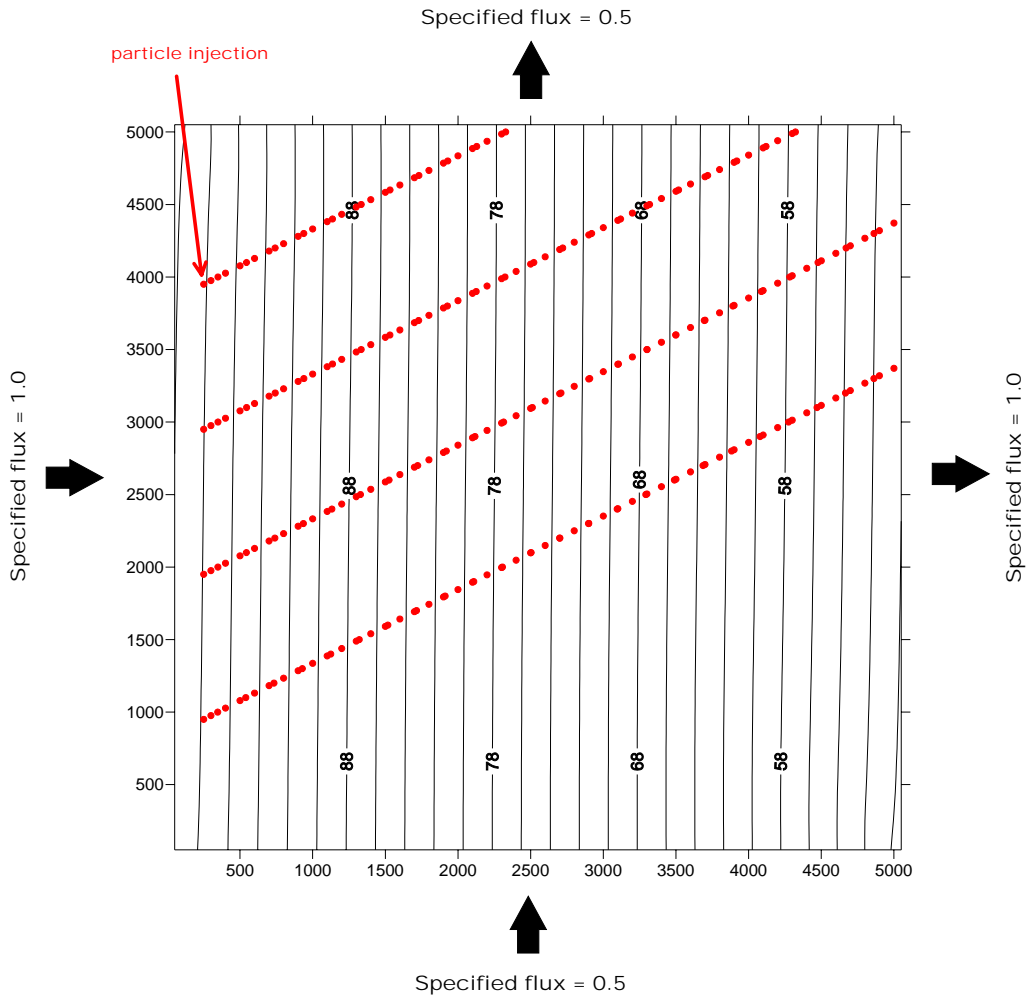


Figure 8. Advective-transport paths simulated using the LDVA capability for the problem presented in figure 6. The paths are superimposed on the hydraulic-head solution from figure 6B.

Illustration and Test of Sensitivities Calculated Using the LVDA Capability

The variable-direction horizontal anisotropy capability is demonstrated using a synthetic problem derived from test case 2 of Hill and others (2000) that includes features common to a complex three-dimensional ground-water flow model. This complex example is also used to perform regression with observations that exactly equal the correct values and that contain sufficient information to estimate all parameters. This constitutes a test of the sensitivities because the regression can only estimate parameter values correctly if the sensitivities are correct. Test case 2 was similarly used to test sensitivities by Hill and others (2000, p. 160).

The model grid for the complex example (fig. 9) has uniform cell dimensions of 1,500 meters (m) in both horizontal directions; the thickness of layers 1, 2, and 3 are 500, 750, and 1500 m, respectively. Constant-head boundaries comprise parts of the western and eastern boundaries, and no flow occurs across the remaining lateral boundaries and the bottom boundary. Springs are represented using either the Drain or General-Head Boundary Packages of McDonald and

Harbaugh (1988) and Harbaugh and others (2000). Wells are simulated at selected nodes and have pumpage rates ranging from 100 to 200 m³/d.

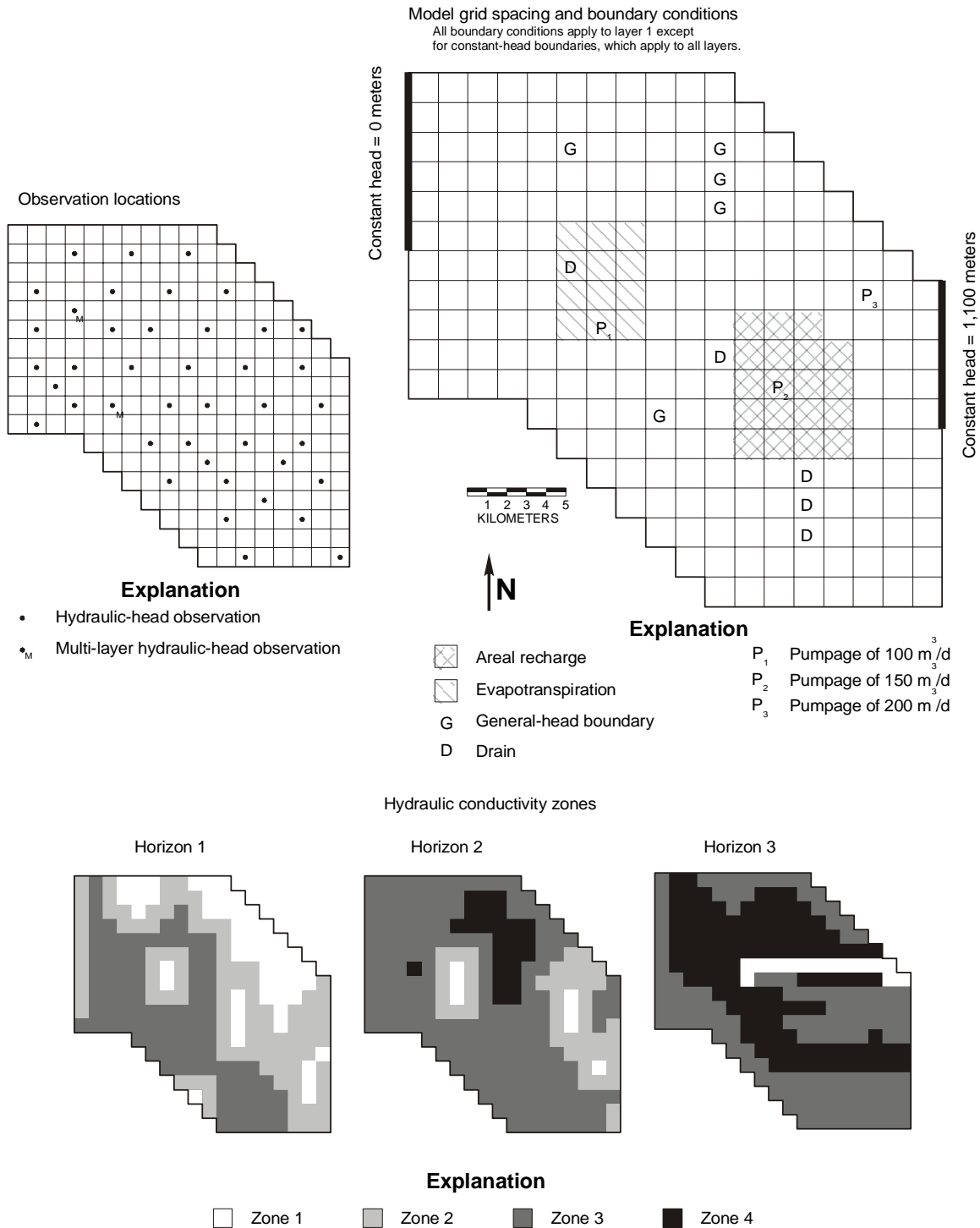


Figure 9. Model grid, boundary conditions, observation locations, and hydraulic-conductivity zones for complex example used to test the calculation of sensitivities. (Modified from Hill and others, 2000.)

The hydraulic-conductivity distribution of the system is divided vertically into three horizons and horizontally into four zones (fig. 9). All four zones are present in the middle horizon; three are present in each of the top and bottom horizons (fig. 9). Each horizon represents a model layer and is defined in the HUF Package using two equal-thickness hydrogeologic units. The hydraulic-conductivity distribution was defined in this manner to test the ability to represent model layers with multiple hydrogeologic units. The hydraulic properties of the model were defined using the fourteen parameters listed in table 1.

The observations (fig. 9) used in the parameter estimation consisted of 44 hydraulic heads, 5 drain flows, and 5 general-head boundary flows. The values were generated by running the model with the true parameter values; no random error was added so that the observations equal the simulated values.

Table 1. Labels, descriptions and true and starting values for the parameters for the complex example

[m/d, meters per day; m²/d, square meters per day; --, no units]

Label	Description	Units	True Value	Initial Value
HK1	Horizontal hydraulic conductivity of zone 1	m/d	1.00	1.3
HK2	Horizontal hydraulic conductivity of zone 2	m/d	1.00x10 ⁻²	1.5x10 ⁻²
HK3	Horizontal hydraulic conductivity of zone 3	m/d	1.00x10 ⁻⁴	1.5x10 ⁻⁴
HK4	Horizontal hydraulic conductivity of zone 4	m/d	1.00x10 ⁻⁵	1.2x10 ⁻⁵
HANI123	Horizontal anisotropy of zones 1 through 3	--	1.00	1.2
HANI4	Horizontal anisotropy of zone 4	--	0.10	0.1
LVDA123	Horizontal-anisotropy direction of zones 1 through 3	degrees	0	0.0
LVDA4	Horizontal-anisotropy direction of zone 4	degrees	45	-55
VANI1234	Vertical anisotropy of hydrogeologic units 1 through 4	--	4.0	4.2
VANI56	Vertical anisotropy of hydrogeologic units 5 and 6	--	1.0	1.2
RCH	Areal recharge rate applied to the area shown in figure 9	m/d	3.10x10 ⁻⁴	3.3x10 ⁻⁴
ETM	Maximum evapotranspiration rate applied to area shown in figure 9	m/d	4.00x10 ⁻⁴	4.2x10 ⁻⁴
GHB	Conductance of head-dependent boundaries ("G") shown in figure 9 represented using the General-Head Boundary Package.	m ² /d	1.00	1.3
KDR	Conductance of the head-dependent boundaries ("D") shown in figure 9 using the Drain Package.	m ² /d	1.00	1.3

To demonstrate how rotating the horizontal anisotropy direction changes the calculated hydraulic heads, the model was run twice with different anisotropy directions in zone 4. The hydraulic-conductivity ellipse for zone 4 is shown in fig. 10(A). First, the model was run with the horizontal anisotropy in zone 4 aligned with the model grid, and the resulting hydraulic-head distribution is shown by the black contour lines in fig. 10(B). Then, the horizontal anisotropy in

zone 4 was rotated 45-degrees clockwise. The resulting hydraulic-head distribution is shown by the red contour lines in fig. 10(B). Values for the remaining parameters were unchanged. The change in hydraulic head between the two runs is shown in figure 10(C).

The results shown in figure 10(C) indicate that rotating the horizontal anisotropy changes the heads the most in layer 3 and progressively less in layers 2 and 1, respectively, as would be expected considering the distribution of zone 4, in which the horizontal anisotropy direction was changed. The change in horizontal anisotropy direction provides a conduit of high hydraulic conductivity and connectivity from the southeast to the northwest of layer 3 where zone 4 is predominantly located. The connectivity in the perpendicular direction, which connects the two constant-head boundaries, is reduced. The head in the southern part of layer 3 decreases as much as 32.5 m and the head in the northern part of layer 3 increases approximately 142 m.

Composite scaled sensitivities were calculated for the 14 parameters at the true values listed in table 1 (fig. 11). The direction of horizontal anisotropy in zones 1 through 3, represented by the LVDA123 parameter, has a zero sensitivity because the hydraulic conductivity in those zones is isotropic. As shown in figures 3 and 4, if the anisotropy ratio were changed, the sensitivity to the LVDA123 parameter would increase. The sensitivities range in value from 0.2 for the HANI4 parameter to 33.5 for the RCH parameter. Using the rule of thumb suggested by Hill (1998, p. 38), the fact that these values span a range of more than two orders of magnitude suggests that estimating all the parameter values by regression may be problematic. The range is just slightly larger than two orders of magnitude. An attempt to estimate all 14 parameters using regression was accomplished successfully using the starting values in table 1. The success of the regression constitutes a test of the sensitivities calculated by the LVDA capability and indicates that they are calculated correctly.

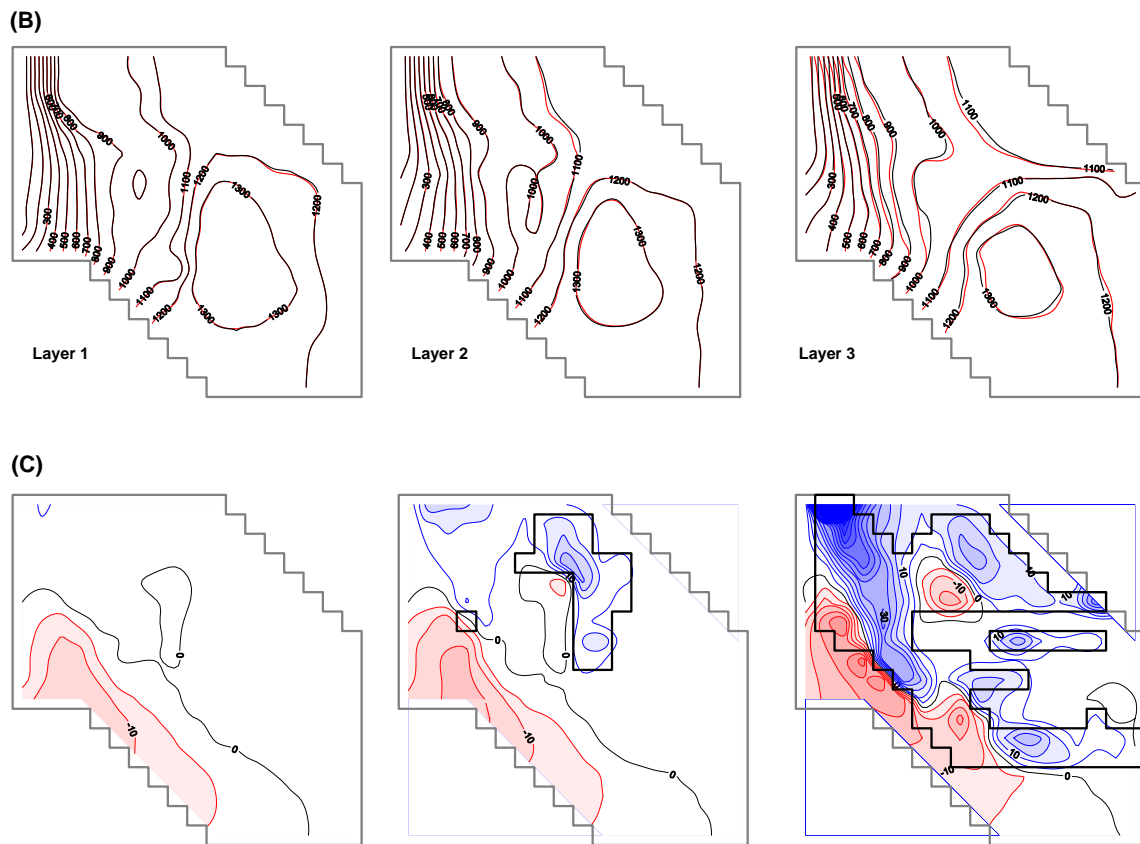
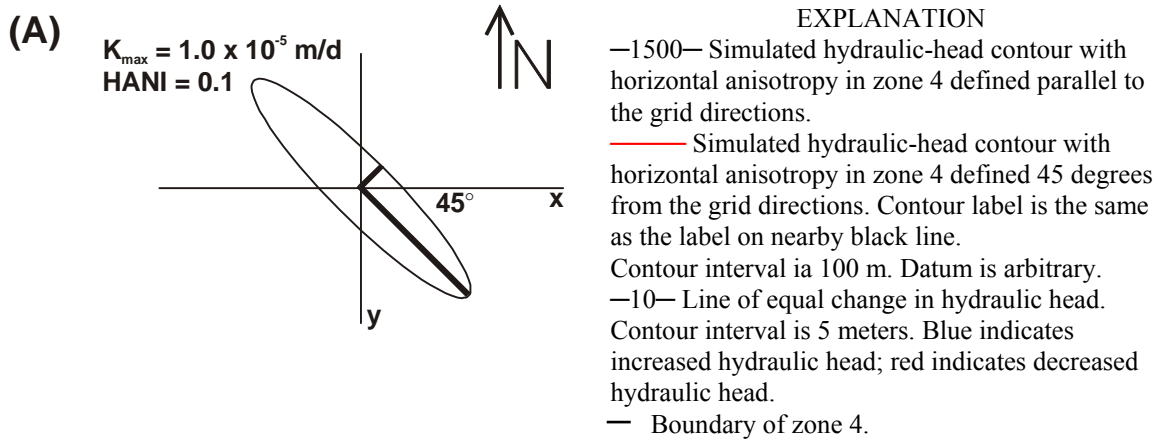


Figure 10. (A) Representation of the hydraulic-conductivity ellipse for zone 4; ANIV is the horizontal anisotropy ratio. (B) Hydraulic-head distribution with anisotropy in zone 4 defined parallel to the grid directions (black lines) and with anisotropy in zone 4 defined 45 degrees from the grid directions (red lines). (C) Change in hydraulic head produced by rotating the direction of horizontal anisotropy in zone 4 (outlined by thick black line) from 0 to 45 degrees.

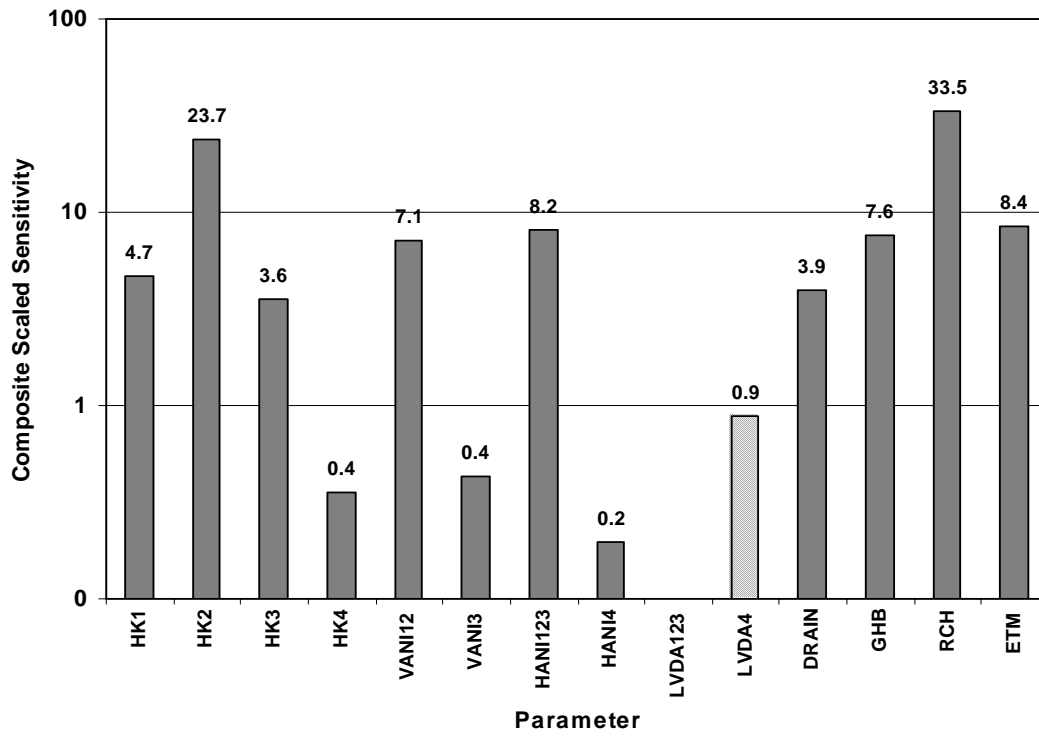


Figure 11. Composite scaled sensitivities at the true values for parameters listed in table 1. Sensitivities for the LVDA parameters shown with cross hatching. The composite scaled sensitivity for LVDA123 is zero because the related horizontal anisotropy ratio equals 1.0.

REFERENCES CITED

- Anderman, E.R., and Hill, M.C., 2000, MODFLOW-2000, the U.S. Geological Survey modular ground-water model – Documentation of the Hydrogeologic-Unit Flow (HUF) Package: U.S. Geological Survey Open-File Report 00-342, 104 p.
- Anderman, E.R. and Hill, M.C., 2001, MODFLOW-2000, the U.S. Geological Survey modular ground-water model -- Documentation of the ADVective-Transport observations (ADV2) Package: U.S. Geological Survey Open-File Report 01-54, 69p.
<http://water.usgs.gov/nrp/gwsoftware/modflow2000/modflow2000.html>
- Anderman, E.R. and Hill, M.C., in review, MODFLOW-2000, the U.S. Geological Survey modular ground-water model – Documentation of the enhanced printing capability of the Hydrogeologic-Unit Flow (HUF) Package: U.S. Geological Survey Open-File Report.
- Dash, Z.V., Zyvoloski, G.A., and Robinson, B.A., 2002, User's manual for the FEHM Application A Finite-Element Heat- and Mass-Transfer Code: Los Alamos, New Mexico, Los Alamos National Laboratory Report LA-13306-M.
- Edwards, M.G., 1998, Cross flow tensors and finite volume approximation with deferred correctio:, *Computer Methods in Applied Mechanics and Engineering*, v. 151, p. 143-161.
- Edwards, M.G. and Rogers, C.F., 1998, Finite volume discretization with imposed flux continuity for the general tensor pressure equation: *Computational Geosciences*, v. 2, p.259-290.
- Edwards, M.G., 2000, M-Matrix flux splitting for general full tensor discretization operators on structured and unstructured grids: *Journal of Computational Physics*, v. 160, p.1-28.
- Harbaugh, A.W., 1990, A computer program for calculating subregional water budgets using results from the U.S. Geological Survey modular three-dimensional ground-water flow model: U.S. Geological Survey Open-File Report 90-392, 46 p.
- Harbaugh, A.W., Banta, E.R., Hill, M.C., and McDonald, M.G., 2000, MODFLOW-2000, the U.S. Geological Survey modular ground-water model – User guide to modularization concepts and the Ground-Water Flow Process: U.S. Geological Survey Open-File Report 00-92, 121 p.
- Henry, R.M., Frind, O.E., and Guiger, Nelson, 1998, Some grid-related limitations of MODFLOW *in* Poeter, Eileen, and others, eds, MODFLOW'98 Conference Proceeding: Colorado School of Mines, October 4-8, 1998, p. 219-226.
- Hill, M.C., 1998, Methods and guidelines for effective model calibration: U.S Geological Survey Water- Resources Investigations Report 98-4005, 90p.
<http://pubs.water.usgs.gov/wri984005/>
- Hill, M.C., 1990, Preconditioned Conjugate-Gradient 2 (PCG2), a computer program for solving ground-water flow equations: U.S. Geological Survey Water-Resources Investigations Report 90-4048, 43 p.
- Hill, M.C., Banta, E.R., Harbaugh, A.W., and Anderman, E.R., 2000, MODFLOW-2000, the U.S. Geological Survey modular ground-water model—User Guide to the Observation, Sensitivity, and Parameter-Estimation Processes and three post-processing programs: U.S. Geological Survey Open-File Report 00-184, 210 p.
- Lin, H.C. J., D.R. Richards, G.-T. Yeh, J.R. Cheng, H.P. Cheng, N.L. Jones, 1997, FEMWATER: A Three-Dimensional Finite Element Computer Model for Simulating Density-Dependent

- Flow and Transport in Variably Saturated Media, Technical Report CHL-97-12, U.S. Army Engineer Waterways Experiment Station, 132 pp.
- McDonald, M.G. and Harbaugh, A.W., 1988, A modular three-dimensional finite difference ground-water flow model: U.S. Geological Survey Techniques of Water Resources Investigations, Book 6, Chapter A1, 586 p.
- Mehl, S.W., and Hill, M.C., 2001, MODFLOW-2000, the U.S. Geological Survey modular ground-water model -- User guide to the Link-AMG (LMG) package for solving matrix equations using an algebraic multigrid solver: U.S. Geological Survey Open-File Report 01-177, 33 p.
- Molson, J.W. and Frind, E.O., 2002a, FLONET/TRANS User Guide: Waterloo, Ontario, Canada, Department of Earth Sciences, University of Waterloo,. 55 p.
- Molson, J.W., and Frind, E.O., 2002b, WATFLOW/WTC User Guide and Documentation, Version 3: Waterloo, Ontario, Canada, Department of Earth Sciences, University of Waterloo,. 75 p.
- Pinder, G.F., 2002, Groundwater modeling using geographical information systems: New York, John Wiley and Sons, 224 p.
- Voss, C.I., and Provost, A.M., 2002, SUTRA - A Model for Saturated-Unsaturated Variable-Density Ground-Water Flow with Solute or Energy Transport: U.S. Geological Survey Water-Resources Investigations Report 02-4231.

APPENDIX A: LVDA INPUT AND OUTPUT

The LVDA capability is a modification to the existing Hydrogeologic-Unit Flow (HUF) Package (Anderman and Hill, 2000). This section describes the new input file needed with the LVDA capability and the changes in the HUF Package output files resulting from using the LVDA capability. There are no changes in the HUF Package output files if the LVDA capability is not used. Although the HUF input file is not changed when using the LVDA capability, the definition of two parameter types does change. The new definitions are presented below.

Printing of the LVDA model layer arrays is not supported by the print capability represented by item 12 of the HUF Package input file. Printing these arrays requires use of the new printing capability for the HUF Package documented by Anderman and Hill (in review).

LVDA Input Instructions

Input for the Model-Layer Variable-Direction Horizontal Anisotropy capability is read from the file that has type “LVDA” in the Name file. Free format is used for reading all values. This file defines the horizontal anisotropy direction for each cell of the finite-difference grid.

FOR EACH SIMULATION

0. [#Text]

Item 0 is optional -- “#” must be in column 1. Item 0 can be repeated multiple times.

1. NPLVDA

2. PARNAM PARTYP Parval NCLU

3. Layer Mltarr Zonarr IZ

Each Item 3 record is called a parameter cluster. Repeat Item 3 NCLU times.

Repeat Items 2 and 3 for each parameter to be defined (that is, NPLVDA times).

Explanation of Variables Read by the LVDA Capability

Text – is a character variable (up to 199 characters) that starts in column 2. Any characters can be included in Text. The “#” character must be in column 1. Text is printed when the file is read.

NPLVDA – is the number of LVDA parameters.

PARNAM – is the name of a parameter to be defined. This name can consist of up to 10 characters and is not case sensitive.

PARTYP – is the parameter type to be defined. For the LVDA capability, the only allowed parameter type is:

LVDA - defines the angle between the grid axis and the principal direction of horizontal hydraulic conductivity. Angle is positive in a clockwise direction with the positive x direction being zero. The angle can vary between –90 and 90 degrees. Hydraulic conductivity along the principal axis (K_{\max} of figure 2) is defined in the HUF Package input file by an HK parameter; the hydraulic conductivity along the minor axis (K_{\min} of figure 2) axis is defined by a HANI parameter in conjunction with the HK parameter. Using the LVDA capability, HANI values need to be less than or equal to 1.

Parval – is the parameter value; however, this value can be replaced by a value specified in the Sensitivity Process input file, or by a value generated by the Parameter-Estimation Process.

NCLU – is the number of clusters required to define the parameter. Each Item-3 record is a cluster (variables Layer, Mltarr, Zonarr, and IZ).

Layer – is the layer to which the direction applies.

Mltarr – is the name of the multiplier array to be used to define array values that are associated with a parameter. The name “NONE” means that there is no multiplier array, and the array values will be set equal to Parval.

Zonarr – is the name of the zone array to be used to define array elements that are associated with a parameter. The name “ALL” means that there is no zone array and that all elements in the layer are part of the parameter.

IZ – is up to 10 zone numbers (separated by spaces) that define the array elements that are associated with a parameter. The first zero or non-numeric value terminates the list. These values are not used if Zonarr is specified as “ALL”.

Example LVDA Input File

The following lines of data illustrate the definition of the LVDA parameter for the three-dimensional complex example described in the ‘Simulation Examples’ section of this report. In this definition, the parameter value of 45 is applied to zone 4 in layers 1, 2, and 3 using a unique zone array for each layer.

```
1                               Item 1:  NPLVDA
LVDA4  LVDA  45.0 3  Item 2:  PARNAM PARTYP PARVAL NCLU
1      NONE  ZLAY1 4  Item 3:  LAYER MLTARR ZONARR IZ
2      NONE  ZLAY2 4  Item 3:  LAYER MLTARR ZONARR IZ
3      NONE  ZLAY3 4  Item 3:  LAYER MLTARR ZONARR IZ
```

LVDA Output

Output from the LVDA capability is sent to the global listing file. The allocate routine prints out the following output:

```
LVDA1 -- MODEL-LAYER VARIABLE-DIRECTION HORIZONTAL ANISOTROPY CAPABILITY, VERSION 2.2.5
ERA, 11/08/2002
INPUT READ FROM UNIT 14
  2 Named Parameters
  11664 ELEMENTS IN X ARRAY ARE USED BY LVDA
  0 ELEMENTS IN IX ARRAY ARE USED BY LVDA
```

The read and prepare routine prints out the following regarding the definition of the LVDA parameter:

```
LVDA1 -- LVDA CAPABILITY
-----
PARAMETER NAME:LVDA4          TYPE:LVDA UNITS:   3
The parameter value from the package file is:  45.000
UNIT: 1 MULTIPLIER:NONE      ZONE:ZLAY1
ZONE VALUES:                4
UNIT: 2 MULTIPLIER:NONE      ZONE:ZLAY2
ZONE VALUES:                4
```

New Definition of Two Parameter Types of the HUF Package Input File

As mentioned above in the explanation of variable PARTYP, the LVDA parameter uses parameter types HK and HANI defined in the HUF Package input. When the LVDA capability is used, HK parameters in the HUF Package input file define hydraulic conductivity along the principal axis (K_{\max} of figure 2); HANI parameters define the ratio used to calculate the hydraulic conductivity along the minor axis (K_{\min} of figure 2) axis as a product of the ratio and the cell hydraulic conductivity along the principal axis. Cell values defined by HANI parameters need to be less than or equal to 1.

Execution Time Issues

Because of its formulation and implementation, MODFLOW-2000 with the HUF Package and the LVDA capability will take longer to run than if the LVDA capability were not active. The increase in execution time will depend on the situation.

For the two-dimensional example of figure 6 in the 'Simulation Examples' section of this report, the model run for the anisotropy parallel to the grid took approximately 9 seconds. The run using the LVDA capability but with the angle set to zero took approximately 13 seconds. The run with the angle set to 45 degrees (the most complex the computation can be) took approximately 76 seconds. Everything was run on the same computer with the same starting hydraulic heads and the PCG solver (Harbaugh and others, 2000) with a head-change convergence criterion of 1.0×10^{-4} m and a residual convergence criterion of 1.0×10^{-4} m³/d.

For the three-dimensional complex example shown in the 'Simulation Examples' section of this report (fig. 8), the model run for the anisotropy parallel to the grid took approximately 0.44 seconds. The run using the LVDA capability but with the angle set to zero took approximately 0.62 seconds. The run with the angle set to 45 degrees, the most complex the computation can be, took approximately 1.8 seconds. All runs were made using the PCG solver with a head-change convergence criterion of 1.0×10^{-6} and a residual convergence criterion of 1.0×10^{-8} .

The relative execution times are shown in figure 11. The LVDA capability will substantially increase model execution times and this needs to be accounted for in model design.

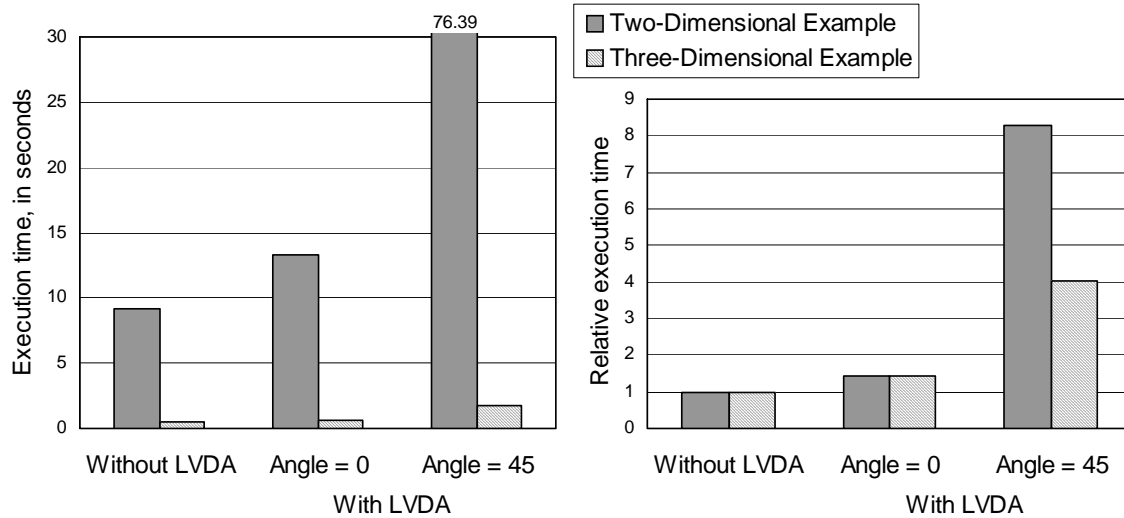


Figure A- 1. Execution times for MODFLOW-2000 models run using the HUF Package without the LDVA capability and with the LVDA capability using angles of horizontal anisotropy of 0 and 45 degrees. The solutions without LDVA and with LDVA using an angle of 0 degrees are identical and execution times differ because of the extra effort required by the LDVA capability. Execution times are reported in seconds and relative to the execution time without the LDVA capability. The three-dimensional example is thought to be more representative of typical applications.

Reference Cited

Anderman, E.R., and Hill, M.C., 2000, MODFLOW-2000, the U.S. Geological Survey modular ground-water model – Documentation of the Hydrogeologic-Unit Flow (HUF) Package: U.S. Geological Survey Open-File Report 00-342, 104 p.

APPENDIX B: MATHEMATICAL DERIVATION FOR SIMULATING VARIABLE-DIRECTION HORIZONTAL ANISOTROPY USING BLOCK-CENTERED FINITE DIFFERENCES

This appendix contains the derivation of the equations needed to simulate variable-direction horizontal anisotropy using a block-centered finite-difference grid. The development presented here is based on the work of Edwards and Rogers (1998). They developed a general theory for curvilinear coordinates but present a full set of coefficients for only the homogeneous case. In this appendix, the coefficients are developed for the heterogeneous case.

Ground-Water Flow Equation

The partial-differential equation for ground-water flow in a saturated medium in a Cartesian coordinate system can be expressed as:

$$S_s \frac{\partial h}{\partial t} - \nabla \cdot \mathbf{K} \nabla h - q = 0; \quad (\text{B-1})$$

where

- h is the hydraulic head [L];
- \mathbf{K} is the porous-medium hydraulic conductivity tensor [L/T];
- S_s is the specific storage [L⁻¹];
- q is the volumetric source flow per unit volume [L³/T-L³] (inflow is positive); and
- t is the time [T].

Generally, the hydraulic-conductivity tensor, \mathbf{K} , is a symmetric full tensor of rank 3 and has the form:

$$\mathbf{K} = \begin{bmatrix} K_{xx} & K_{xy} & K_{xz} \\ K_{xy} & K_{yy} & K_{yz} \\ K_{xz} & K_{yz} & K_{zz} \end{bmatrix}. \quad (\text{B-2a})$$

The values of \mathbf{K} can vary spatially, so that each element of the matrix in equation B-2a can be a function of the spatial coordinates x , y , and z .

For the LVDA capability, one principal axis of hydraulic conductivity (the vertical axis) is aligned with the z -direction, so that $K_{xz} = K_{yz} = 0$ and equation B-2a becomes:

$$\mathbf{K} = \begin{bmatrix} K_{xx} & K_{xy} & 0 \\ K_{xy} & K_{yy} & 0 \\ 0 & 0 & K_{zz} \end{bmatrix}. \quad (\text{B-2b})$$

The flow equation is assumed to be parabolic which requires that

$$K_{xy}^2 \leq K_{xx} K_{yy} \quad (\text{B-2c})$$

This requirement is always met given how anisotropy is defined in the LVDA input file and, in general, for physically realizable ground-water flow problems.

All z-direction terms remain unchanged in MODFLOW, so that in this appendix only the two dimensional (x-y) version of equation B-1 needs to be considered. By integrating equation B-1 over the aquifer thickness, the two-dimensional form is derived as:

$$S \frac{\partial h}{\partial t} - \nabla \cdot \mathbf{T}' \nabla h - Q = 0 ; \quad (\text{B-3})$$

where

- \mathbf{T}' is the porous-medium transmissivity tensor [L^2/T];
- S is the storage coefficient [-]; and
- Q is the volumetric source flow per unit area [$L^3/T-L^2$] (positive is into the region).

The Block-Centered Finite-Difference Grid and the Continuity Equation

The classical finite-difference method (for example, Wang and Anderson, 1982) is used to discretize equation B-3 in space and time. Only spatial discretization is of concern in this work; time discretization remains the same as described by McDonald and Harbaugh (1988).

The first step in the spatial discretization is to construct a two-dimensional grid (fig. B-1). The x and y coordinate axes are defined to follow the rows and columns of the grid (as shown in figure B-1). Creating the grid is equivalent to specifying the locations of the planes that form the walls of the finite-difference cells in each coordinate direction. The intersections of these planes form the grid of rectangular cells. A node point is located in the center of each cell. The grid described is called a two-dimensional block- or cell-centered grid. Each cell is used as a volume, called a control volume, over which flow is balanced to give the finite-difference equations.

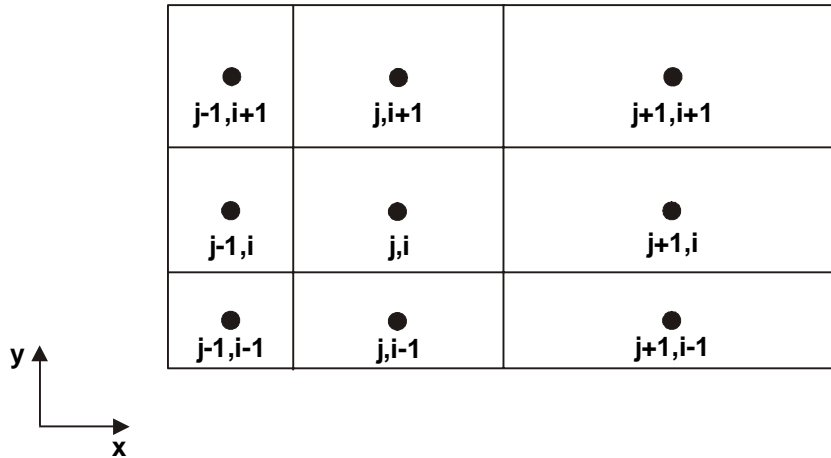


Figure B-1. Two-dimensional cell-centered grid in x-y plane. The row indexing convention is the same as that used in MODFLOW, when observed from below, with j used to index the x axis and i used to index the y axis.

McDonald and Harbaugh (1988) derived the discretized ground-water flow equations by simply applying Darcy's Law to the control volumes, but proper accounting of variable-direction anisotropy requires integral equations over the cell. The more complicated-looking equations required by the LVDA capability achieve volumetric conservation of water or conservation of

mass, just as McDonald and Harbaugh (1988) did using Darcy's Law in that the flow through each side of each finite-difference cell needs to come from or go to the neighboring cell.

Using the integral approach, the finite-difference flow equation is derived by integrating equation B-3 over the two-dimensional control volumes (cell areas). The resulting area integrals of flow are transformed into line integrals of flow perpendicular to the cell boundaries using the Gauss theorem in a plane, which is expressed as

$$\int_{\Omega_m} \nabla \cdot (\mathbf{T}' \nabla h) dS_m = \oint_{\partial\Omega_p} (\mathbf{T}' \nabla h) \cdot \hat{\mathbf{n}} ds_m \quad (\text{B-4})$$

where

- Ω_m is the surface area of cell m [L^2];
- $\partial\Omega_p$ is the boundary line of cell m [L];
- dS_m is the differential surface area of cell m [L^2],
- ds_m is the differential boundary line of cell m [L]; and
- $\hat{\mathbf{n}}$ is the outward unit normal to the boundary line of cell m [-].

The heterogeneous transmissivity is represented by a piecewise constant function over each control volume. The hydraulic head distribution within the cell is approximated using several piecewise linear functions over each control volume.

Computational Coordinates

The line integral on the right-hand side of equation B-4 can be evaluated with more manageable algebraic expressions if the Cartesian coordinate system that defines the physical situation is mapped to local computational coordinates such that the rectangular grid cells are transformed into unit squares. For the equations presented here, this allows the dx 's and dy 's to be omitted from the lengthy equations. In more generally deformable grids, converting to local unit-square grid coordinates is more important and, therefore, used in the development by Edwards and Rogers (1998). Here, we use the transformation to take advantage of the simplification of the equations and to coordinate with the development by Edwards and Rogers (1998).

Local computational coordinates are developed by mapping control volumes that are rectangular in the x - y plane to a unit square in the ξ - η plane. The mapping is defined by the relations $x = x(\xi)$ and $y = y(\eta)$ where the relations, using vector notation, are:

$$\begin{bmatrix} x \\ y \end{bmatrix} = \begin{bmatrix} (1-\xi)x_1 + \xi x_2 \\ (1-\eta)y_1 + \eta y_2 \end{bmatrix} \quad (\text{B-5})$$

where x_1, y_1 ; x_1, y_2 ; x_2, y_1 ; and x_2, y_2 are the coordinates of the corners of the rectangular cell in the x - y plane [L]. Figure B-2 shows the mapping with cell dimensions.

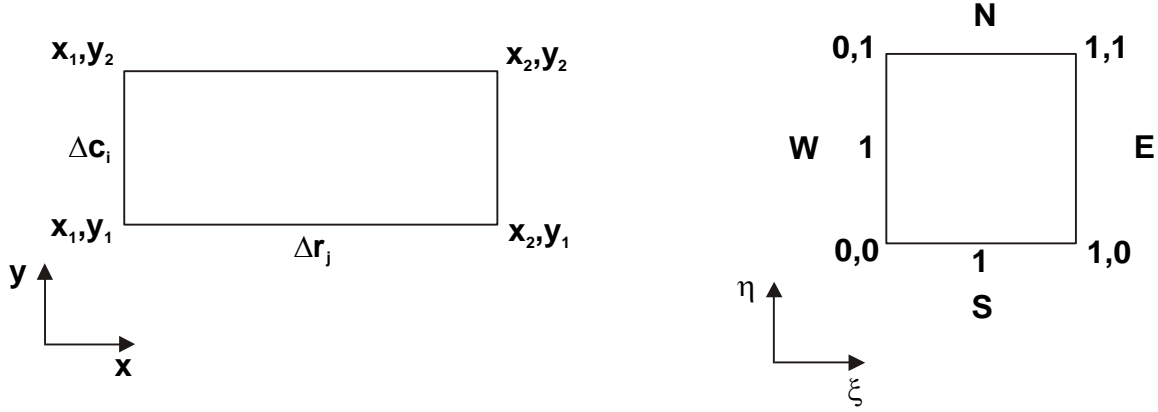


Figure B-2. A two-dimensional cell in the x - y plane mapped into a unit square cell in the ξ - η plane. For convenient referencing in the text, the four sides of the unit square are labeled N (north), S (south), E (east), and W (west). Δc_i is the cell dimension along the y axis, which is parallel to the columns of the grid; Δr_j is the cell dimension along the x axis, which is parallel to the rows of the grid.

With this mapping, equation B-4 can be expressed as in equation B-6. The letters, E, W, N and S identify the cell sides shown in figure B-2:

$$\begin{aligned}
 \oint_{\partial\Omega_p} (T' \nabla h) \cdot \hat{\mathbf{n}} ds_m &= \int_{1,0}^{1,1} (T_{aa} h_\xi + T_{ab} h_\eta) d\eta - \int_{0,0}^{0,1} (T_{aa} h_\xi + T_{ab} h_\eta) d\eta \\
 &+ \int_{0,1}^{1,1} (T_{ab} h_\xi + T_{bb} h_\eta) d\xi - \int_{0,0}^{1,0} (T_{ab} h_\xi + T_{bb} h_\eta) d\xi
 \end{aligned} \tag{B-6}$$

E
W
N
S

where h_ξ and h_η are head gradients in the two directions and T_{aa} , T_{ab} , and T_{bb} are elements of the transmissivity tensor of the unit square. Here, the subscripts a and b are used on the transmissivity coefficients to coordinate with the notation of Edwards and Rogers (1998), but these subscripts could be replaced by ξ and η , respectively. Each integral in equation B-6 defines the flow across one cell face. The terms associated with transmissivities T_{aa} and T_{bb} are the flow terms caused by the normal gradient of hydraulic head across (that is, perpendicular to) the cell faces. The terms associated with T_{ab} are the flows caused by the gradients along (that is, parallel or tangential to) the cell faces and the horizontal anisotropy, which produces flow across the cell face because of the T_{ab} term. (also discussed in connection with eq. 6)

The transmissivity tensor T in the ξ - η coordinate system relates to the transmissivity tensor T' in the x - y system as:

$$\begin{aligned}
T_{aa_{j,i,k}} &= T'_{xx_{j,i,k}} \left(\frac{\Delta c_i}{\Delta r_j} \right) \\
T_{ab_{j,i,k}} &= T'_{xy_{j,i,k}} \\
T_{bb_{j,i,k}} &= T'_{yy_{j,i,k}} \left(\frac{\Delta r_j}{\Delta c_i} \right)
\end{aligned} \tag{B-7}$$

where

Δc_i is the cell width of row i [L],

Δr_j is the cell width of column j [L],

$$\begin{aligned}
T'_{xx_{j,i,k}} &= \frac{T'_{maj_{j,i,k}} + T'_{min_{j,i,k}}}{2} + \frac{T'_{maj_{j,i,k}} - T'_{min_{j,i,k}}}{2} \cos(2\theta_{j,i,k}) \text{ [L}^2\text{/T]}, \\
T'_{xy_{j,i,k}} &= \frac{T'_{maj_{j,i,k}} - T'_{min_{j,i,k}}}{2} \sin(2\theta_{j,i,k}) \text{ [L}^2\text{/T]}, \\
T'_{yy_{j,i,k}} &= \frac{T'_{maj_{j,i,k}} + T'_{min_{j,i,k}}}{2} - \frac{T'_{maj_{j,i,k}} - T'_{min_{j,i,k}}}{2} \cos(2\theta_{j,i,k}) \text{ [L}^2\text{/T]},
\end{aligned}$$

and

$T'_{maj_{j,i,k}}$ is the transmissivity along the major axis of the anisotropy ellipse [L²/T],

$T'_{min_{j,i,k}}$ is the transmissivity along the minor axis of the anisotropy ellipse [L²/T],

defined as $T'_{maj_{j,i,k}} HANI_{j,i,k}$,

$HANI_{j,i,k}$ is the horizontal anisotropy ratio [-],

$\theta_{j,i,k}$ is the angle between the principal axis of anisotropy and the model grid, where clockwise is a positive angle, values can range from -90 to 90 degrees, and

$\theta_{j,i,k}$ is defined as $\sum \theta_l m_l_{j,i,k}$,

θ_l is the value of the variable-direction horizontal anisotropy parameter l , and

$m_l_{j,i,k}$ is the multiplication factor for the variable-direction horizontal anisotropy parameter l .

Defining $\theta_{j,i,k}$ as $\sum \theta_l m_l_{j,i,k}$ allows the angle to be defined using additive parameters, as

described by Harbaugh and others (2000, p. 16-19). The option of defining $\theta_{j,i,k}$ using additive parameters is available because nearly all parameters defined in MODFLOW-2000 are additive. It is not expected that this option will be used in many applications.

Finite-Difference Equations for Flow

Each integral in equation B-6 defines the flow across one cell face. To form the mass conservation equations for the entire finite-difference grid, equation B-6 needs to be further developed. This is done first by evaluating flow in one dimension and focusing on some basic ideas and the terms with gradients that are normal to the cell faces. The one-dimensional analysis

also yields the harmonic mean conductance terms developed by McDonald and Harbaugh (1988). After the one-dimension discussion, flow in two dimensions is discussed.

Flow Equations in One Dimension

The one-dimensional classical cell-centered approximation to the flow through a cell boundary in terms of the nodal hydraulic heads can be used to present some ideas and concepts needed in the formulation for the general anisotropic two-dimensional case discussed in this report. From figure B-3, the flow per unit width through the cell boundary at $j+1/2$ is given by

$$F_{j+1/2} = -\frac{T_{j+1/2}(h_{j+1} - h_j)}{\frac{1}{2}(\Delta r_j + \Delta r_{j+1})} \quad (\text{B-8})$$

where

$F_{j+1/2}$ is the flow per unit width through the cell boundary at $j+1/2$ [$L^3/T-L$], and

Δr_j is the length of cell j and $(\frac{1}{2}(\Delta r_j + \Delta r_{j+1}))$ is the distance between nodes j and $j+1$ [L].

Figure B-3 also shows the piecewise linear variation for hydraulic head.

Here, transmissivity, T , is piecewise constant over a cell, the flow and the hydraulic heads are continuous across the cell boundary, and the gradient of the head is discontinuous across the cell boundary. By introducing an intermediate unknown head, h_f at the cell face, an equation for flow continuity can be written for the flow per unit width as

$$-\frac{T_j(h_f - h_j)}{\frac{1}{2}\Delta r_j} = -\frac{T_{j+1}(h_{j+1} - h_f)}{\frac{1}{2}\Delta r_{j+1}} \quad (\text{B-9})$$

Equation B-9 can be solved for the intermediate hydraulic head at the cell face yielding

$$h_f = \frac{h_j T_j / \Delta r_j + h_{j+1} T_{j+1} / \Delta r_{j+1}}{T_j / \Delta r_j + T_{j+1} / \Delta r_{j+1}} \quad (\text{B-10})$$

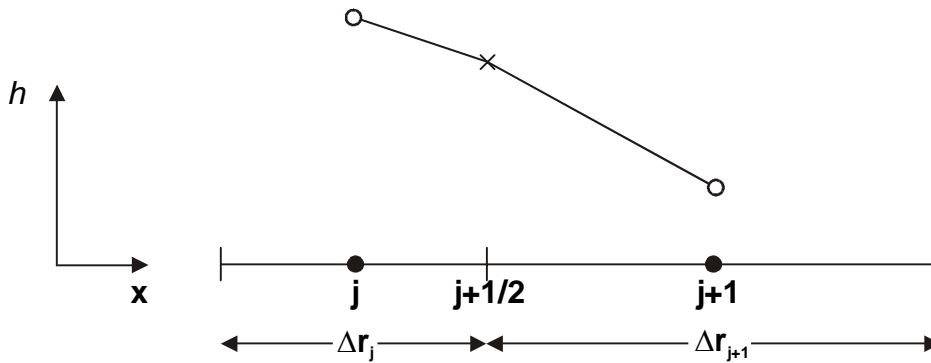


Figure B-3. One-dimensional cells with piecewise linear hydraulic-head variation.

Substituting equation B-10 into the left-hand side of equation B-9 and equating with $F_{j+1/2}$, then comparing with equation B-8 gives the classical finite-difference approximation for the flow per unit width at the cell face:

$$F_{j+\frac{1}{2}} = \frac{-2T_j T_{j+1}}{T_j \Delta r_{j+1} + T_{j+1} \Delta r_j} (h_{j+1} - h_j) \quad (\text{B-11})$$

Using the terminology of McDonald and Harbaugh (1988), the fraction on the right-hand side of equation B-11 is the conductance per unit width of the cell, and equals the harmonic mean of the transmissivity of the two cells connected at $j + \frac{1}{2}$.

To prepare for two-dimensional equations, note that part of the mapping defined in equation B-5 can be used to map a chain of one-dimensional cells into a chain of cells of unit length. The piecewise linear basis functions can be used to define a continuous variation in hydraulic head as:

$$h = 2(1 - \xi)h_j + 2(\xi - \frac{1}{2})h_f; \quad \frac{1}{2} \leq \xi \leq 1 \quad \text{in cell } j; \quad (\text{B-12.1})$$

$$h = (1 - 2\xi)h_f + 2\xi h_{j+1}; \quad 0 \leq \xi \leq \frac{1}{2} \quad \text{in cell } j+1. \quad (\text{B-12.2})$$

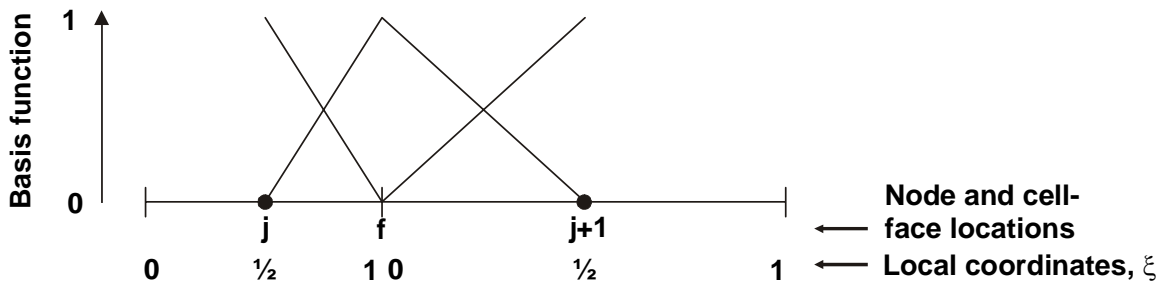


Figure B-4. Piecewise-linear basis functions. Global finite-difference nodes j and $j+1$ are shown with f , the location of the finite-difference cell boundary. Local coordinates which range from 0 to 1 for each cell also are shown

In figure B-4, the basis functions from equation B-12.1 are drawn for cell j and the basis functions from equation B-12.2 are drawn for cell $j+1$. The basis function multiplying h_j in equation B-12.1 varies from 1 at node j to 0 at cell boundary f in figure B-4, the basis function multiplying h_f in equation B-12.1 varies from 0 at node j to 1 at cell boundary f in figure B-4, and so on. Figure B-4, therefore, shows the basis functions covering the region accounted for by one of the conductance terms of the type shown in equation B-11. Basis functions could be avoided when considering flow in one dimension, but are important when considering flow in two dimensions.

Flow Equations in Two Dimensions

In two dimensions the role of the piecewise linear basis functions in one dimension for hydraulic head is played by linear triangular basis functions, and the areas of coverage are shown in figure B-5. The areas of coverage possess piecewise constant spatial gradients. After introducing one additional hydraulic head unknown at each face of each cell, local triangular basis functions are used over each quarter of a cell with a piecewise linear hydraulic head. Figure

B-5 shows a cell and its eight neighbors in the unit-square ξ - η coordinate system with the active support triangles for the hydraulic head shown as shaded. For notational convenience, the local nine-cell numbering scheme shown in figure B-5 is used in the following equations. The global (j,i) indexing can be restored at the end of the equation development.

A typical triangle from cell 1 with corner labels and adjoining triangles is shown in figure B-6. Representation of hydraulic head h and the unit-square cell coordinates ξ and η using the piecewise linear basis functions over the shaded triangle in cell 1 are given by

$$h = (1 - u - v)h_1 + uh_s + vh_w \quad (\text{B-13.1})$$

$$\begin{aligned} \xi &= (1 - u - v)x_1 + ux_s + vx_w \\ &= (1 - u)x_1 + ux_s \end{aligned} \quad (\text{B-13.2})$$

$$\begin{aligned} \eta &= (1 - u - v)y_1 + uy_s + vy_w \\ &= (1 - v)y_1 + vy_w \end{aligned} \quad (\text{B-13.3})$$

where

ξ, η are the coordinates in the unit-square cell system mapping;
 u, v are the local area coordinates for the shaded triangle in cell 1 in figure B-6.

The subscripts define locations shown in figure B-6. Local coordinate u increases linearly from 0 at the cell center to 1 at cell boundary S; v increases linearly from 0 at the cell center to 1 at cell boundary W. The local area coordinate system used here is from Norrie and De Vries (1973, p. 86). This is the fourth and final coordinate system used in this report; all the coordinate systems are listed in Table 2.

Hydraulic head is continuous over each triangle in figure B-5 or B-6 and also continuous at the common vertices. Using the N, S, E, and W notation of figure B-6, local gradients of potential can be determined using equation B-13.1. For example, for the shaded triangle of cell 1 in figure B-13.1:

$$h_\xi = 2(h_s - h_1) \quad (\text{B-14.1})$$

$$h_\eta = 2(h_w - h_1) \quad (\text{B-14.2})$$

where h_ξ and h_η are gradients of head in the ξ and η directions, and $h_s, h_1,$ and h_w are the heads at locations 1, S, and W in figure B-6. The 2 occurs in equations B-14 because the length between h_1 and either h_s or h_w is $\frac{1}{2}$ of the unit square. Introduction of the hydraulic heads at the cell faces enables flow across the cell faces (normal flow) and the hydraulic head at the cell faces to be point-wise continuous. The normal flow is continuous, but the tangential flow may be discontinuous across a cell face.

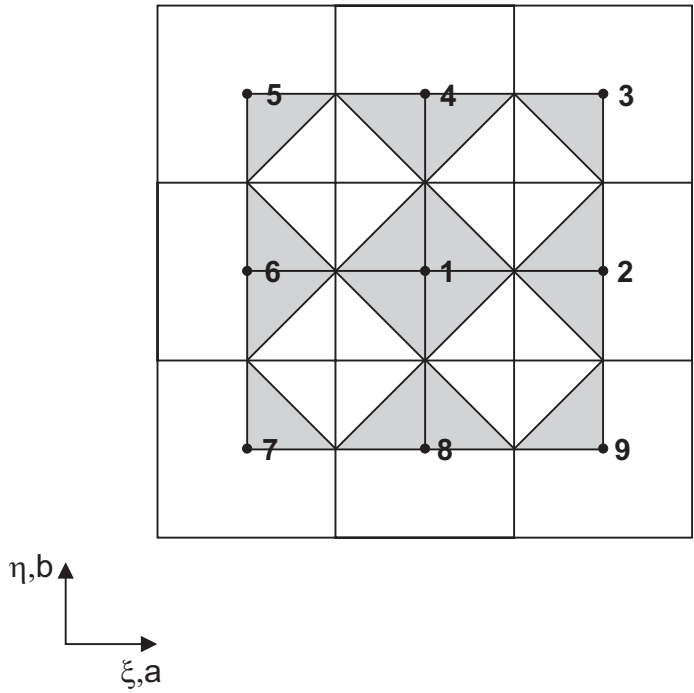


Figure B-5. Unit-square grid with areas covered by piecewise linear triangular basis functions shaded gray.

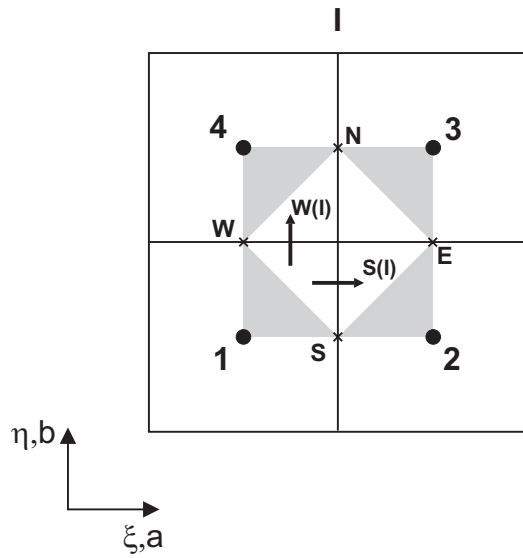


Figure B-6. Areas covered by the triangular basis functions associated with the $j+\frac{1}{2}$ and $i+\frac{1}{2}$ faces of cell 1. For convenient referencing in the text, the four added nodes on the sides of the finite-difference cells are labeled N (north), S (south), E (east), and W (west). The I at the top of the figure identifies this set of four cells as cell 1 of figure B-5 plus bordering cells 2, 3, and 4.

Table 2. Coordinate system notation used in this report

Shape of cells	Rectangle	Unit square
Global coordinates	xy	
Local spatial coordinates (range from 0 to 1 from one side of the cell to the other). The two sets are equivalent, but the ab set is retained to conform with the notation of Edwards and Rogers (1998).		ab, $\xi\eta$
Local area coordinates (range from 0 to 1 from the cell center to the sides of the cell)		uv

Flow Continuity for the General Anisotropic Tensor

Figure B-5 shows the nine cells that control triangular basis-function support for a representative interior cell in the transformed domain of a uniform square grid. To impose normal flow continuity while accounting for tangential flows, eight flows are defined for the central cell and are shown in figure B-7. These flows are formulated by taking four subsets with four cells each of the nine cells of figure B-5. Figure B-8 shows all four subsets of four cells with each location of the additional hydraulic heads denoted by an X; a set of four cells with the triangular areas of defined basis functions is shown in figure B-6. Each subset of cells actually has four additional hydraulic head locations on the cell boundaries, but only the locations pertaining to cell 1 appear in figure B-8.

The four cell-face hydraulic heads for cell 1 are introduced at the locations denoted N,S,E,W in figures B-6 and B-8. They are located on each cell face at the midpoint. Other locations are possible (Edwards and Rogers, 1998), but will not be considered for this development. The location chosen has the advantage of producing a symmetrical A matrix in equations 8 and B-25. The locations shown also have the advantage of producing the standard 5-point difference equations in the case of a diagonal hydraulic-conductivity tensor, which results if the principal axes of anisotropy are aligned with the coordinate axes.

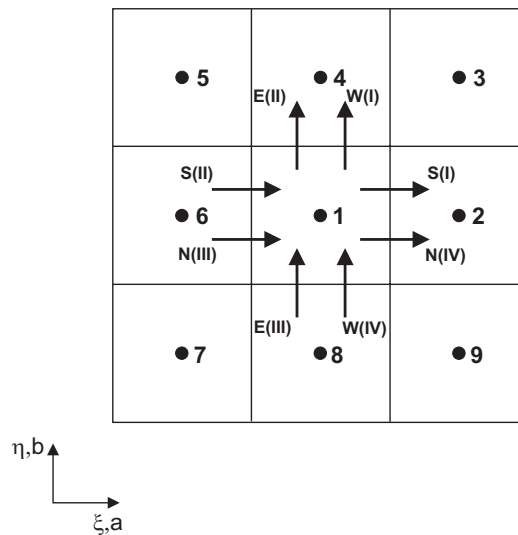


Figure B-7. Control volume quadrant flows.

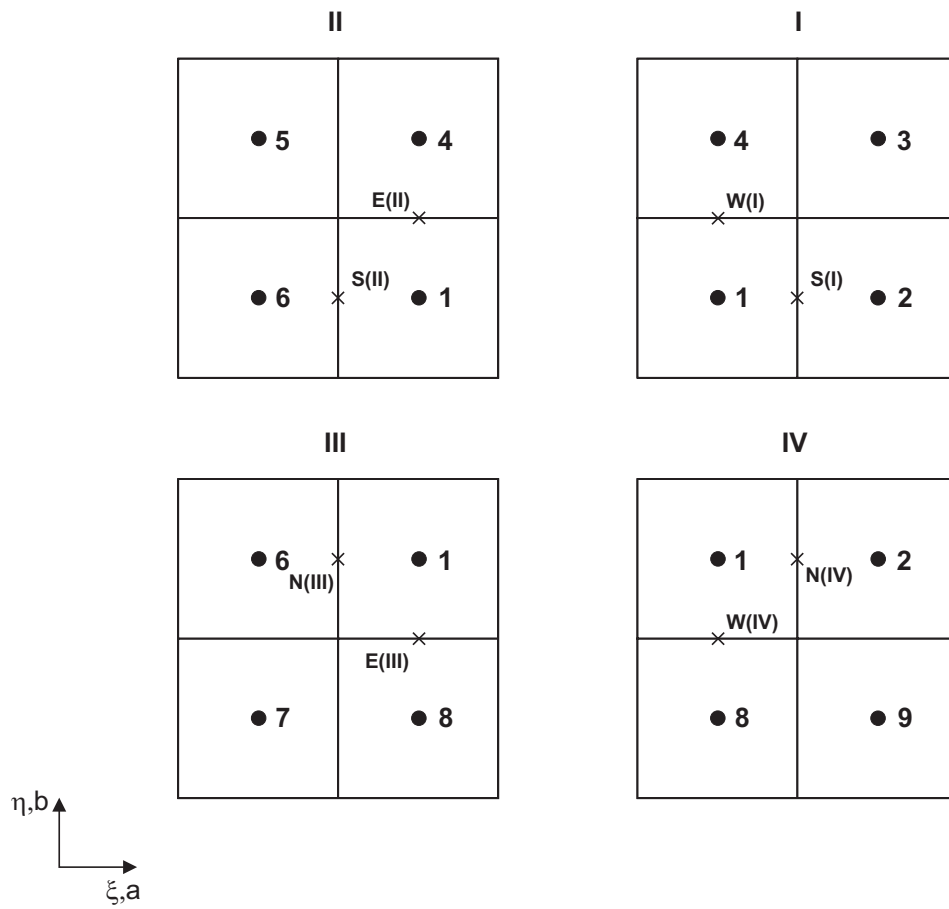


Figure B-8. Four subsets of the nine-cell grid associated with cell 1. Locations of additional hydraulic heads are marked by 'x's. Subset I was also shown in figure B-6

When continuity of normal flow is imposed across the four cell faces, and using the four points (N,S,E,W) at which the hydraulic head is specified as continuous, the flow continuity conditions for figure B-6 written as functions of unit length of cell boundary are given by

$$\text{W(I): } -(T_{aa}h_\xi + T_{ab}h_\eta) \Big|_S^1 = -(T_{aa}h_\xi + T_{ab}h_\eta) \Big|_S^2 \quad (\text{B-15.1})$$

$$\text{S(I): } -(T_{aa}h_\xi + T_{ab}h_\eta) \Big|_N^3 = -(T_{aa}h_\xi + T_{ab}h_\eta) \Big|_N^4 \quad (\text{B-15.2})$$

$$\text{E(I): } -(T_{ab}h_\xi + T_{bb}h_\eta) \Big|_E^2 = -(T_{ab}h_\xi + T_{bb}h_\eta) \Big|_E^3 \quad (\text{B-15.3})$$

$$\text{N(I): } -(T_{ab}h_\xi + T_{bb}h_\eta) \Big|_W^1 = -(T_{ab}h_\xi + T_{bb}h_\eta) \Big|_W^4 \quad (\text{B-15.4})$$

Substituting from equation B-14 and similar ones (not shown) for the other cells and noting that the cell width for the unit square is 1 yields the following equations for cell subset I of figure B-8, which also is shown in figure B-6.

$$-(T_{aa}^1 2(h_S - h_1) + T_{ab}^1 2(h_W - h_1)) = -(T_{aa}^2 2(h_2 - h_S) + T_{ab}^2 2(h_E - h_2)) \quad (\text{B-16.1})$$

$$-(T_{aa}^3 2(h_3 - h_N) + T_{ab}^3 2(h_3 - h_E)) = -(T_{aa}^4 2(h_N - h_4) + T_{ab}^4 2(h_4 - h_W)) \quad (\text{B-16.2})$$

$$-(T_{ab}^2 2(h_2 - h_S) + T_{bb}^2 2(h_E - h_2)) = -(T_{ab}^3 2(h_3 - h_N) + T_{bb}^3 2(h_3 - h_E)) \quad (\text{B-16.3})$$

$$-(T_{ab}^1 2(h_S - h_1) + T_{bb}^1 2(h_W - h_1)) = -(T_{ab}^4 2(h_N - h_4) + T_{bb}^4 2(h_4 - h_W)) \quad (\text{B-16.4})$$

Similar equations can be written for the other three subsets of four cells of figure B-8. Each set of four equations can be solved simultaneously for the four introduced hydraulic heads at the cell faces. The solution for equation set B-16 is given by

$$\begin{aligned} h_S = \left(\frac{1}{D} \right) \{ & [(T_{aa}^3 + T_{aa}^4)(T_{bb}^1 + T_{bb}^4)(T_{bb}^2 + T_{bb}^3) - (T_{ab}^3)^2(T_{bb}^1 + T_{bb}^4) - (T_{ab}^4)^2(T_{bb}^2 + T_{bb}^3)](T_{aa}^1 + T_{ab}^1) \\ & + [(T_{ab}^1(T_{ab}^3)^2 - T_{ab}^1(T_{aa}^3 + T_{aa}^4)(T_{bb}^2 + T_{bb}^3) - T_{ab}^2 T_{ab}^3 T_{ab}^4](T_{bb}^1 + T_{ab}^1)h_1 \\ & + [(T_{aa}^3 + T_{aa}^4)(T_{bb}^1 + T_{bb}^4)(T_{bb}^2 + T_{bb}^3) - (T_{ab}^3)^2(T_{bb}^1 + T_{bb}^4) - (T_{ab}^4)^2(T_{bb}^2 + T_{bb}^3)](T_{aa}^2 - T_{ab}^2) \\ & + [T_{ab}^1 T_{ab}^3 T_{ab}^4 + T_{ab}^2(T_{aa}^3 + T_{aa}^4)(T_{bb}^1 + T_{bb}^4) - T_{ab}^2(T_{ab}^4)^2](T_{bb}^2 - T_{ab}^2)h_2 \\ & + [(-T_{ab}^1 T_{ab}^4(T_{bb}^2 + T_{bb}^3) - T_{ab}^2 T_{ab}^3(T_{bb}^1 + T_{bb}^4)](T_{aa}^3 + T_{ab}^3) \\ & + [T_{ab}^1 T_{ab}^3 T_{ab}^4 + T_{ab}^2(T_{aa}^3 + T_{aa}^4)(T_{bb}^1 + T_{bb}^4) - T_{ab}^2(T_{ab}^4)^2](T_{bb}^3 + T_{ab}^3)h_3 \\ & + [(-T_{ab}^1 T_{ab}^4(T_{bb}^2 + T_{bb}^3) - T_{ab}^2 T_{ab}^3(T_{bb}^1 + T_{bb}^4)](T_{aa}^4 - T_{ab}^4) \\ & + [T_{ab}^1(T_{ab}^3)^2 - T_{ab}^1(T_{aa}^3 + T_{aa}^4)(T_{bb}^2 + T_{bb}^3) - T_{ab}^2 T_{ab}^3 T_{ab}^4](T_{bb}^4 - T_{ab}^4)h_4 \} \end{aligned} \quad (\text{B-17.1})$$

$$\begin{aligned}
h_E = & \left(\frac{1}{D} \right) \left\{ ([T_{ab}^1 T_{ab}^3 T_{ab}^4 + T_{ab}^2 (T_{aa}^3 + T_{aa}^4)(T_{bb}^1 + T_{bb}^4) - T_{ab}^2 (T_{ab}^4)^2](T_{aa}^1 + T_{ab}^1) \right. \\
& + [-T_{ab}^1 T_{ab}^2 (T_{aa}^3 + T_{aa}^4) - T_{ab}^3 T_{ab}^4 (T_{aa}^1 + T_{aa}^2)](T_{bb}^1 + T_{ab}^1) h_1 \\
& + ([T_{ab}^1 T_{ab}^3 T_{ab}^4 + T_{ab}^2 (T_{aa}^3 + T_{aa}^4)(T_{bb}^1 + T_{bb}^4) - T_{ab}^2 (T_{ab}^4)^2](T_{aa}^2 - T_{ab}^2) \\
& + [(T_{aa}^1 + T_{aa}^2)(T_{aa}^3 + T_{aa}^4)(T_{bb}^1 + T_{bb}^4) - (T_{ab}^1)^2 (T_{aa}^3 + T_{aa}^4) - (T_{ab}^4)^2 (T_{aa}^1 + T_{aa}^2)](T_{bb}^2 - T_{ab}^2) h_2 \\
& + [(T_{ab}^1)^2 T_{ab}^3 - T_{ab}^3 (T_{aa}^1 + T_{aa}^2)(T_{bb}^1 + T_{bb}^4) - T_{ab}^1 T_{ab}^2 T_{ab}^4](T_{aa}^3 + T_{ab}^3) \\
& + [(T_{aa}^1 + T_{aa}^2)(T_{aa}^3 + T_{aa}^4)(T_{bb}^1 + T_{bb}^4) - (T_{ab}^1)^2 (T_{aa}^3 + T_{aa}^4) - (T_{ab}^4)^2 (T_{aa}^1 + T_{aa}^2)](T_{bb}^3 + T_{ab}^3) h_3 \\
& + [(T_{ab}^1)^2 T_{ab}^3 - T_{ab}^3 (T_{aa}^1 + T_{aa}^2)(T_{bb}^1 + T_{bb}^4) - T_{ab}^1 T_{ab}^2 T_{ab}^4](T_{aa}^4 - T_{ab}^4) \\
& + [-T_{ab}^1 T_{ab}^2 (T_{aa}^3 + T_{aa}^4) - T_{ab}^3 T_{ab}^4 (T_{aa}^1 + T_{aa}^2)](T_{bb}^4 - T_{ab}^4) h_4 \left. \right\}
\end{aligned} \tag{B-17.2}$$

$$\begin{aligned}
h_N = & \left(\frac{1}{D} \right) \left\{ ([-T_{ab}^1 T_{ab}^4 (T_{bb}^2 + T_{bb}^3) - T_{ab}^2 T_{ab}^3 (T_{bb}^1 + T_{bb}^4)](T_{aa}^1 + T_{ab}^1) \right. \\
& + [T_{ab}^1 T_{ab}^2 T_{ab}^3 + T_{ab}^4 (T_{aa}^1 + T_{aa}^2)(T_{bb}^2 + T_{bb}^3) - (T_{ab}^2)^2 T_{ab}^4](T_{bb}^1 + T_{ab}^1) h_1 \\
& + ([-T_{ab}^1 T_{ab}^4 (T_{bb}^2 + T_{bb}^3) - T_{ab}^2 T_{ab}^3 (T_{bb}^1 + T_{bb}^4)](T_{aa}^2 - T_{ab}^2) \\
& + [(T_{ab}^1)^2 T_{ab}^3 - T_{ab}^1 T_{ab}^2 T_{ab}^4 - T_{ab}^3 (T_{aa}^1 + T_{aa}^2)(T_{bb}^1 + T_{bb}^4)](T_{bb}^2 - T_{ab}^2) h_2 \\
& + [(T_{aa}^1 + T_{aa}^2)(T_{bb}^1 + T_{bb}^4)(T_{bb}^2 + T_{bb}^3) - (T_{ab}^1)^2 (T_{bb}^2 + T_{bb}^3) - (T_{ab}^2)^2 (T_{bb}^1 + T_{bb}^4)](T_{aa}^3 + T_{ab}^3) \\
& + [(T_{ab}^1)^2 T_{ab}^3 - T_{ab}^1 T_{ab}^2 T_{ab}^4 - T_{ab}^3 (T_{aa}^1 + T_{aa}^2)(T_{bb}^1 + T_{bb}^4)](T_{bb}^3 - T_{ab}^3) h_3 \\
& + [(T_{aa}^1 + T_{aa}^2)(T_{bb}^1 + T_{bb}^4)(T_{bb}^2 + T_{bb}^3) - (T_{ab}^1)^2 (T_{bb}^2 + T_{bb}^3) - (T_{ab}^2)^2 (T_{bb}^1 + T_{bb}^4)](T_{aa}^4 - T_{ab}^4) \\
& + [T_{ab}^1 T_{ab}^2 T_{ab}^3 + T_{ab}^4 (T_{aa}^1 + T_{aa}^2)(T_{bb}^2 + T_{bb}^3) - (T_{ab}^2)^2 T_{ab}^4](T_{bb}^4 - T_{ab}^4) h_4 \left. \right\}
\end{aligned} \tag{B-17.3}$$

$$\begin{aligned}
h_W = & \left(\frac{1}{D} \right) \left\{ ([T_{ab}^1 (T_{ab}^3)^2 - T_{ab}^2 T_{ab}^3 T_{ab}^4 - T_{ab}^1 (T_{aa}^3 + T_{aa}^4)(T_{bb}^2 + T_{bb}^3)](T_{aa}^1 + T_{ab}^1) \right. \\
& + [(T_{aa}^1 + T_{aa}^2)(T_{aa}^3 + T_{aa}^4)(T_{bb}^2 + T_{bb}^3) - (T_{ab}^2)^2 (T_{aa}^3 + T_{aa}^4) - (T_{ab}^3)^2 (T_{aa}^1 + T_{aa}^2)](T_{bb}^1 + T_{ab}^1) h_1 \\
& + ([T_{ab}^1 (T_{ab}^3)^2 - T_{ab}^2 T_{ab}^3 T_{ab}^4 - T_{ab}^1 (T_{aa}^3 + T_{aa}^4)(T_{bb}^2 + T_{bb}^3)](T_{aa}^2 - T_{ab}^2) \\
& + [-T_{ab}^1 T_{ab}^2 (T_{aa}^3 + T_{aa}^4) - T_{ab}^3 T_{ab}^4 (T_{aa}^1 + T_{aa}^2)](T_{bb}^2 - T_{ab}^2) h_2 \\
& + [(T_{ab}^1 T_{ab}^2 T_{ab}^3 + T_{ab}^4 (T_{aa}^1 + T_{aa}^2)(T_{bb}^2 + T_{bb}^3) - (T_{ab}^2)^2 T_{ab}^4](T_{aa}^3 + T_{ab}^3) \\
& + [-T_{ab}^1 T_{ab}^2 (T_{aa}^3 + T_{aa}^4) - T_{ab}^3 T_{ab}^4 (T_{aa}^1 + T_{aa}^2)](T_{bb}^3 + T_{ab}^3) h_3 \\
& + [(T_{ab}^1 T_{ab}^2 T_{ab}^3 + T_{ab}^4 (T_{aa}^1 + T_{aa}^2)(T_{bb}^2 + T_{bb}^3) - (T_{ab}^2)^2 T_{ab}^4](T_{aa}^4 - T_{ab}^4) \\
& + [(T_{aa}^1 + T_{aa}^2)(T_{aa}^3 + T_{aa}^4)(T_{bb}^2 + T_{bb}^3) - (T_{ab}^2)^2 (T_{aa}^3 + T_{aa}^4) - (T_{ab}^3)^2 (T_{aa}^1 + T_{aa}^2)](T_{bb}^4 - T_{ab}^4) h_4 \left. \right\}
\end{aligned} \tag{B-17.4}$$

where

$$\begin{aligned}
D &= (T_{ab}^1 T_{ab}^3 - T_{ab}^2 T_{ab}^4)^2 \\
&+ (T_{aa}^1 + T_{aa}^2)(T_{aa}^3 + T_{aa}^4)(T_{bb}^1 + T_{bb}^4)(T_{bb}^2 + T_{bb}^3) \\
&- (T_{ab}^1)^2 (T_{aa}^3 + T_{aa}^4)(T_{bb}^2 + T_{bb}^3) - (T_{ab}^2)^2 (T_{aa}^3 + T_{aa}^4)(T_{bb}^1 + T_{bb}^4) \\
&- (T_{ab}^3)^2 (T_{aa}^1 + T_{aa}^2)(T_{bb}^1 + T_{bb}^4) - (T_{ab}^4)^2 (T_{aa}^1 + T_{aa}^2)(T_{bb}^2 + T_{bb}^3)
\end{aligned} \tag{B-17.5}$$

Flow Terms in the Finite-Difference Equation

As shown in figure B-7, there are eight cell-face contributions to the flow for control-volume cell 1. To form the finite-difference approximation to equation B-1, the following terms need to be represented in the x-y plane.

$$F_{j+\frac{1}{2},i} = F_{N(IV)} + F_{S(I)} \tag{B-18.1}$$

$$F_{j,i+\frac{1}{2}} = F_{E(II)} + F_{W(I)} \tag{B-18.2}$$

$$F_{j-\frac{1}{2},i} = F_{N(III)} + F_{S(II)} \tag{B-18.3}$$

$$F_{j,i-\frac{1}{2}} = F_{E(III)} + F_{W(IV)} \tag{B-18.4}$$

where $F_{d(n)}$ terms represent the flow rate at the cell boundary, and d is $N, S, E,$ or W and n is $I, II, III,$ or IV . The subscripts N, S, E, W refer to figure B-7, and the quadrant numbers I, II, III, IV refer to the four positions of the sub-sets of the nine-cell grid shown in figure B-8. The flow components on the right-hand sides of equations B-18 can be approximated by difference equations involving the nodal hydraulic heads and the additional hydraulic heads at the cell faces.

$$F_{S(I)} = -T_{aa}^1 (h_{S(I)} - h_1) - T_{ab}^1 (h_{W(I)} - h_1) \tag{B-19.1}$$

$$F_{W(I)} = -T_{ab}^1 (h_{S(I)} - h_1) - T_{bb}^1 (h_{W(I)} - h_1) \tag{B-19.2}$$

$$F_{S(II)} = -T_{aa}^1 (h_1 - h_{S(II)}) - T_{ab}^1 (h_{E(II)} - h_1) \tag{B-19.3}$$

$$F_{E(II)} = -T_{ab}^1 (h_1 - h_{S(II)}) - T_{bb}^1 (h_{E(II)} - h_1) \tag{B-19.4}$$

$$F_{E(III)} = -T_{ab}^1 (h_1 - h_{N(III)}) - T_{bb}^1 (h_1 - h_{E(III)}) \tag{B-19.5}$$

$$F_{N(III)} = -T_{aa}^1 (h_1 - h_{N(III)}) - T_{ab}^1 (h_1 - h_{E(III)}) \tag{B-19.6}$$

$$F_{W(IV)} = -T_{ab}^1 (h_{N(IV)} - h_1) - T_{bb}^1 (h_1 - h_{W(IV)}) \tag{B-19.7}$$

$$F_{N(IV)} = -T_{aa}^1 (h_{N(IV)} - h_1) - T_{ab}^1 (h_1 - h_{W(IV)}) \tag{B-19.8}$$

The factors of 2 in equations like B-14 are canceled by the cell-boundary length associated with each F term of equations B-18 being exactly $\frac{1}{2}$. The eight flows in equations B-19 can be expressed in terms of only the cell (node) hydraulic heads by eliminating the potentials at the cell

faces using equation B-17 for quadrant I and similar equations obtained by permuting the indices of cell numbers for quadrants II through IV. Then

$$F_{S(I)} = -T_{aa}^1 (a_{S1}(1,2,3,4)h_1 + a_{S2}(1,2,3,4)h_2 + a_{S3}(1,2,3,4)h_3 + a_{S4}(1,2,3,4)h_4 - h_1) - T_{ab}^1 (a_{W1}(1,2,3,4)h_1 + a_{W2}(1,2,3,4)h_2 + a_{W3}(1,2,3,4)h_3 + a_{W4}(1,2,3,4)h_4 - h_1) \quad (\text{B-20.1})$$

$$F_{W(I)} = -T_{ab}^1 (a_{S1}(1,2,3,4)h_1 + a_{S2}(1,2,3,4)h_2 + a_{S3}(1,2,3,4)h_3 + a_{S4}(1,2,3,4)h_4 - h_1) - T_{bb}^1 (a_{W1}(1,2,3,4)h_1 + a_{W2}(1,2,3,4)h_2 + a_{W3}(1,2,3,4)h_3 + a_{W4}(1,2,3,4)h_4 - h_1) \quad (\text{B-20.2})$$

$$F_{S(II)} = -T_{aa}^1 (h_1 - (a_{S1}(6,1,4,5)h_6 + a_{S2}(6,1,4,5)h_1 + a_{S3}(6,1,4,5)h_4 + a_{S4}(6,1,4,5)h_5)) - T_{ab}^1 (a_{E1}(6,1,4,5)h_6 + a_{E2}(6,1,4,5)h_1 + a_{E3}(6,1,4,5)h_4 + a_{E4}(6,1,4,5)h_5 - h_1) \quad (\text{B-20.3})$$

$$F_{E(II)} = -T_{ab}^1 (h_1 - (a_{S1}(6,1,4,5)h_6 + a_{S2}(6,1,4,5)h_1 + a_{S3}(6,1,4,5)h_4 + a_{S4}(6,1,4,5)h_5)) - T_{bb}^1 (a_{E1}(6,1,4,5)h_6 + a_{E2}(6,1,4,5)h_1 + a_{E3}(6,1,4,5)h_4 + a_{E4}(6,1,4,5)h_5 - h_1) \quad (\text{B-20.4})$$

$$F_{E(III)} = -T_{ab}^1 (h_1 - (a_{N1}(7,8,1,6)h_7 + a_{N2}(7,8,1,6)h_8 + a_{N3}(7,8,1,6)h_1 + a_{N4}(7,8,1,6)h_6)) - T_{bb}^1 (h_1 - (a_{E1}(7,8,1,6)h_7 + a_{E2}(7,8,1,6)h_8 + a_{E3}(7,8,1,6)h_1 + a_{E4}(7,8,1,6)h_6)) \quad (\text{B-20.5})$$

$$F_{N(III)} = -T_{aa}^1 (h_1 - (a_{N1}(7,8,1,6)h_7 + a_{N2}(7,8,1,6)h_8 + a_{N3}(7,8,1,6)h_1 + a_{N4}(7,8,1,6)h_6)) - T_{ab}^1 (h_1 - (a_{E1}(7,8,1,6)h_7 + a_{E2}(7,8,1,6)h_8 + a_{E3}(7,8,1,6)h_1 + a_{E4}(7,8,1,6)h_6)) \quad (\text{B-20.6})$$

$$F_{W(IV)} = -T_{ab}^1 (a_{N1}(8,9,2,1)h_8 + a_{N2}(8,9,2,1)h_9 + a_{N3}(8,9,2,1)h_2 + a_{N4}(8,9,2,1)h_1 - h_1) - T_{bb}^1 (h_1 - (a_{W1}(8,9,2,1)h_8 + a_{W2}(8,9,2,1)h_9 + a_{W3}(8,9,2,1)h_2 + a_{W4}(8,9,2,1)h_1)) \quad (\text{B-20.7})$$

$$F_{N(IV)} = -T_{aa}^1 (a_{N1}(8,9,2,1)h_8 + a_{N2}(8,9,2,1)h_9 + a_{N3}(8,9,2,1)h_2 + a_{N4}(8,9,2,1)h_1 - h_1) - T_{ab}^1 (h_1 - (a_{W1}(8,9,2,1)h_8 + a_{W2}(8,9,2,1)h_9 + a_{W3}(8,9,2,1)h_2 + a_{W4}(8,9,2,1)h_1)) \quad (\text{B-20.8})$$

where the coefficients can be expressed generally as $a_{dm}(n_1, n_2, n_3, n_4)$, and d is N, S, E , or W , m is $1, 2, 3$, or 4 , and each of the n_i are integer values between 1 and 9. Equations for the $a_{dm}(n_1, n_2, n_3, n_4)$ coefficients are:

For quadrant I:

$$a_{S1}(1,2,3,4) = \left(\frac{1}{D(1,2,3,4)} \right) \left\{ [(T_{aa}^3 + T_{aa}^4)(T_{bb}^1 + T_{bb}^4)(T_{bb}^2 + T_{bb}^3) - (T_{ab}^3)^2(T_{bb}^1 + T_{bb}^4) - (T_{ab}^4)^2(T_{bb}^2 + T_{bb}^3)](T_{aa}^1 + T_{ab}^1) + [(T_{ab}^1(T_{ab}^3)^2 - T_{ab}^1(T_{aa}^3 + T_{aa}^4)(T_{bb}^2 + T_{bb}^3) - T_{ab}^2 T_{ab}^3 T_{ab}^4)](T_{bb}^1 + T_{ab}^1) \right\} \quad (\text{B-21.1})$$

$$a_{S2}(1,2,3,4) = \left(\frac{1}{D(1,2,3,4)} \right) \left\{ [(T_{aa}^3 + T_{aa}^4)(T_{bb}^1 + T_{bb}^4)(T_{bb}^2 + T_{bb}^3) - (T_{ab}^3)^2(T_{bb}^1 + T_{bb}^4) - (T_{ab}^4)^2(T_{bb}^2 + T_{bb}^3)](T_{aa}^2 - T_{ab}^2) + [(T_{ab}^1 T_{ab}^3 T_{ab}^4 + T_{ab}^2(T_{aa}^3 + T_{aa}^4)(T_{bb}^1 + T_{bb}^4) - T_{ab}^2(T_{ab}^4)^2)](T_{bb}^2 - T_{ab}^2) \right\} \quad (\text{B-21.2})$$

$$a_{S_3}(1,2,3,4) = \left(\frac{1}{D(1,2,3,4)} \right) \left\{ [-T_{ab}^1 T_{ab}^4 (T_{bb}^2 + T_{bb}^3) - T_{ab}^2 T_{ab}^3 (T_{bb}^1 + T_{bb}^4)] (T_{aa}^3 + T_{ab}^3) \right. \\ \left. + [T_{ab}^1 T_{ab}^3 T_{ab}^4 + T_{ab}^2 (T_{aa}^3 + T_{aa}^4) (T_{bb}^1 + T_{bb}^4) - T_{ab}^2 (T_{ab}^4)^2] (T_{bb}^3 + T_{ab}^3) \right\} \quad (\text{B-21.3})$$

$$a_{S_4}(1,2,3,4) = \left(\frac{1}{D(1,2,3,4)} \right) \left\{ [-T_{ab}^1 T_{ab}^4 (T_{bb}^2 + T_{bb}^3) - T_{ab}^2 T_{ab}^3 (T_{bb}^1 + T_{bb}^4)] (T_{aa}^4 - T_{ab}^4) \right. \\ \left. + [T_{ab}^1 (T_{ab}^3)^2 - T_{ab}^1 (T_{aa}^3 + T_{aa}^4) (T_{bb}^2 + T_{bb}^3) - T_{ab}^2 T_{ab}^3 T_{ab}^4] (T_{bb}^4 - T_{ab}^4) \right\} \quad (\text{B-21.4})$$

$$a_{W_1}(1,2,3,4) = \left(\frac{1}{D(1,2,3,4)} \right) \left\{ [(T_{ab}^1 (T_{ab}^3)^2 - T_{ab}^2 T_{ab}^3 T_{ab}^4 - T_{ab}^1 (T_{aa}^3 + T_{aa}^4) (T_{bb}^2 + T_{bb}^3))] (T_{aa}^1 + T_{ab}^1) \right. \\ \left. + [(T_{aa}^1 + T_{aa}^2) (T_{aa}^3 + T_{aa}^4) (T_{bb}^2 + T_{bb}^3) - (T_{ab}^2)^2 (T_{aa}^3 + T_{aa}^4) \right. \\ \left. - (T_{ab}^3)^2 (T_{aa}^1 + T_{aa}^2)] (T_{bb}^1 + T_{ab}^1) \right\} \quad (\text{B-21.5})$$

$$a_{W_2}(1,2,3,4) = \left(\frac{1}{D(1,2,3,4)} \right) \left\{ [T_{ab}^1 (T_{ab}^3)^2 - T_{ab}^2 T_{ab}^3 T_{ab}^4 - T_{ab}^1 (T_{aa}^3 + T_{aa}^4) (T_{bb}^2 + T_{bb}^3)] (T_{aa}^2 - T_{ab}^2) \right. \\ \left. + [-T_{ab}^1 T_{ab}^2 (T_{aa}^3 + T_{aa}^4) - T_{ab}^3 T_{ab}^4 (T_{aa}^1 + T_{aa}^2)] (T_{bb}^2 - T_{ab}^2) \right\} \quad (\text{B-21.6})$$

$$a_{W_3}(1,2,3,4) = \left(\frac{1}{D(1,2,3,4)} \right) \left\{ [T_{ab}^1 T_{ab}^2 T_{ab}^3 + T_{ab}^4 (T_{aa}^1 + T_{aa}^2) (T_{bb}^2 + T_{bb}^3) - (T_{ab}^2)^2 T_{ab}^4] (T_{aa}^3 + T_{ab}^3) \right. \\ \left. + [-T_{ab}^1 T_{ab}^2 (T_{aa}^3 + T_{aa}^4) - T_{ab}^3 T_{ab}^4 (T_{aa}^1 + T_{aa}^2)] (T_{bb}^3 + T_{ab}^3) \right\} \quad (\text{B-21.7})$$

$$a_{W_4}(1,2,3,4) = \left(\frac{1}{D(1,2,3,4)} \right) \left\{ [(T_{ab}^1 T_{ab}^2 T_{ab}^3 + T_{ab}^4 (T_{aa}^1 + T_{aa}^2) (T_{bb}^2 + T_{bb}^3) - (T_{ab}^2)^2 T_{ab}^4] (T_{aa}^4 - T_{ab}^4) \right. \\ \left. + [(T_{aa}^1 + T_{aa}^2) (T_{aa}^3 + T_{aa}^4) (T_{bb}^2 + T_{bb}^3) - (T_{ab}^2)^2 (T_{aa}^3 + T_{aa}^4) \right. \\ \left. - (T_{ab}^3)^2 (T_{aa}^1 + T_{aa}^2)] (T_{bb}^4 - T_{ab}^4) \right\} \quad (\text{B-21.8})$$

where

$$D(1,2,3,4) = (T_{ab}^1 T_{ab}^3 - T_{ab}^2 T_{ab}^4)^2 \\ + (T_{aa}^1 + T_{aa}^2) (T_{aa}^3 + T_{aa}^4) (T_{bb}^1 + T_{bb}^4) (T_{bb}^2 + T_{bb}^3) \\ - (T_{ab}^1)^2 (T_{aa}^3 + T_{aa}^4) (T_{bb}^2 + T_{bb}^3) - (T_{ab}^2)^2 (T_{aa}^3 + T_{aa}^4) (T_{bb}^1 + T_{bb}^4) \\ - (T_{ab}^3)^2 (T_{aa}^1 + T_{aa}^2) (T_{bb}^1 + T_{bb}^4) - (T_{ab}^4)^2 (T_{aa}^1 + T_{aa}^2) (T_{bb}^2 + T_{bb}^3) \quad (\text{B-21.9})$$

For quadrant II:

$$a_{S_1}(6,1,4,5) = \left(\frac{1}{D(6,1,4,5)} \right) \left\{ [(T_{aa}^4 + T_{aa}^5)(T_{bb}^6 + T_{bb}^5)(T_{bb}^1 + T_{bb}^4) - (T_{ab}^4)^2(T_{bb}^6 + T_{bb}^5) - (T_{ab}^5)^2(T_{bb}^1 + T_{bb}^4)](T_{aa}^6 + T_{ab}^6) \right. \\ \left. + [(T_{ab}^6(T_{ab}^4)^2 - T_{ab}^6(T_{aa}^4 + T_{aa}^5)(T_{bb}^1 + T_{bb}^4) - T_{ab}^1 T_{ab}^4 T_{ab}^5)](T_{bb}^6 + T_{ab}^6) \right\} \quad (\text{B-22.1})$$

$$a_{S_2}(6,1,4,5) = \left(\frac{1}{D(6,1,4,5)} \right) \left\{ [(T_{aa}^4 + T_{aa}^5)(T_{bb}^6 + T_{bb}^5)(T_{bb}^1 + T_{bb}^4) - (T_{ab}^4)^2(T_{bb}^6 + T_{bb}^5) - (T_{ab}^5)^2(T_{bb}^1 + T_{bb}^4)](T_{aa}^1 - T_{ab}^1) \right. \\ \left. + [(T_{ab}^6 T_{ab}^4 T_{ab}^5 + T_{ab}^1(T_{aa}^4 + T_{aa}^5)(T_{bb}^6 + T_{bb}^5) - T_{ab}^1(T_{ab}^5)^2)](T_{bb}^1 - T_{ab}^1) \right\} \quad (\text{B-22.2})$$

$$a_{S_3}(6,1,4,5) = \left(\frac{1}{D(6,1,4,5)} \right) \left\{ [-T_{ab}^6 T_{ab}^5(T_{bb}^1 + T_{bb}^4) - T_{ab}^1 T_{ab}^4(T_{bb}^6 + T_{bb}^5)](T_{aa}^4 + T_{ab}^4) \right. \\ \left. + [T_{ab}^6 T_{ab}^4 T_{ab}^5 + T_{ab}^1(T_{aa}^4 + T_{aa}^5)(T_{bb}^6 + T_{bb}^5) - T_{ab}^1(T_{ab}^5)^2](T_{bb}^4 + T_{ab}^4) \right\} \quad (\text{B-22.3})$$

$$a_{S_4}(6,1,4,5) = \left(\frac{1}{D(6,1,4,5)} \right) \left\{ [-T_{ab}^6 T_{ab}^5(T_{bb}^1 + T_{bb}^4) - T_{ab}^1 T_{ab}^4(T_{bb}^6 + T_{bb}^5)](T_{aa}^5 - T_{ab}^5) \right. \\ \left. + [T_{ab}^6(T_{ab}^4)^2 - T_{ab}^6(T_{aa}^4 + T_{aa}^5)(T_{bb}^1 + T_{bb}^4) - T_{ab}^1 T_{ab}^4 T_{ab}^5](T_{bb}^5 - T_{ab}^5) \right\} \quad (\text{B-22.4})$$

$$a_{E_1}(6,1,4,5) = \left(\frac{1}{D(6,1,4,5)} \right) \left\{ ([T_{ab}^6 T_{ab}^4 T_{ab}^5 + T_{ab}^1(T_{aa}^4 + T_{aa}^5)(T_{bb}^6 + T_{bb}^5) - T_{ab}^1(T_{ab}^5)^2](T_{aa}^6 + T_{ab}^6) \right. \\ \left. + [-T_{ab}^4 T_{ab}^5(T_{aa}^6 + T_{aa}^1) - T_{ab}^6 T_{ab}^1(T_{aa}^4 + T_{aa}^5)](T_{bb}^6 + T_{ab}^6) \right\} \quad (\text{B-22.5})$$

$$a_{E_2}(6,1,4,5) = \left(\frac{1}{D(6,1,4,5)} \right) \left\{ [(T_{ab}^6 T_{ab}^4 T_{ab}^5 + T_{ab}^1(T_{aa}^4 + T_{aa}^5)(T_{bb}^6 + T_{bb}^5) - T_{ab}^1(T_{ab}^5)^2](T_{aa}^1 - T_{ab}^1) \right. \\ \left. + [(T_{aa}^6 + T_{aa}^1)(T_{aa}^4 + T_{aa}^5)(T_{bb}^6 + T_{bb}^5) - (T_{ab}^5)^2(T_{aa}^6 + T_{aa}^1) - (T_{ab}^6)^2(T_{aa}^4 + T_{aa}^5)](T_{bb}^1 - T_{ab}^1) \right\} \quad (\text{B-22.6})$$

$$a_{E_3}(6,1,4,5) = \left(\frac{1}{D(6,1,4,5)} \right) \left\{ [(T_{ab}^6)^2 T_{ab}^4 - T_{ab}^4(T_{aa}^6 + T_{aa}^1)(T_{bb}^6 + T_{bb}^5) - T_{ab}^6 T_{ab}^1 T_{ab}^5](T_{aa}^4 + T_{ab}^4) \right. \\ \left. + [(T_{aa}^6 + T_{aa}^1)(T_{aa}^4 + T_{aa}^5)(T_{bb}^6 + T_{bb}^5) - (T_{ab}^5)^2(T_{aa}^6 + T_{aa}^1) - (T_{ab}^6)^2(T_{aa}^4 + T_{aa}^5)](T_{bb}^4 + T_{ab}^4) \right\} \quad (\text{B-22.7})$$

$$a_{E_4}(6,1,4,5) = \left(\frac{1}{D(6,1,4,5)} \right) \left\{ [(T_{ab}^6)^2 T_{ab}^4 - T_{ab}^4(T_{aa}^6 + T_{aa}^1)(T_{bb}^6 + T_{bb}^5) - T_{ab}^6 T_{ab}^1 T_{ab}^5](T_{aa}^5 - T_{ab}^5) \right. \\ \left. + (-T_{ab}^4 T_{ab}^5(T_{aa}^6 + T_{aa}^1) - T_{ab}^6 T_{ab}^1(T_{aa}^4 + T_{aa}^5)](T_{bb}^5 - T_{ab}^5) \right\} \quad (\text{B-22.8})$$

where

$$\begin{aligned}
D(6,1,4,5) &= (T_{ab}^6 T_{ab}^4 - T_{ab}^1 T_{ab}^5)^2 \\
&+ (T_{aa}^6 + T_{aa}^1)(T_{aa}^4 + T_{aa}^5)(T_{bb}^6 + T_{bb}^5)(T_{bb}^1 + T_{bb}^4) \\
&- (T_{ab}^6)^2 (T_{aa}^4 + T_{aa}^5)(T_{bb}^1 + T_{bb}^4) - (T_{ab}^1)^2 (T_{aa}^4 + T_{aa}^5)(T_{bb}^6 + T_{bb}^5) \\
&- (T_{ab}^4)^2 (T_{aa}^6 + T_{aa}^1)(T_{bb}^6 + T_{bb}^5) - (T_{ab}^5)^2 (T_{aa}^6 + T_{aa}^1)(T_{bb}^1 + T_{bb}^4)
\end{aligned} \tag{B-22.9}$$

For quadrant III:

$$\begin{aligned}
a_{N1}(7,8,1,6) &= \left(\frac{1}{D(7,8,1,6)} \right) \left\{ [-T_{ab}^8 T_{ab}^1 (T_{bb}^7 + T_{bb}^6) - T_{ab}^7 T_{ab}^6 (T_{bb}^8 + T_{bb}^1)] (T_{aa}^7 + T_{aa}^7) \right. \\
&\quad \left. + [T_{ab}^7 T_{ab}^8 T_{ab}^1 + T_{ab}^6 (T_{aa}^7 + T_{aa}^8)(T_{bb}^8 + T_{bb}^1) - (T_{ab}^8)^2 T_{ab}^6] (T_{bb}^7 + T_{bb}^7) \right\}
\end{aligned} \tag{B-23.1}$$

$$\begin{aligned}
a_{N2}(7,8,1,6) &= \left(\frac{1}{D(7,8,1,6)} \right) \left\{ [-T_{ab}^8 T_{ab}^1 (T_{bb}^7 + T_{bb}^6) - T_{ab}^7 T_{ab}^6 (T_{bb}^8 + T_{bb}^1)] (T_{aa}^8 - T_{aa}^8) \right. \\
&\quad \left. + [(T_{ab}^7)^2 T_{ab}^1 - T_{ab}^7 T_{ab}^8 T_{ab}^6 - T_{ab}^1 (T_{aa}^7 + T_{aa}^8)(T_{bb}^7 + T_{bb}^6)] (T_{bb}^8 - T_{bb}^8) \right\}
\end{aligned} \tag{B-23.2}$$

$$\begin{aligned}
a_{N3}(7,8,1,6) &= \left(\frac{1}{D(7,8,1,6)} \right) \left\{ [(T_{aa}^7 + T_{aa}^8)(T_{bb}^7 + T_{bb}^6)(T_{bb}^8 + T_{bb}^1) - (T_{ab}^8)^2 (T_{bb}^7 + T_{bb}^6) \right. \\
&\quad \left. - (T_{ab}^7)^2 (T_{bb}^8 + T_{bb}^1)] (T_{aa}^1 + T_{aa}^1) \right. \\
&\quad \left. + [(T_{ab}^7)^2 T_{ab}^1 - T_{ab}^7 T_{ab}^8 T_{ab}^6 - T_{ab}^1 (T_{aa}^7 + T_{aa}^8)(T_{bb}^7 + T_{bb}^6)] (T_{bb}^1 + T_{bb}^1) \right\}
\end{aligned} \tag{B-23.3}$$

$$\begin{aligned}
a_{N4}(7,8,1,6) &= \left(\frac{1}{D(7,8,1,6)} \right) \left\{ [(T_{aa}^7 + T_{aa}^8)(T_{bb}^7 + T_{bb}^6)(T_{bb}^8 + T_{bb}^1) - (T_{ab}^8)^2 (T_{bb}^7 + T_{bb}^6) \right. \\
&\quad \left. - (T_{ab}^7)^2 (T_{bb}^8 + T_{bb}^1)] (T_{aa}^6 - T_{aa}^6) \right. \\
&\quad \left. + [T_{ab}^7 T_{ab}^8 T_{ab}^1 + T_{ab}^6 (T_{aa}^7 + T_{aa}^8)(T_{bb}^8 + T_{bb}^1) - (T_{ab}^8)^2 T_{ab}^6] (T_{bb}^6 - T_{bb}^6) \right\}
\end{aligned} \tag{B-23.4}$$

$$\begin{aligned}
a_{E1}(7,8,1,6) &= \left(\frac{1}{D(7,8,1,6)} \right) \left\{ [(T_{ab}^7 T_{ab}^1 T_{ab}^6 + T_{ab}^8 (T_{aa}^1 + T_{aa}^6)(T_{bb}^7 + T_{bb}^6) - T_{ab}^8 (T_{ab}^6)^2] (T_{aa}^7 + T_{aa}^7) \right. \\
&\quad \left. + [-T_{ab}^1 T_{ab}^6 (T_{aa}^7 + T_{aa}^8) - T_{ab}^7 T_{ab}^8 (T_{aa}^1 + T_{aa}^6)] (T_{bb}^7 + T_{bb}^7) \right\}
\end{aligned} \tag{B-23.5}$$

$$\begin{aligned}
a_{E2}(7,8,1,6) &= \left(\frac{1}{D(7,8,1,6)} \right) \left\{ [T_{ab}^7 T_{ab}^1 T_{ab}^6 + T_{ab}^8 (T_{aa}^1 + T_{aa}^6)(T_{bb}^7 + T_{bb}^6) - T_{ab}^8 (T_{ab}^6)^2] (T_{aa}^8 - T_{aa}^8) \right. \\
&\quad \left. + [(T_{aa}^7 + T_{aa}^8)(T_{aa}^1 + T_{aa}^6)(T_{bb}^7 + T_{bb}^6) - (T_{ab}^6)^2 (T_{aa}^7 + T_{aa}^8) \right. \\
&\quad \left. - (T_{ab}^7)^2 (T_{aa}^1 + T_{aa}^6)] (T_{bb}^8 - T_{bb}^8) \right\}
\end{aligned} \tag{B-23.6}$$

$$\begin{aligned}
a_{E3}(7,8,1,6) = & \left(\frac{1}{D(7,8,1,6)} \right) \left\{ [(T_{ab}^7)^2 T_{ab}^1 - T_{ab}^1 (T_{aa}^7 + T_{aa}^8)(T_{bb}^7 + T_{bb}^6) - T_{ab}^7 T_{ab}^8 T_{ab}^6](T_{aa}^1 + T_{ab}^1) \right. \\
& + [T_{aa}^7 + T_{aa}^8)(T_{aa}^1 + T_{aa}^6)(T_{bb}^7 + T_{bb}^6) - (T_{ab}^6)^2 (T_{aa}^7 + T_{aa}^8) \\
& \left. - (T_{ab}^7)^2 (T_{aa}^1 + T_{aa}^6)](T_{bb}^1 + T_{ab}^1) \right\} \quad (\text{B-23.7})
\end{aligned}$$

$$\begin{aligned}
a_{E4}(7,8,1,6) = & \left(\frac{1}{D(7,8,1,6)} \right) \left\{ [(T_{ab}^7)^2 T_{ab}^1 - T_{ab}^1 (T_{aa}^7 + T_{aa}^8)(T_{bb}^7 + T_{bb}^6) - T_{ab}^7 T_{ab}^8 T_{ab}^6](T_{aa}^6 - T_{ab}^6) \right. \\
& \left. + [-T_{ab}^1 T_{ab}^6 (T_{aa}^7 + T_{aa}^8) - T_{ab}^7 T_{ab}^8 (T_{aa}^1 + T_{aa}^6)](T_{bb}^6 - T_{ab}^6) \right\} \quad (\text{B-23.8})
\end{aligned}$$

where

$$\begin{aligned}
D(7,8,1,6) = & (T_{ab}^7 T_{ab}^1 - T_{ab}^8 T_{ab}^6)^2 \\
& + (T_{aa}^7 + T_{aa}^8)(T_{aa}^1 + T_{aa}^6)(T_{bb}^7 + T_{bb}^6)(T_{bb}^8 + T_{bb}^1) \\
& - (T_{ab}^7)^2 (T_{aa}^1 + T_{aa}^6)(T_{bb}^8 + T_{bb}^1) - (T_{ab}^8)^2 (T_{aa}^1 + T_{aa}^6)(T_{bb}^7 + T_{bb}^6) \\
& - (T_{ab}^1)^2 (T_{aa}^7 + T_{aa}^8)(T_{bb}^7 + T_{bb}^6) - (T_{ab}^6)^2 (T_{aa}^7 + T_{aa}^8)(T_{bb}^8 + T_{bb}^1) \quad (\text{B-23.9})
\end{aligned}$$

For quadrant IV:

$$\begin{aligned}
a_{N1}(8,9,2,1) = & \left(\frac{1}{D(8,9,2,1)} \right) \left\{ ([-T_{ab}^9 T_{ab}^2 (T_{bb}^8 + T_{bb}^1) - T_{ab}^8 T_{ab}^1 (T_{bb}^9 + T_{bb}^2)](T_{aa}^8 + T_{ab}^8) \right. \\
& \left. + [T_{ab}^8 T_{ab}^9 T_{ab}^2 + T_{ab}^1 (T_{aa}^8 + T_{aa}^9)(T_{bb}^9 + T_{bb}^2) - (T_{ab}^9)^2 T_{ab}^1](T_{bb}^8 + T_{ab}^8) \right\} \quad (\text{B-24.1})
\end{aligned}$$

$$\begin{aligned}
a_{N2}(8,9,2,1) = & \left(\frac{1}{D(8,9,2,1)} \right) \left\{ [-T_{ab}^9 T_{ab}^2 (T_{bb}^8 + T_{bb}^1) - T_{ab}^8 T_{ab}^1 (T_{bb}^9 + T_{bb}^2)](T_{aa}^9 - T_{ab}^9) \right. \\
& \left. + [(T_{ab}^8)^2 T_{ab}^2 - T_{ab}^8 T_{ab}^9 T_{ab}^1 - T_{ab}^2 (T_{aa}^8 + T_{aa}^9)(T_{bb}^8 + T_{bb}^1)](T_{bb}^9 - T_{ab}^9) \right\} \quad (\text{B-24.2})
\end{aligned}$$

$$\begin{aligned}
a_{N3}(8,9,2,1) = & \left(\frac{1}{D(8,9,2,1)} \right) \left\{ [(T_{aa}^8 + T_{aa}^9)(T_{bb}^8 + T_{bb}^1)(T_{bb}^9 + T_{bb}^2) - (T_{ab}^9)^2 (T_{bb}^8 + T_{bb}^1) \right. \\
& \left. - (T_{ab}^8)^2 (T_{bb}^9 + T_{bb}^2)](T_{aa}^2 + T_{ab}^2) \right. \\
& \left. + [(T_{ab}^8)^2 T_{ab}^2 - T_{ab}^8 T_{ab}^9 T_{ab}^1 - T_{ab}^2 (T_{aa}^8 + T_{aa}^9)(T_{bb}^8 + T_{bb}^1)](T_{bb}^2 + T_{ab}^2) \right\} \quad (\text{B-24.3})
\end{aligned}$$

$$\begin{aligned}
a_{N4}(8,9,2,1) = & \left(\frac{1}{D(8,9,2,1)} \right) \left\{ [(T_{aa}^8 + T_{aa}^9)(T_{bb}^8 + T_{bb}^1)(T_{bb}^9 + T_{bb}^2) - (T_{ab}^9)^2 (T_{bb}^8 + T_{bb}^1) \right. \\
& \left. - (T_{ab}^8)^2 (T_{bb}^9 + T_{bb}^2)](T_{aa}^1 - T_{ab}^1) \right. \\
& \left. + [T_{ab}^8 T_{ab}^9 T_{ab}^2 + T_{ab}^1 (T_{aa}^8 + T_{aa}^9)(T_{bb}^9 + T_{bb}^2) - (T_{ab}^9)^2 T_{ab}^1](T_{bb}^1 - T_{ab}^1) \right\} \quad (\text{B-24.4})
\end{aligned}$$

$$a_{w_1}(8,9,2,1) = \left(\frac{1}{D(8,9,2,1)} \right) \left\{ [(T_{ab}^8 (T_{ab}^2)^2 - T_{ab}^9 T_{ab}^2 T_{ab}^1 - T_{ab}^8 (T_{aa}^2 + T_{aa}^1)(T_{bb}^9 + T_{bb}^2))(T_{aa}^8 + T_{aa}^8) + [(T_{aa}^8 + T_{aa}^9)(T_{aa}^2 + T_{aa}^1)(T_{bb}^9 + T_{bb}^2) - (T_{ab}^9)^2 (T_{aa}^2 + T_{aa}^1) - (T_{ab}^2)^2 (T_{aa}^8 + T_{aa}^9)](T_{bb}^8 + T_{ab}^8)] \right\} \quad (\text{B-24.5})$$

$$a_{w_2}(8,9,2,1) = \left(\frac{1}{D(8,9,2,1)} \right) \left\{ [T_{ab}^8 (T_{ab}^2)^2 - T_{ab}^9 T_{ab}^2 T_{ab}^1 - T_{ab}^8 (T_{aa}^2 + T_{aa}^1)(T_{bb}^9 + T_{bb}^2)](T_{aa}^9 - T_{ab}^9) + [-T_{ab}^8 T_{ab}^9 (T_{aa}^2 + T_{aa}^1) - T_{ab}^2 T_{ab}^1 (T_{aa}^8 + T_{aa}^9)](T_{bb}^9 - T_{ab}^9) \right\} \quad (\text{B-24.6})$$

$$a_{w_3}(8,9,2,1) = \left(\frac{1}{D(8,9,2,1)} \right) \left\{ [T_{ab}^8 T_{ab}^9 T_{ab}^2 + T_{ab}^1 (T_{aa}^8 + T_{aa}^9)(T_{bb}^9 + T_{bb}^2) - (T_{ab}^9)^2 T_{ab}^1](T_{aa}^2 + T_{ab}^2) + [-T_{ab}^8 T_{ab}^9 (T_{aa}^2 + T_{aa}^1) - T_{ab}^2 T_{ab}^1 (T_{aa}^8 + T_{aa}^9)](T_{bb}^2 + T_{ab}^2) \right\} \quad (\text{B-24.7})$$

$$a_{w_4}(8,9,2,1) = \left(\frac{1}{D(8,9,2,1)} \right) \left\{ [T_{ab}^8 T_{ab}^9 T_{ab}^2 + T_{ab}^1 (T_{aa}^8 + T_{aa}^9)(T_{bb}^9 + T_{bb}^2) - (T_{ab}^9)^2 T_{ab}^1](T_{aa}^1 - T_{ab}^1) + [(T_{aa}^8 + T_{aa}^9)(T_{aa}^2 + T_{aa}^1)(T_{bb}^9 + T_{bb}^2) - (T_{ab}^9)^2 (T_{aa}^2 + T_{aa}^1) - (T_{ab}^2)^2 (T_{aa}^8 + T_{aa}^9)](T_{bb}^1 - T_{ab}^1) \right\} \quad (\text{B-24.8})$$

where

$$D(8,9,2,1) = (T_{ab}^8 T_{ab}^2 - T_{ab}^9 T_{ab}^1)^2 + (T_{aa}^8 + T_{aa}^9)(T_{aa}^2 + T_{aa}^1)(T_{bb}^8 + T_{bb}^1)(T_{bb}^9 + T_{bb}^2) - (T_{ab}^8)^2 (T_{aa}^2 + T_{aa}^1)(T_{bb}^9 + T_{bb}^2) - (T_{ab}^9)^2 (T_{aa}^2 + T_{aa}^1)(T_{bb}^8 + T_{bb}^1) - (T_{ab}^2)^2 (T_{aa}^8 + T_{aa}^9)(T_{bb}^8 + T_{bb}^1) - (T_{ab}^1)^2 (T_{aa}^8 + T_{aa}^9)(T_{bb}^9 + T_{bb}^2) \quad (\text{B-24.9})$$

Obtaining the Final Coefficients

The finite-difference approximation for the second term of equation B-3 is obtained from equations B-18.1 to B-18.4 with substitution of equations B-20.1 to B-20.8 and equations B-21.1 to B-24.9 for the coefficients. Finally, the local node numbering scheme in figure B-7 needs to be converted to the set of j, i indices as shown in figure B-9.

For inactive cells adjacent to a boundary of the region, the appropriate transmissivities, T_{aa}^m , T_{bb}^m , and T_{ab}^m will be zero. The conductances for cell faces forming external boundaries will automatically be computed to be zero, giving the natural boundary condition of no flow across the boundaries of the region. However, some terms in equations B- 21.1 through B- 24.9 can become quotients of zero over zero, and this becomes more likely when two or more cells have zero conductances. Taking the limits of these quotients algebraically as the conductance per unit width goes to zero will give the correct terms, but evaluating all possible combinations is tedious. Instead, for numerical evaluation, very small non-zero transmissivities are used at the cells outside the region. It is this approximation that leads to the error shown in figure 6B. More rigorous treatment is possible but is not included in this version of the LVDA capability.

The conductance per unit cell width for the z-direction remains the harmonic mean expressions as before because the principal axis of vertical anisotropy continues to be aligned with the z-coordinate axis. In the case of the principal axes of anisotropy being aligned with the x,y coordinate directions, the formulation presented also reduces to the harmonic mean conductance expressions.

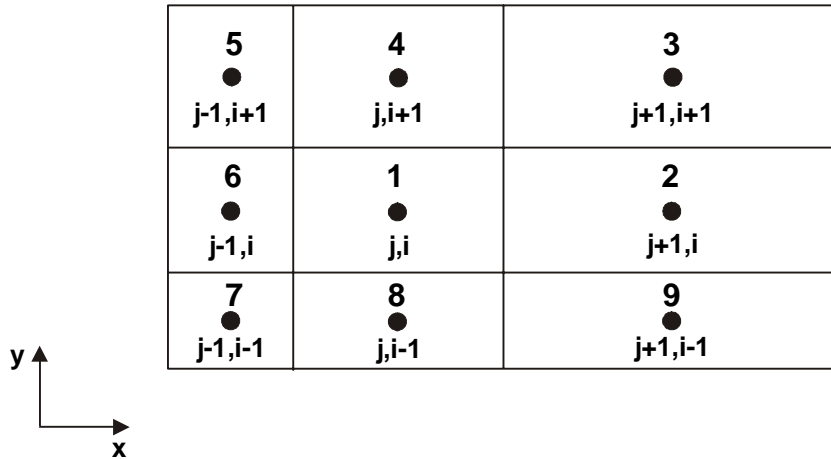


Figure B-9. Finite-difference grid showing local numbering and global indices used for the derivation of variable-direction horizontal anisotropy.

Final Matrix Equation

The eight flow terms shown in figure B-7 are expressed in terms of only the node hydraulic heads by eliminating the added heads at the cell faces. This was accomplished by enforcing normal flow continuity and resulted in equations B-20 with the coefficients of equations B-21 through B-24. Using these results, a finite-difference matrix equation can be constructed to approximate the steady-state form of the ground-water flow equation in two dimensions (B-3). The resulting form of the matrix equation is

$$\mathbf{A}^{(9)}h = f \tag{B-25}$$

where

- $\mathbf{A}^{(9)}$ is the matrix of finite-difference coefficients [L^2/T];
- h is the vector of hydraulic head at the node points [L]; and
- f is the vector of volumetric source flow-rate at each cell [L^3/T] (positive is into the region).

Equation B-25 is the same as equation 8.

The superscript on the \mathbf{A} matrix indicates that each difference equation contains up to nine non-zero coefficients forming a matrix with terms on the diagonal and eight off-diagonals; whereas only four off-diagonals are needed when horizontal anisotropy is parallel to the grid directions. For a three-dimensional system, terms occur on two additional off-diagonals, but these are not affected by horizontal anisotropy and are not discussed in this report.

Diagonal Dominance

The property of diagonal dominance, in which for each row of the matrix the absolute value of the diagonal term is greater than the sum of the absolute values of the off-diagonals, is important to solving matrix equations (Golub and van Loan, 1996, p. 120). Matrices that are not diagonally dominant are very difficult to solve. Edwards (1998) has shown conditional diagonal dominance for a uniform (homogeneous) anisotropic conductance tensor. In particular, diagonal dominance is ensured for the $\mathbf{A}^{(9)}$ matrix constructed by locating the points of pressure continuity at the midpoints of each cell face as was done in this report if the following condition is satisfied.

$$T_{aa} = T_{bb} = |T_{ab}| \quad (\text{B-26})$$

Equation B-26 describes rather restrictive conditions. The Mohr's circle diagram (Bear, 1972 p. 142), shows that the angle between the principal axes of the conductivity tensor and the coordinate system must be 45 degrees and the hydraulic conductivity in the direction of the minor principal axis must be zero. Thus, the matrix for the full set of difference equations will almost never be diagonally dominant.

Operator Splitting

Solving matrix equations such as equation B-25 generally occupies most of the execution time of most ground-water simulations. Matrix $\mathbf{A}^{(9)}$ of equation B-25 is especially difficult for iterative solvers, because it is not diagonally dominant. In addition, equation B-25 does not satisfy a maximum principle, as discussed in the 'Modifying the equations for traditional solvers' section of this report. To obtain a set of equations that can be more easily solved, operator splitting (matrix splitting) can be very useful and has the advantage of possessing a maximum principle.

An operator splitting of the finite-difference equations is developed such that a matrix involving only the 5-point stencil of cells needs to be solved to obtain the hydraulic head field. Splitting at the matrix and cell-flow level will be discussed; results showed that consistent splitting requires splitting at the cell-flow level. Some properties concerning operator splitting error, iteration stability and convergence, and matrix diagonal dominance will be presented. The operator splitting used in this report is adapted from Edwards (1998, 2000), who developed a general theory for consistent flow representation for anisotropic conductivity for finite-element and finite-difference methods on several types of grids and for a family of control-volume integration algorithms. He also described an operator splitting algorithm and its properties. In this report, only the Edwards (1998, 2000) methods that are relevant to the cell-centered finite-difference method are presented and the representative equations of Edwards (1998, 2000) are expanded to include the whole set of flow equations needed for a 2-dimensional cell-centered grid.

The \mathbf{A} matrix of equation B-25 can be split into a pentadiagonal matrix and a residual matrix

$$\mathbf{A}^{(9)} = \mathbf{A}^{(5)} + \mathbf{A}^{(9-5)} \quad (\text{B-27})$$

where

- $\mathbf{A}^{(5)}$ is the pentadiagonal matrix;
- $\mathbf{A}^{(9-5)}$ is the residual matrix.

The residual matrix may have 4 or 9 diagonals depending on the splitting performed.

Splitting at the Matrix Level

There are many ways to split the $\mathbf{A}^{(9)}$ matrix. One way is a matrix level splitting that keeps all the matrix elements that multiply $h_1, h_2, h_4, h_6,$ and h_8 of fig. B-9 in the $\mathbf{A}^{(5)}$ matrix and put all the matrix elements that multiply $h_3, h_5, h_7,$ and h_9 into the $\mathbf{A}^{(9-5)}$ matrix. However, this splitting gives an $\mathbf{A}^{(5)}$ matrix which is not guaranteed to be diagonally dominant, because the cross derivative terms both add to and subtract from the diagonal of the matrix. Furthermore, the computed flow rates are not conservative across the cell faces unless iteration to convergence is done, thus what are called outer iterations in the PCG2 and LMG solvers are needed (Hill, 1990; Mehl and Hill, 2001). Finally, the velocity field calculated from the hydraulic head solution with this splitting will have a discretization error of order one if the transmissivity field is not uniform. To avoid these limitations, operator splitting at the flow level needs to be considered.

Splitting at the Flow Level

A consistent splitting is done at the flow level by splitting each flow in equation B-20.1 to B-20.8 into a normal-gradient component and a tangential-gradient component. Thus, for example, for the flow rate of equation B-20.1

$$F_{S(I)} = F_{S(I)}^{(5)} + F_{S(I)}^{(9-5)} \quad (\text{B-28})$$

The other 7 flow rates are treated similarly. The normal-gradient component comprises those flows that arise from the terms with T_{aa} and T_{bb} in equation B-6 and the tangential-gradient component comprises those flows that arise from terms with T_{ab} . This consistent operator splitting retains both local conservation of fluid and a divergence-free velocity field on a cell-by-cell basis.

Assembling the split flows into equation B-28 yields the form of equation B-27 for an operator splitting at the matrix level. The resulting $\mathbf{A}^{(9-5)}$ cross-flow matrix has 9 diagonals, while the $\mathbf{A}^{(5)}$ matrix is diagonally dominant.

Although it is possible in principle to derive analytical equations for the elements of $\mathbf{A}^{(9-5)}$, it is difficult to start with equations B-20.1 through B-20.8 and separate the normal-gradient flows from the tangential-gradient flows. The terms in equations B-20.1 to B-20.8 contain ratios of polynomials in $T_{aa}, T_{bb},$ and T_{ab} that do not separate easily. A more productive approach is to use the definition of equation B-28 and specify the normal-gradient components based on the classical 5-point differencing scheme for ground-water flow. Then the tangential-gradient components are calculated as the difference between the total components and the normal-gradient components. Thus, it is not necessary to derive explicit equations for the tangential-gradient terms.

The Split Flow Components

The normal-gradient flow components are written as

$$F_{S(I)}^{(5)} = - \left[\frac{T_{aa}^1 T_{aa}^2}{T_{aa}^1 + T_{aa}^2} (h_2 - h_1) \right] \quad (\text{B-29.1})$$

$$F_{W(I)}^{(5)} = - \left[\frac{T_{bb}^1 T_{bb}^4}{T_{bb}^1 + T_{bb}^4} (h_4 - h_1) \right] \quad (\text{B-29.2})$$

$$F_{S(II)}^{(5)} = - \left[\frac{T_{aa}^6 T_{aa}^1}{T_{aa}^6 + T_{aa}^1} (h_1 - h_6) \right] \quad (\text{B-29.3})$$

$$F_{E(II)}^{(5)} = - \left[\frac{T_{bb}^1 T_{bb}^4}{T_{bb}^1 + T_{bb}^4} (h_4 - h_1) \right] \quad (\text{B-29.4})$$

$$F_{E(III)}^{(5)} = - \left[\frac{T_{bb}^8 T_{bb}^1}{T_{bb}^8 + T_{bb}^1} (h_1 - h_8) \right] \quad (\text{B-30.5})$$

$$F_{N(III)}^{(5)} = - \left[\frac{T_{aa}^6 T_{aa}^1}{T_{aa}^6 + T_{aa}^1} (h_1 - h_6) \right] \quad (\text{B-29.6})$$

$$F_{W(IV)}^{(5)} = - \left[\frac{T_{bb}^8 T_{bb}^1}{T_{bb}^8 + T_{bb}^1} (h_1 - h_8) \right] \quad (\text{B-29.7})$$

$$F_{N(IV)}^{(5)} = - \left[\frac{T_{aa}^1 T_{aa}^2}{T_{aa}^1 + T_{aa}^2} (h_2 - h_1) \right] \quad (\text{B-29.8})$$

where T_{aa} and T_{bb} are given by equation B-7.

Then the tangential-gradient flow components are given by

$$F_{S(I)}^{(9-5)} = F_{S(I)} - F_{S(I)}^{(5)} \quad (\text{B-30.1})$$

$$F_{W(I)}^{(9-5)} = F_{W(I)} - F_{W(I)}^{(5)} \quad (\text{B-30.2})$$

$$F_{S(II)}^{(9-5)} = F_{S(II)} - F_{S(II)}^{(5)} \quad (\text{B-30.3})$$

$$F_{E(II)}^{(9-5)} = F_{E(II)} - F_{E(II)}^{(5)} \quad (\text{B-30.4})$$

$$F_{E(III)}^{(9-5)} = F_{E(III)} - F_{E(III)}^{(5)} \quad (\text{B-30.5})$$

$$F_{N(III)}^{(9-5)} = F_{N(III)} - F_{N(III)}^{(5)} \quad (\text{B-30.6})$$

$$F_{W(IV)}^{(9-5)} = F_{W(IV)} - F_{W(IV)}^{(5)} \quad (\text{B-30.7})$$

$$F_{N(IV)}^{(9-5)} = F_{N(IV)} - F_{N(IV)}^{(5)} \quad (\text{B-30.8})$$

The full $F_{D(n)}$ terms, with D=N,S,E, or W and n=I,II,III, or IV, are given by equations B-20.1 through B-20.8.

Equations B-30.1 through B-30.8 and equations B-29.1 through B-29.8 define the operator splitting at the flow level. The \mathbf{A} matrix equations can be assembled from these terms after converting the local cell numbers into global grid indices following figure B-9.

Solving the Finite-Difference Equations

After operator splitting has been done and the finite-difference equations have been assembled for steady state or transient flow, solution can proceed with or without iteration.

Semi-Implicit without Iteration

The first approach is applicable to a transient flow equation with no nonlinearities such as water-table conditions or nonlinear head-dependent boundaries. Looking only at the flow balance terms and ignoring the storage terms, operator splitting suggests a semi-implicit form of equation B-25 as

$$\mathbf{A}^{(5)}h^{n+1} = f - \mathbf{A}^{(9-5)}h^n \quad (\text{B-31})$$

where n and $n + 1$ indicate the time levels. Equation B-31 defines a non-iterative semi-implicit approximation to equation B-25 for h . The solutions for h are obtained at each discrete time level without iteration.

It can be shown that the operator splitting gives rise to a splitting truncation error of order Δt for the full anisotropic conductivity tensor (Edwards, 2000). This error can be reduced by iteration using the procedure described in the following section, or kept under control by restriction of the time-step length. Generally, MODFLOW models are nonlinear in some manner and require iteration; the method represented by equation B-31 would be rarely used and is not provided as an option in the LDVA capability.

Semi-Implicit with Iteration

The second approach is applicable to either a steady-state or transient flow equation. Equations B-25 and B-27 are combined and written in the form of an iteration cycle as

$$\mathbf{A}^{(5)}h^{\gamma+1} = f - \mathbf{A}^{(9-5)}h^\gamma \quad (\text{B-32})$$

where

γ is the iteration counter.

The iterations are equivalent to outer iterations of MODFLOW's PCG or LMG solvers.

The solution for h from equation B-32 is free of the error due to operator splitting mentioned above. However, it is not clear that this iteration is unconditionally stable, as discussed below.

Stability

The semi-implicit algorithms with and without iteration obtained by operator splitting are stable provided that the spectral radius is less than one. Stability is expected if $\mathbf{A}^{(9)}$ is diagonally dominant. Unfortunately, the full difference-equation matrix is only conditionally diagonally dominant with rather restrictive conditions, as discussed above. Numerical experimentation will likely be necessary to determine the robustness of a solution algorithm for h based on equations B-31 or B-32.

References Cited

- Anderman, E.R., and Hill, M.C., 2000, MODFLOW-2000, the U.S. Geological Survey modular ground-water model – Documentation of the Hydrogeologic-Unit Flow (HUF) Package: U.S. Geological Survey Open-File Report 00-342, 104 p.
- Bear, Jacob, 1972, Dynamics of fluid in porous media: New York, American Elsevier, 764p.
- Edwards, M.G., 1998, Cross flow tensors and finite volume approximation with deferred correction, Computer Methods in Applied Mechanics and Engineering, 151, p. 143-161.
- Edwards, M.G., 2000, M-Matrix flux splitting for general full tensor discretization operators on structured and unstructured grids, Journal of Computational Physics, 160, p.1-28.
- Edwards, M.G. and Rogers, C.F., 1998, Finite volume discretization with imposed flux continuity for the general tensor pressure equation, Computational Geosciences, 2, p.259-290.
- Golub, G.H and van Loan, C.F., 1996, Matrix computations, third edition: Baltimore, the Johns Hopkins University Press, 694p.
- Hill, M.C., 1990, Preconditioned Conjugate-Gradient 2 (PCG2), a computer program for solving ground-water flow equations: U.S. Geological Survey Water-Resources Investigations Report 90-4048, 43 p.
- McDonald, M.G. and Harbaugh, A.W., 1988, A modular three-dimensional finite difference ground-water flow model: U.S. Geological Survey Techniques of Water Resources Investigations, Book 6, Chapter A1. 586 p.
- Mehl, S.W., and Hill, M.C., 2001, MODFLOW-2000, the U.S. Geological Survey modular ground-water model -- User guide to the Link-AMG (LMG) Package for solving matrix equations using an algebraic multigrid solver: U.S. Geological Survey Open-File Report 01-177, 33 p.
- Norrie, D.H., and de Vries, Gerard, 1973, The finite element method: New York, Academic Press, 322p.
- Wang, H.F. and Anderson, M.P., 1982, Introduction to groundwater modeling, Finite difference and finite element methods: San Francisco, W.H Freeman and Company, 237p.

APPENDIX C: SENSITIVITIES

Using the operator splitting presented in Appendix B, the modified ground-water flow equation used by the LVDA capability can be expressed as:

$$\mathbf{A}^{(5)} h^{n+1} = f - (f^9 - f^5) \quad (\text{C-1})$$

where

- $\mathbf{A}^{(5)}$ is the pentadiagonal coefficient matrix [L^2/T],
- h^n is a vector of hydraulic heads [L],
- n is the solver-iteration counter,
- f is the forcing function vector [L^3/T],
- f^9 is a vector of flows calculated as $A^9 h$ [L^3/T], and
- f^5 is a vector of flows calculated as $A^5 h$ [L^3/T].

Equations for sensitivities are derived by taking the derivative of equation C-1 with respect to a general parameter b_l and applying the chain rule (see any basic calculus text) yields:

$$\mathbf{A}^{(5)} \frac{\partial h^{n+1}}{\partial b_l} = \frac{\partial f}{\partial b_l} - \frac{\partial f^9}{\partial b_l} + \frac{\partial f^5}{\partial b_l} - \frac{\partial \mathbf{A}^{(5)}}{\partial b_l} h^{n+1} \quad (\text{C-2})$$

The $\mathbf{A}^{(5)}$ matrix is calculated as discussed in appendix B. The first term on the right-hand side is already calculated as described by Hill and others (2000, p. 69). Evaluation of the other three terms is described below.

The f^9 Term

Figure B-7 shows that accounting for flow through the boundaries of a finite-difference cell requires involves calculating eight flow components:

$$f_{i,j,k}^9 = F_{S(II)_{i,j,k}} + F_{N(III)_{i,j,k}} - F_{S(I)_{i,j,k}} - F_{N(IV)_{i,j,k}} + F_{E(III)_{i,j,k}} + F_{W(IV)_{i,j,k}} - F_{E(II)_{i,j,k}} - F_{W(I)_{i,j,k}} \quad (\text{C-3})$$

Taking the derivative of C-3 with respect to parameter b_l produces:

$$\begin{aligned} \frac{\partial f_{i,j,k}^9}{\partial b_l} = & \frac{\partial F_{S(II)_{i,j,k}}}{\partial b_l} + \frac{\partial F_{N(III)_{i,j,k}}}{\partial b_l} - \frac{\partial F_{S(I)_{i,j,k}}}{\partial b_l} - \frac{\partial F_{N(IV)_{i,j,k}}}{\partial b_l} \\ & + \frac{\partial F_{E(III)_{i,j,k}}}{\partial b_l} + \frac{\partial F_{W(IV)_{i,j,k}}}{\partial b_l} - \frac{\partial F_{E(II)_{i,j,k}}}{\partial b_l} - \frac{\partial F_{W(I)_{i,j,k}}}{\partial b_l} \end{aligned} \quad (\text{C-4})$$

The first term on the right-hand side of equation C-4 was defined by equation B-20.3. Rearranging slightly produces:

$$\begin{aligned} F_{S(II)_{i,j,k}} = & -T_{aa_{i,j,k}} \left(h_{i,j,k} - a_{S1}(6,1,4,5)h_{i,j-1,k} - a_{S2}(6,1,4,5)h_{i,j,k} \right) \\ & - T_{ab_{i,j,k}} \left(a_{E1}(6,1,4,5)h_{i,j-1,k} + a_{E2}(6,1,4,5)h_{i,j,k} \right. \\ & \left. + a_{E3}(6,1,4,5)h_{i+1,j,k} + a_{E4}(6,1,4,5)h_{i+1,j-1,k} - h_{i,j,k} \right) \end{aligned} \quad (\text{C-5})$$

Taking the derivative with respect to b_l and applying the chain rule yields:

$$\begin{aligned}
\frac{\partial F_{S(II)_{i,j,k}}}{\partial b_l} = & -\frac{\partial T_{aa_{i,j,k}}}{\partial b_l} \left(h_{i,j,k} - a_{S1}(6,1,4,5)h_{i,j-1,k} - a_{S2}(6,1,4,5)h_{i,j,k} \right. \\
& \left. - a_{S3}(6,1,4,5)h_{i+1,j,k} - a_{S4}(6,1,4,5)h_{i+1,j-1,k} \right) \\
& - T_{aa_{i,j,k}} \left(\frac{\partial h_{i,j,k}}{\partial b_l} \right. \\
& \left. - \frac{\partial a_{S1}(6,1,4,5)}{\partial b_l} h_{i,j-1,k} - a_{S1}(6,1,4,5) \frac{\partial h_{i,j-1,k}}{\partial b_l} \right. \\
& \left. - \frac{\partial a_{S2}(6,1,4,5)}{\partial b_l} h_{i,j,k} - a_{S2}(6,1,4,5) \frac{\partial h_{i,j,k}}{\partial b_l} \right. \\
& \left. - \frac{\partial a_{S3}(6,1,4,5)}{\partial b_l} h_{i+1,j,k} - a_{S3}(6,1,4,5) \frac{\partial h_{i+1,j,k}}{\partial b_l} \right. \\
& \left. - \frac{\partial a_{S4}(6,1,4,5)}{\partial b_l} h_{i+1,j-1,k} - a_{S4}(6,1,4,5) \frac{\partial h_{i+1,j-1,k}}{\partial b_l} \right) \\
& - \frac{\partial T_{ab_{i,j,k}}}{\partial b_l} \left(a_{E1}(6,1,4,5)h_{i,j-1,k} + a_{E2}(6,1,4,5)h_{i,j,k} \right. \\
& \left. + a_{E3}(6,1,4,5)h_{i+1,j,k} + a_{E4}(6,1,4,5)h_{i+1,j-1,k} - h_{i,j,k} \right) \\
& - T_{ab_{i,j,k}} \left(\frac{\partial a_{E1}(6,1,4,5)}{\partial b_l} h_{i,j-1,k} + a_{E1}(6,1,4,5) \frac{\partial h_{i,j-1,k}}{\partial b_l} \right. \\
& \left. + \frac{\partial a_{E2}(6,1,4,5)}{\partial b_l} h_{i,j,k} + a_{E2}(6,1,4,5) \frac{\partial h_{i,j,k}}{\partial b_l} \right. \\
& \left. + \frac{\partial a_{E3}(6,1,4,5)}{\partial b_l} h_{i+1,j,k} + a_{E3}(6,1,4,5) \frac{\partial h_{i+1,j,k}}{\partial b_l} \right. \\
& \left. + \frac{\partial a_{E4}(6,1,4,5)}{\partial b_l} h_{i+1,j-1,k} + a_{E4}(6,1,4,5) \frac{\partial h_{i+1,j-1,k}}{\partial b_l} \right. \\
& \left. - \frac{\partial h_{i,j,k}}{\partial b_l} \right) \tag{C-6}
\end{aligned}$$

Similar equations can be derived for the other 7 flows. The equations require evaluation of derivatives of T_{aa} , T_{ab} and T_{bb} terms, which are defined using equation B-7. Taking the derivative and applying the chain rule yields:

$$\frac{\partial T_{aa_{i,j,k}}}{\partial b_l} = \left(\frac{\Delta c_i}{\Delta r_j} \right) \left[\frac{\frac{\partial TR_{i,j,k}}{\partial b_l} + \frac{\partial TC_{i,j,k}}{\partial b_l}}{2} + \frac{\frac{\partial TR_{i,j,k}}{\partial b_l} - \frac{\partial TC_{i,j,k}}{\partial b_l}}{2} \cos(2\theta_{i,j,k}) \right. \\
\left. + \frac{TR_{i,j,k} - TC_{i,j,k}}{2} \frac{\partial \cos(2\theta_{i,j,k})}{\partial b_l} \right] \tag{C-7}$$

$$\frac{\partial Tab_{i,j,k}}{\partial b_l} = \frac{\frac{\partial TR_{i,j,k}}{\partial b_l} - \frac{\partial TC_{i,j,k}}{\partial b_l}}{2} \sin(2\theta_{i,j,k}) + \frac{TR_{i,j,k} - TC_{i,j,k}}{2} \frac{\partial \sin(2\theta_{i,j,k})}{\partial b_l} \quad (C-8)$$

$$\frac{\partial Tbb_{i,j,k}}{\partial b_l} = \left(\frac{\Delta r_j}{\Delta c_i} \right) \left[\begin{array}{c} \frac{\frac{\partial TR_{i,j,k}}{\partial b_l} + \frac{\partial TC_{i,j,k}}{\partial b_l}}{2} - \frac{\frac{\partial TR_{i,j,k}}{\partial b_l} - \frac{\partial TC_{i,j,k}}{\partial b_l}}{2} \cos(2\theta_{i,j,k}) \\ - \frac{TR_{i,j,k} - TC_{i,j,k}}{2} \frac{\partial \cos(2\theta_{i,j,k})}{\partial b_l} \end{array} \right] \quad (C-9)$$

The derivatives on the right-hand side of equation C-7 to C-9 are non-zero only for parameters defining horizontal hydraulic conductivity (Kh_l), horizontal anisotropy ($HANI_l$), and the angle of anisotropy (θ_l).

$$\frac{\partial TR_{i,j,k}}{\partial Kh_l} = \sum_{p=1}^n m_{l,i,j,p} thk_{p,i,j,k} \quad (C-10)$$

$$\frac{\partial TC_{i,j,k}}{\partial Kh_l} = \sum_{p=1}^n m_{l,i,j,p} thk_{p,i,j,k} HANI_{i,j,p} \quad (C-11)$$

$$\frac{\partial TC_{i,j,k}}{\partial Hani_l} = \sum_{p=1}^n KH_{i,j,p} m_{l,i,j,p} thk_{p,i,j,k} \quad (C-12)$$

$$\frac{\partial \sin(2\theta_{i,j,k})}{\partial \theta_{i,j,k}} = 2 \cos(2\theta_{i,j,k}) \quad (C-13.1)$$

$$\frac{\partial \cos(2\theta_{i,j,k})}{\partial \theta_{i,j,k}} = -2 \sin(2\theta_{i,j,k}) \quad (C-13.2)$$

The complexity of the equations for a_{S1} , a_{S2} , and so on in equation C-6, indicates that their derivatives cannot be calculated analytically without considerable effort. Therefore, perturbation sensitivities are calculated for these terms by perturbing parameter values, calculating the change in the coefficient, and dividing by the change in the parameter value. In the current version of the LDVA capability, a fixed perturbation step size of 10 percent is used, except that when the angle is zero, a step size of 15 degrees is used. While the equations for the coefficients are nonlinear with respect to the parameter values, this approach worked well in the simulation examples presented in this report.

The f^5 Term

Next, focusing on f^5 , equation B-29 can be rearranged to yield:

$$f_{i,j,k}^5 = FL_{i,j,k}^5 + FT_{i,j,k}^5 + FR_{i,j,k}^5 + FB_{i,j,k}^5 \quad (C-14)$$

where

$$FL_{i,j,k}^5 = \frac{2T_{aa}^6 T_{aa}^1}{T_{aa}^6 + T_{aa}^1} (\phi_6 - \phi_1) = CRL_{i,j,k} (\phi_6 - \phi_1) \quad (C-15.1)$$

$$FT_{i,j,k}^5 = \frac{2T_{bb}^8 T_{bb}^1}{T_{bb}^8 + T_{bb}^1} (\phi_8 - \phi_1) = CCT_{i,j,k} (\phi_8 - \phi_1) \quad (C-15.2)$$

$$FR_{i,j,k}^5 = \frac{2T_{aa}^1 T_{aa}^2}{T_{aa}^1 + T_{aa}^2} (\phi_2 - \phi_1) = CRR_{i,j,k} (\phi_2 - \phi_1) \quad (C-15.3)$$

$$FB_{i,j,k}^5 = \frac{2T_{bb}^4 T_{bb}^1}{T_{bb}^4 + T_{bb}^1} (\phi_4 - \phi_1) = CCB_{i,j,k} (\phi_4 - \phi_1) \quad (C-15.4)$$

Taking the derivative of equation C-14 yields:

$$\frac{\partial f_{i,j,k}^5}{\partial b_l} = \frac{\partial FL_{i,j,k}^5}{\partial b_l} + \frac{\partial FT_{i,j,k}^5}{\partial b_l} + \frac{\partial FR_{i,j,k}^5}{\partial b_l} + \frac{\partial FB_{i,j,k}^5}{\partial b_l} \quad (C-16)$$

where

$$\frac{\partial FL_{i,j,k}^5}{\partial b_l} = \frac{\partial CRL_{i,j,k}}{\partial b_l} (\phi_6 - \phi_1) + CRL_{i,j,k} \left(\frac{\partial \phi_6}{\partial b_l} - \frac{\partial \phi_1}{\partial b_l} \right) \quad (C-17.1)$$

$$\frac{\partial FR_{i,j,k}^5}{\partial b_l} = \frac{\partial CRR_{i,j,k}}{\partial b_l} (\phi_2 - \phi_1) + CRR_{i,j,k} \left(\frac{\partial \phi_2}{\partial b_l} - \frac{\partial \phi_1}{\partial b_l} \right) \quad (C-17.2)$$

$$\frac{\partial FT_{i,j,k}^5}{\partial b_l} = \frac{\partial CCT_{i,j,k}}{\partial b_l} (\phi_8 - \phi_1) + CCT_{i,j,k} \left(\frac{\partial \phi_8}{\partial b_l} - \frac{\partial \phi_1}{\partial b_l} \right) \quad (C-17.3)$$

$$\frac{\partial FB_{i,j,k}^5}{\partial b_l} = \frac{\partial CCB_{i,j,k}}{\partial b_l} (\phi_4 - \phi_1) + CCB_{i,j,k} \left(\frac{\partial \phi_4}{\partial b_l} - \frac{\partial \phi_1}{\partial b_l} \right) \quad (C-17.4)$$

To derive the sensitivity of the conductance terms in C-17, consider the following steps. Basic calculus yields:

$$\frac{\partial}{\partial b} \left[\frac{u}{v} \right] = \frac{v \frac{\partial u}{\partial b} - u \frac{\partial v}{\partial b}}{v^2} \quad (C-18)$$

For $CRL_{i,j,k}$ u and v are defined as:

$$u = 2T_{aa}^6 T_{aa}^1 \quad (C-19)$$

$$v = T_{aa}^6 + T_{aa}^1 \quad (C-20)$$

Taking the derivative of equation C-19 with respect to b_l yields:

$$\frac{\partial u}{\partial b_l} = 2 \left[\frac{\partial T_{aa}^6}{\partial b_l} T_{aa}^1 + T_{aa}^6 \frac{\partial T_{aa}^1}{\partial b_l} \right] \quad (C-21)$$

and taking the derivative of equation C-20 with respect to b_i yields:

$$\frac{\partial v}{\partial b_i} = \frac{\partial Taa^6}{\partial b_i} + \frac{\partial Taa^1}{\partial b_i} \quad (C-22)$$

The Final Term

The $\mathbf{A}^{(5)}$ matrix is composed of the conductance terms that are shown in equations C-15, and the generalized derivative of each term is calculated using equations C-18 through C-22. The resulting matrix is then multiplied by the hydraulic heads already calculated for time step n+1.

APPENDIX D: CALCULATION OF HORIZONTAL CELL-FACE VELOCITIES AND SENSITIVITIES

Horizontal cell-face velocities are used by the Advective-Transport Observations (ADV2) Package (Anderman and Hill, 2001). These velocities change as the direction of horizontal anisotropy changes, as discussed in this appendix.

Horizontal Cell-Face Velocities

The velocity on the left x-face of cell i,j,k is defined as the flow rate through the cell face divided by the effective area of flow:

$$v_{x_{i,j-1/2,k}} = \frac{2Q_{x_{i,j-1/2,k}}}{n_{i,j,k}\Delta c_i(l_{i,j-1,k} + l_{i,j,k})} \quad (\text{D-1})$$

where

- $v_{x_{i,j-1/2,k}}$ is the velocity on face $i,j-1/2,k$ [L/T],
- $Q_{x_{i,j-1/2,k}}$ is the cell-face flow rate [L³/T],
- Δc_i is the cell width of row i [L],
- $n_{i,j,k}$ is the effective porosity of cell i,j,k , and
- $l_{i,j,k}$ is the saturated thickness of unconfined cell i,j,k or thickness of confined cell i,j,k [L].

The cell-face velocities are calculated using an average saturated thickness, instead of the single-cell saturated thickness used in MODPATH, because the original method produces discontinuities in velocity, and thus in sensitivity, at cell boundaries. For the LVDA Capability, the flow for a given cell face is calculated as the sum of the two flows calculated using equation B-20.

Horizontal Cell-Face Velocity Sensitivity

The sensitivity of the horizontal cell-face velocities are obtained by taking the derivative of equation D-1 with respect to a general parameter, yielding

$$\frac{\partial v_{x_{i,j-1/2,k}}}{\partial b_l} = \frac{2}{n_{i,j,k}\Delta c_i} \left[\frac{\frac{\partial Q_{x_{i,j-1/2,k}}}{\partial b_l} (l_{i,j-1,k} + l_{i,j,k}) + Q_{x_{i,j-1/2,k}} \left(\frac{\partial h_{i,j-1,k}}{\partial b_l} + \frac{\partial h_{i,j,k}}{\partial b_l} \right)}{(l_{i,j-1,k} + l_{i,j,k})^2} \right] \quad (\text{D-2})$$

which depends on the sensitivity of the flow and of the saturated thickness. Sensitivities of the flows are calculated using equation C-6 in subroutine SSEN1HUF2VDF9.